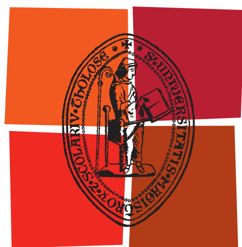

THÈSE

En vue de l'obtention du

DOCTORAT DE L'UNIVERSITÉ DE TOULOUSE

Délivré par :

Institut Supérieur de l'Aéronautique et de l'Espace (ISAE)

Présentée et soutenue par :
Sara SICONOLFI

le vendredi 15 janvier 2016

Titre :

Modèle physique de prédiction des effets des événements singuliers destructifs dans les composants électroniques de puissance

A physical prediction model of destructive Single Event Effects in power electronics devices

---

École doctorale et discipline ou spécialité :

ED GEET : Génie électrique

Unité de recherche :

Équipe d'accueil ISAE-ONERA OLIMPES

Directeur(s) de Thèse :

M. Jean-Pierre DAVID (directeur de thèse)
M. Guillaume HUBERT (co-directeur de thèse)

Jury :

M. Patrick AUSTIN - Président du Jury
M. Frédéric DARRACQ
M. Julien MEKKI
M. Jean-Luc LERAY - Rapporteur
M. Raoul VELAZCO - Rapporteur
M. Jean-Pierre DAVID - Directeur de thèse

Sara Siconolfi

A physical prediction model of destructive Single Event Effects in power electronics devices

COLOPHON
This thesis was typeset using the LaTeX typesetting system with the book class. The body text is set to 11pt. Typographical decisions were made to improve readers' comfort and minimize their concentration effort. Drawings are created with Inkscape and Gnuplot.
Version for reviewers: November 06, 2014
Final version: March 31, 2015

Ai miei genitori
Ai miei maestri e professori

Aknowledgments

> People often say that motivation doesn't last. Well, neither does bathing, that's why we recommend it daily.
>
> Zig Ziglar

At the end of my Ph.D. experience, my desk and drawers at Onera have been emptied, and all that is left is this manuscript and a few folders on a HD drive. On a less material level, the heritage of this three-year-journey is unforgettable, both in terms of lessons learnt for me, and of people I have met.

The lessons learnt are so many and so profound, that it has been a difficult task to try and summarize them in the few epigraphs I put at the beginning of each chapter.

What I would like to indulge in now, is an acknowledgement of the people who made this experience not only possible, but awesome.

Guillaume Hubert, my first contact and mentor at Onera, the promoter of the Ph.D. subject, the man who pushed me beyond my limits and taught me the lesson of strategy: thank you.

Jean-Pierre David, official *Directeur de thèse*, office-mate, pace maker, who taught me to take care of the small strokes to make the picture beautiful and functional: thank you.

I owe a lot to my *rapporteurs*, who were kind enough to be interested in my work and give it the best scientific evaluation I could ever ask. Particularly, I want to thank Raoul Velazco for his precious and detailed review of this manuscript, and Jean-Luc Leray for giving me the last push of scientific confidence I needed before the defence.

I would like to thank Patrick Austin for our constructive discussions, both before and during the defence itself: having him as president of the jury has been truly enriching and has permitted me to look at my work from other perspectives.

A special thank to Frédéric Darracq, with whom I had a pleasant technical exchange during my first year of Ph.D.: his data, his expert contribution, and his presence in the jury have been the quintessence of the scientific dialogue.

And of course Julien Mekki: I hope he knows how much his contribution meant to me, both during our collaboration, and as member of the jury. He has made our dialogue dynamic, efficient and rewarding. I want to thank him for giving me the opportunity and the funds to establish an enriching collaboration: his interest in my work has brought it to the next level.

I also take the chance to thank Pascal Oser and Giovanni Spiezia for their work at CERN and the role they played in our joint study, in terms of technical contribution and pleasant exchanges.

My special gratitude goes to Annie Carles-Bailhé, whose support, advice and personal engagement made all this possible.

Thank you to Sophie Duzellier and Jean-François Roussel for the way they lead respectively ECM group and DESP department. On a personal level, they have gifted me the freedom to embrace my challenges.

A special thank you to Laurent Artola for his Jedi guidance through the world of TCAD.

I struggle to resume in a few lines my gratitude to the big family of DESP department: you will all be truly missed with your triathlons, games, cakes, coffees and microphones. I will never forget the way you welcomed and improved me and my weird Italian accent.

Claude and Stephane, I wish I could find one of you in every office I go; unfortunately (luckily?) you are unique.

I want to thank all the people from Onera who gave me their time and professionalism, and very pleasant moments. Thank you also to my theatre buddies and to EChO fellows.

Thank you to all the Ph.D. students, post-docs and interns who shared their journey with me.

A Ph.D. is a quite trying moment, and I believe I made it through thanks to the support of my friends.

Some of them are not in Toulouse, but I know they are with me: Andrea, Stefano, Bordone, Nucci, João, Manuel, César, David, Leticia, Daniela, Francesca, Betta, thank you. For sure distance has never been an obstacle with Manuela: our friendship has found new ways every single day to share our lives and Ph.D. adventures.

Life in Toulouse has been a blast and I am grateful for the great people I have met there and for what we have shared: *apéros* with Tiziana, good laughs and food with Luigi and Elisa, beers and languages with Alice, wine tasting with Remi. Thank you guys. A special thought for Gerardo and Paulo: thank you for being always there for me and for letting me cook pasta for you.

Gianluca, which category (and in which language) shall I put you in? You were next to me with your advices and your patience, literally from the first to the last day of my Ph.D.: thank you, and *poi vediamo*.

Last but actually first, my family, to whom I will address a few words in Italian.

Grazie alla mia grande famiglia con tanti zii, zie e cugini, e la certezza che tutti fanno il tifo per me, anche da lontano.

Grazie a Francesco, un amore di fratello, che condivide la mia testa dura e i miei sogni, e che tante volte mi ha fatto tornare il sorriso.

Grazie ai miei genitori, che hanno saputo ascoltare e comprendere tutti i miei sforzi; il loro incoraggiamento è stato fondamentale per raggiungere questo traguardo, ed è per questo che la tesi è ad essi dedicata, sperando di averli resi un pizzico più orgogliosi.

Contents

1 Introduction **1**

2 Review of Single Event Burnout in power MOSFETs **5**

2.1 Power MOSFET 5
2.1.1 Power MOSFET configurations 5
2.1.2 Power MOSFET characteristics 9
2.2 Natural radiation environment 10
2.2.1 Space radiation environment 10
2.2.2 Atmospheric radiation environment 11
2.3 Introduction of useful definitions 12
2.3.1 Cross section 12
2.3.2 Linear Energy Transfer 13
2.3.3 Range 14
2.4 Interaction between particle and material 14
2.4.1 Total Ionizing Dose 16
2.4.2 Single Event Effects 16
2.5 Single Event Burnout 18
2.5.1 Literature survey of SEB in power MOSFETs 18
2.5.2 Summary of the state of the art 24

3 Calculation of SEB triggering criteria via 2D TCAD simulation **27**

3.1 Construction of an operational 2D MOSFET structure 27
3.1.1 Introduction to simulated physical models 29
3.1.2 Comparison with component datasheet 32
3.1.3 Evaluation of scale factor between 3D component and its 2D simulation 33
3.1.4 Comparison of 2D and 3D diffusion phenomena 34
3.2 Study of SEB physics by means of heavy ion injection 35

3.2.1 Proposition of study methodology and choice of SEB triggering criterion . . . 37
3.2.2 SEB prints in terms of drain current and electric field . . . 38
3.2.3 Determination of SEB threshold charge dependencies on physical parameters . . . 41
3.3 Extraction of SEB triggering law . . . 50
3.3.1 Synthesis of SEB physical parameters dependencies . . . 51
3.3.2 Choice of a mathematical representation of SEB physics . . . 54

4 Construction of SEB rate prediction model based on deposited charge and electric field 57
4.1 Proposition of a methodology for transition from TCAD analysis to prediction model . . . 57
4.1.1 Discussion of the empirical law for threshold charge . . . 58
4.1.2 Definition of SEB prediction criterion . . . 59
4.1.3 Derivation of model INPUTs and OUTPUTs . . . 59
4.2 Development of DELPHY for SEB generated by heavy ions . . . 60
4.2.1 DELPHY geometry for HEXFET topology . . . 61
4.2.2 DELPHY geometry for STRIPFET topology . . . 62
4.2.3 Implementation of the threshold charge criterion . . . 63
4.2.4 Cross section calculation for heavy ion generated SEB . . . 65
4.3 Comparison with heavy ion irradiation data . . . 69
4.3.1 Test configuration . . . 69
4.3.2 Comparison . . . 70
4.3.3 Effect of mathematical fitting of $k(x)$ . . . 70
4.3.4 Effect of 2D/3D diffusion . . . 70
4.4 Cross section calculation for proton generated SEB . . . 71
4.4.1 Secondary heavy ion generation by proton impact . . . 71
4.4.2 Proton SEB cross section calculation . . . 73
4.5 Comparison with proton irradiation data of STRIPFET . . . 74
4.5.1 Test configuration . . . 75
4.5.2 Comparison . . . 75

5 Extension of SEB cross section calculation from irradiation data 77
5.1 Motivation of SEB sensitivity calculation from irradiation data . . . 77
5.2 Test configuration and results for IRF360 . . . 78
5.3 Calculation of proton cross section . . . 79
5.4 Calculation of heavy ion cross section . . . 80

6 Discussion 85
6.1 Choice of 2D simulations . . . 85
6.2 Choice of triggering criterion . . . 86

6.3 Choice of simulated physical models 86
6.4 Confirmation of SEB trends 87
6.5 Identification of triggering law 87
6.6 Discussion of RPP methodology 88
6.7 Proton induced SEB 88
6.8 SEB calculation from experimental data 89

7 Conclusions 91

References 93

Résumé français 105
1 Introduction 105
2 Single Event Burnout dans les MOSFETs de puissance 107
3 Calcul des critères de déclenchement SEB à travers la simulation composant 2D TCAD 107
3.1 Construction d'une structure MOSFET 2D 107
3.2 Etude de la physique SEB par injection d'ions lourds 110
3.3 Extraction d'une loi empirique 110
4 Construction d'un modèle de prédiction SEB basé sur le champ électrique et la charge critique 112
4.1 Définition d'un critère de prédiction SEB 112
4.2 Développement de DELPHY pour SEB généré par ions lourds 112
4.3 Comparaison avec les données d'irradiation 114
4.4 Calcul des sections efficaces pour SEB proton 114
4.5 Comparaison avec les données d'irradiation 122
5 Extension du calcul des sections efficaces SEB à partir des données d'irradiation 122
5.1 Calcul des sections efficaces proton 122
5.2 Calcul des sections efficaces ion lourd 122
6 Discussions 122
6.1 Choix des simulations 2D 122
6.2 Choix du critère de déclenchement 124
6.3 Choix des modèles physiques simulés 124
6.4 Confirmation des allures SEB 126
6.5 Identification de la loi de déclenchement 126
6.6 Discussion de la méthodologie RPP 127
6.7 Calcul SEB à partir des données expérimentales 127
7 Conclusions 127

Nomenclature

η	Number of atoms per unit volume
Λ	Strip length
λ	Scale factor
μ	Mobility
Φ	Total radiative particle flux
ρ	Density
σ	Cross section
θ	Tilt
ϱ	Nuclei radius
ξ	Sensitive width of model cell
ζ	Range

c	Secondary ions generation probability
E	Energy
EF	Electric Field
h	Thickness
I	Current

N	Number of scattering centres
n	Neutron
p	Proton
q	Charge
R	Total width of model cell
V	Voltage
Z	Atomic number
L	Channel length
S	Stopping power
W	Channel width

Superscripts

D	Datasheet
H	HEXFET
S	STRIPFET
T	TCAD

Subscripts

B	Bremssthralung
D	Drain
DS	Drain to source
epi	Epitaxial layer
GS	Gate to source
HI	Heavy Ion
I	Ionizing
LET	Linear Energy Transfer
m	Microscopic
N	Nuclear

n	electron
th	Threshold

Acronyms

BJT	Bipolar Junction Transistor
CERN	European Organisation for Nuclear Research
CIA	Current Induced Avalanche
CME	Coronal Mass Ejection
CNES	Centre National d'Etudes Spatiales
COTS	(Commercial) Off-the-Shelf
DELPHY	Destructive effects prEdiction modeL based on PHysical analYsis
DUT	Device Under Test
ehp	Electron-hole pair
FEM	Finite Elements Method
GCR	Galactic Cosmic Ray
IEEE	Institute of Electrical and Electronics Engineers
IGBT	Insulated Gate Bipolar Transistor
IR	International Rectifier
LET	Linear Energy Transfer
LHC	Large Hadron Collider
MBU	Multiple Bit Upset
MCU	Multiple Cell Upset
MOSFET	Metal Oxide Semiconductor Field Effect Transistor
ONERA	Office National d'Etudes et Recherches Aérospatiales
RADECS	Radiation Effects on Components and Systems
RPP	Rectangular Parallelepiped
S-J	Super-Junction power MOSFET

SEB	Single Event Burnout
SEE	Single Event Effects
SEGR	Single Event Gate Rupture
SEL	Single Event Latch-up
SET	Single Event Transient
SEU	Single Event Upset
SiC	Silicon Carbide
SIMS	Secondary Ion Mass Spectrometry
SOA	Safe Operating Area
TCAD	Technology Computer-Aided Design
TPA	Two-photon Absorption
VIP	Vertical Intelligent Power

List of Figures

2.1 Schematics of lateral and vertical MOSFET configurations 6
2.2 VMOS (left) and DMOS (right) configurations 6
2.3 Schematics of planar and trench MOSFET technologies [63] 7
2.4 HEXFET schematics 7
2.5 Reverse engineering shows the internal HEXFET structure (courtesy of F. Darracq) 8
2.6 Top view of a generic STRIPFET technology 8
2.7 Trench power MOSFET featuring the typical gate thrench structure [63] 8
2.8 Drain current characteristics versus drain to source bias voltage . . . 9
2.9 Drain current characteristics versus gate to source voltage 9
2.10 Earth's magnetosphere, from [6] 11
2.11 Impact of cosmic rays on the atmosphere and generation of secondary particles [7] 12
2.12 Microscopic cross section 13
2.13 A generic LET shape with respect to energy E [35] 14
2.14 Path of a magnesium ion, initial energy is 500 MeV (left) and of an electron, initial energy is 100 keV (right), inside a 500 μm silicon target 15
2.15 Schematic diagram of the vertical cross sections of a DMOS (left) and the parasite *npn* transistor (right) [96] 18
2.16 Ionization rates for holes and electrons in silicon [84] 19
2.17 Extent of sensitive volume at different laser energies and at different bias [19] 21
2.18 Liu's circuit level model for SEB [51] 22
2.19 Schematics of non destructive test circuits from Oberg and Wert [69] (left), and from Fischer [25] (right) 22
2.20 Backside laser mapping of IRFU420 [56] 23
2.21 Physics of SEB 24

3.1 Detail and surface dimensions of the studied devices 28

3.2 Different 2D sections of MOSFET cell 30
3.3 Basic 2D MOSFET cell for TCAD simulations 30
3.4 Detail and surface dimensions of the studied devices 31
3.5 Mesh used in TCAD simulations; it is refined inside the epitaxial layer 32
3.6 Drain current I_D comparison between datasheet and TCAD for HEXFET 33
3.7 TCAD simulated diffusion in 2D (left) and 3D (right) for HEXFET 36
3.8 Drain current I_D patterns plotted with time. Curve 3 is the SEB case, with $LET = 13\ MeVcm^2/mg$. Curves 1 and 2 are the noSEB case, respectively with $LET = 2\ MeVcm^2/mg$ and $LET = 10\ MeVcm^2/mg$ 39
3.9 Current density prints inside MOSFET epitaxial layer, at significant times. On the left *(a, c, e)* is represented a transient phenomenon, while on the right *(b, d, f)* is represented a SEB. Current reference scale is provided in *(a)* 40
3.10 Electric field plotted in time at different particle LET. Its value is averaged inside epitaxial layer. Curve 3 is the SEB case, with $LET = 13\ MeVcm^2/mg$. Curves 1 and 2 are the noSEB case, respectively with $LET = 2\ MeVcm^2/mg$ and $LET = 10\ MeVcm^2/mg$ 41
3.11 Electric field inside HEXFET, as given by TCAD simulations, before injection of the ionizing particle (black solid curve), and at the end of SEB evolution (red dotted curve) 43
3.12 Safe Operating Area of simulated components, according to respective datasheets 44
3.13 A, B, C are the heavy ion impact locations studied inside the elementary cell 44
3.14 Critical charge q_{th} as a function of impact location in a HEXFET cell. Epitaxial layer thickness h_{epi} is 30 μm and voltage bias V_{DS} is 40 V (upper curve) and 50 V (lower curve) 45
3.15 Critical charge q_{th} as a function of impact location in a STRIPFET cell. Epitaxial layer thickness h_{epi} is 4 μm 45
3.16 α, β, γ and δ are the heavy ion impact angles studied inside the elementary cell 46
3.17 A and B are the injection conditions studied with short track length. SC is the track length which short circuits the epitaxial layer 47
3.18 A, B, C are the epitaxial layer thicknesses studied inside the HEXFET elementary cell 48
3.19 Critical charge q_{th} as a function of epitaxial layer thickness, at $V_{DS} = 40\ V$ and in three impact locations A (low curve), B (middle curve) and C (high curve) 49
3.20 Drain current I_D time evolutions at different epitaxial layer doping values, $V_{DS} = 30\ V$ and $LET = 13\ MeVcm^2/mg$ 50

3.21 Threshold charge versus average electric field at impact locations A, B, C inside the HEXFET structure. Each curve shows threshold charge for different values of epitaxial layer thickness 52
3.22 Threshold charge as a function of average electric field inside the HEXFET topology. The 3 curves represents the three impact locations A, B, C 53
3.23 Threshold charge as a function of average electric field inside the STRIPFET topology 53

4.1 $k(x)$ values versus heavy ion impact location, from TCAD simulations of a HEXFET structure, and piecewise linear law 58
4.2 Piecewise linear law to express $k(x)$ in the STRIPFET structure . . 59
4.3 INPUTs and OUTPUTs of DELPHY 60
4.4 Transition from TCAD geometry to model geometry for a HEXFET structure 61
4.5 Transition from TCAD geometry to model geometry for a STRIPFET structure 63
4.6 Geometrical illustration of SEB criterion used in this work for HEXFET ans STRIPFET topologies 64
4.7 Elementary cell and hexagon annulus as visual representation of SEB cross section σ_{HI} in HEXFET technology 65
4.8 Transition from TCAD and model geometries to σ_{HI} cross section calculation in HEXFET technology 66
4.9 Elementary cell and rectangle as visual representation of SEB cross section σ_{HI} in STRIPFET technology 67
4.10 Transition from TCAD and model geometries to σ_{HI} cross section calculation in STRIPFET technology 67
4.11 σ_{HI} cross section per cell versus LET 68
4.12 Heavy ion SEB cartographies for the HEXFET component, calculated by DELPHY. Red area is SEB sensitive 68
4.13 Heavy ion irradiation data from [10] 69
4.14 σ_{HI} cross section per cell versus LET: black continuous curve is calculated with prediction model, while red dots are from [10] 70
4.15 Total differential probability per μm to generate a heavy ion by proton impact, versus proton energy. 71
4.16 LET spectra of secondary ions generation differential probability, as a function of proton energy 72
4.17 Calculation of protons SEB cross section by convolution of secondary ions SEB cross section and secondary ions generation probability. Proton energy is 200 MeV 74
4.18 Proton SEB cross section versus proton energy 75

5.1 Proton irradiation data from [10] 78
5.2 Picture of proton induced SEB in a IRF360 ($V_{DS} = 320\ V$ and $V_{GS} = 0\ V$), from [10] 79
5.3 Proton SEB calculation (dotted black line) compared with proton irradiation data from [10] (solid red line) 80
5.4 Heavy ion SEB calculation by DELPHY(dots), compared with heavy ion irradiation data from [10] (solid line) 81
5.5 Overview of the methodology: SEB prediction (bottom row) is achieved from experimental data (top row), through differential probability of secondary ions generation 82

F.1 Détails et dimensions de la surface des dispositifs étudiés 108
F.2 Cellule élémentaire étudiée dans les deux topologies MOSFET 108
F.3 Comparaison du courant de drain pour HEXFET 109
F.4 Charge seuil comme fonction du champ électrique moyen dans la topologie HEXFET. Les trois courbes représentent les trois lieux d'injection A, B, C 111
F.5 Charge seuil comme fonction du champ électrique moyen dans la topologie STRIPFET. Les trois courbes représentent les trois lieux d'injection A, B, C 111
F.6 Entrées et sorties de DELPHY 113
F.7 Transition de la géométrie TCAD à la géométrie du modèle pour une structure HEXFET 113
F.8 Transition de la géométrie TCAD à la géométrie du modèle pour une structure STRIPFET 114
F.9 Illustration géométrique du critère SEB utilisé dans ces travaux pour les topologies HEXFET et STRIPFET 115
F.10 Cellule élémentaire et couronne hexagonale comme représentation visuelle de la section efficace σ_{HI} dans la technologie HEXFET 116
F.11 Transition des géométries TCAD et modèle au calcul de la section efficace σ_{HI} dans la technologie HEXFET 116
F.12 Cellule élémentaire et rectangle comme représentation visuelle de la section efficace σ_{HI} dans la technologie STRIPFET 117
F.13 Transition des géométries TCAD et modèle au calcul de la section efficace σ_{HI} dans la technologie STRIPFET 117
F.14 Section efficace σ_{HI} par cellule, en fonction du LET 118
F.15 Cartographies SEB ion lourd pour le composant HEXFET, calculées par DELPHY. La partie rouge est sensible au SEB 118
F.16 Section efficace σ_{HI} par cellule, en fonction du LET : la courbe continue noire est calculée avec le modèle de prédiction ; les points rouges viennent de [10] 119

F.17 Spectre *LET* de la probabilité de génération des ions secondaires, en fonction de l'énergie du proton 120
F.18 Calcul des sections efficaces SEB proton, pour une énergie proton de 200 MeV 121
F.19 Section efficace SEB proton en fonction de l'énergie proton 121
F.20 Section efficace proton calculée (en noir pointillé) comparée avec les données d'irradiation proton (en rouge continu) [10] 123
F.21 Section efficace ion lourd calcaluée (points) comparée avec les données d'irradiation ion lourd (en rouge continu) [10] 124
F.22 Vue générale de la méthodologie 125

List of Tables

2.1 Parameters which have an influence on SEB 18

3.1 MOSFETs regions thicknesses 29
3.2 Drain current I_D values, from HEXFET datasheet and TCAD simulations 34
3.3 Drain current I_D values, from STRIPFET datasheet and TCAD simulations 34
3.4 Selection of TCAD simulated parameters among all the variables which have an influence on SEB 37
3.5 Impact location effect on SEB threshold charge $q_{th}(pC)$ in HEXFET and STRIPFET technologies. Voltage bias V_{DS} is 40 V 43
3.6 Tilt effect on SEB threshold charge $q_{th}(pC)$ in HEXFET and STRIPFET technologies. Voltage bias V_{DS} is 30 V and threshold charge is calculated according to (3.4) 47
3.7 Effect of track length on threshold charge 48
3.8 Epitaxial layer doping values studied via TCAD, at $V_{DS} = 30\ V$ and $LET = 13\ MeV cm^2/mg$ 49
3.9 HEXFET, values of k and z coefficients at different injection locations 54
3.10 STRIPFET, values of k and z coefficients at different injection locations 54

4.1 Linear and piecewise linear laws to describe $k(x)$ in the STRIPFET structure 69
4.2 Proton SEB cross section by CERN and by DELPHY 76

F.1 Sélection des paramétrés simulés avec TCAD 110
F.2 Sections efficaces SEB proton : données CERN et calcul DELPHY . 122

Chapter 1

Introduction

> Habille-moi lentement, je suis pressé.
>
> Napoléon

Power MOSFETs (Metal Oxide Semiconductor Field Effect Transistor) are widely used electronic devices capable of delivering high power levels. They are also subject to severe failures caused by the impact of a radiative particle on them. The harsh radiative environment is in fact one of the fundamental aspects that has to be taken into account in design.

Among the possible radiation effects, this work addresses Single Event Burnout (SEB), which is caused by one single particle depositing charge inside the device and thus switching ON the parasitic Bipolar Junction Transistor (BJT) structure. This leads to an electron current which activates the epitaxial/substrate junction and thus generates a hole current if a high electric field is present. The phenomenon is self-sustained and leads to thermal destruction of the device. That may have catastrophic effects at circuit, system or even mission level.

Because of its destructive and permanent nature, SEB is to be studied in order to design electronic systems that are both efficient and reliable. Traditional reliability approaches are not applicable to SEB: for example derating, i.e. using the component at a power level lower than its nominal capabilities, would be in contrast with power MOSFET purpose; as well as redundancy, that would not be advantageous because of the large number of devices used. For this reason, prediction appears to be an extremely useful approach to deal with SEB.

In order to build a valuable prediction tool, one has to move from a deep physical knowledge of SEB, that has been widely studied in the last 30 years. In fact, already in 1985, the existence of SEB has been postulated for the very first time. Its physical consequences at a device level were already known, and studies were conducted to investigate its electrical characteristics at a semiconductor level. In the following

years it has been shown that SEB sensitivity increases with voltage bias and particle energy, while it decreases with temperature and epitaxial layer thickness. Based on these considerations, some hardening solutions have been proposed over the years, but none of them showed to totally avoid the occurrence of SEB.

Several test protocols have also been defined, especially non destructive ones, in order to save facilities time and cost. They are either based on restraining the injected charge inside the component, or on facilitating current evacuation.

Thanks to non destructive tests, to 2D computer aided simulations and to laser mapping, component sensitivity characterization appears as an easy way to evaluate and try to predict the occurrence of SEB in specific devices. However, there are other factors that must be taken into account, such as part-to-part variability, cost and time consumption of characterization itself. Most of all, none of the cited methods guarantees a complete and reliable appreciation of SEB sensitivity for a given component. Different MOSFET configurations have also been characterised in terms of SEB sensitivity, such as STRIPFET, Silicon Carbide (SiC) and Super-Junction (S-J).

Hence, physical knowledge of SEB mechanisms has been deeply enhanced, thus permitting to understand its dynamics development. What is still missing is a SEB rate prediction tool, that would allow to assess SEB risk for a given mission, device and working condition.

The lack of a SEB rate prediction tool justifies the work here presented. It consists in developing an operational prediction model of SEB rate in power MOSFET.

In this thesis, in order to build a SEB rate prediction model, first SEB inside power MOSFET has been simulated, in order to study the effects of each parameter on SEB phenomenon. To do that, a 2D power MOSFET structure has been built in two different technology configurations: HEXFET and STRIPFET. Once the structure validated by comparison to datasheet, a heavy ion striking the device has been simulated, in order to trigger an SEB. This basic simulation has been repeated several times, while changing, one at a time, device geometry and doping, injection parameters and polarisation, in order to study the effects of each of them on SEB triggering. All these effects have been modelled as functions of electric field inside epitaxial layer, and the SEB triggering criterion has been identified as the deposited charge inside it. Thus, all simulation results have been summarized with an empirical triggering law, which states that threshold charge depends on the average electric field inside the epitaxial layer, through a coefficient that describes the injection location effect. (Chapter 3)

The empirical law has been exploited through basic mathematical fitting, and the triggering criterion has been determined as a comparison between deposited charge and threshold charge, thus setting the base of DELPHY prediction model (Destructive effects prEdiction modeL based on PHysical analYsis). These part of the work

has been presented to IEEE Conference on Radiation Effects on Components and Systems (RADECS) and permitted to set the bases of proton SEB estimation in the occasion of a joint study ONERA-CERN, in order to characterize power MOSFETs for the future generation of power converters inside the Large Hadron Collider.

To calculate proton SEB cross sections, a wide GEANT4 database of secondary reactions has been filtered at ONERA in order to extract the pertinent secondary reactions for the present study, and a differential generation probability has been calculated. It has then been convoluted with heavy ion cross sections to determine a proton SEB cross section, which has shown agreement in the order of magnitude with the experimental cross section. In fact, the calculated cross sections better agreed with experimental results in the case of STRIPFET technology which is indeed more integrated than the HEXFET. (Chapter 4)

The concept used to predict proton induced SEB has been extended to the calculation of heavy ion SEB sensitivity from proton SEB test data, and its reciprocal: in both cases, the predicted heavy ion cross section agrees in the order of magnitude to the experimental one, thus establishing the validity of the procedure. (Chapter 5).

Chapter

2 Review of Single Event Burnout in power MOSFETs

> In science, moreover, the work of the individual is so bound up with that of his scientific predecessors and contemporaries that it appears almost as an impersonal product of his generation.
>
> A. Einstein

The natural radiation environment has proven to be very harsh on power electronics. This chapter presents the effects of the radiation environment on power electronics devices, and in particularly focuses on Single Event Burnout in power MOSFETs.

2.1 Power MOSFET

A power MOSFET is a transistor capable of delivering considerable levels of voltage and current. It shares the same structure of a MOSFET: they both have three terminals (gate, source and drain), but power MOSFET features a vertical current flow, thus utilizing the silicon more effectively and so permitting to handle higher levels of power. The two different configurations are shown in fig. 2.1.

2.1.1 Power MOSFET configurations

The first power MOSFET was introduced in the market in the late 1970s, and was called VMOS because of its V-groove design. Its structure is visible on the left of fig. 2.2. The device is normally off; when a positive gate voltage V_{GS} is applied, electrons form a very thin n^+ layer under the gate. This n^+ layer is called "channel" inside the p region, and "accumulation layer" into the n region. When a positive drain to source bias V_{DS} is applied, electrons flow through the channel, from the

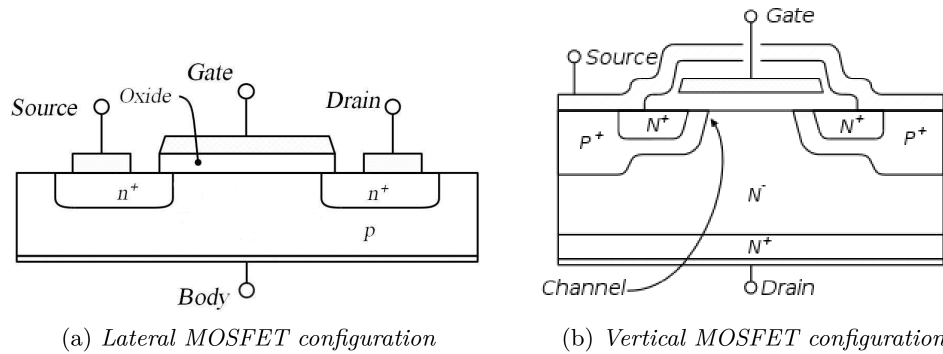

(a) *Lateral MOSFET configuration* (b) *Vertical MOSFET configuration*

Figure 2.1 – Schematics of lateral and vertical MOSFET configurations

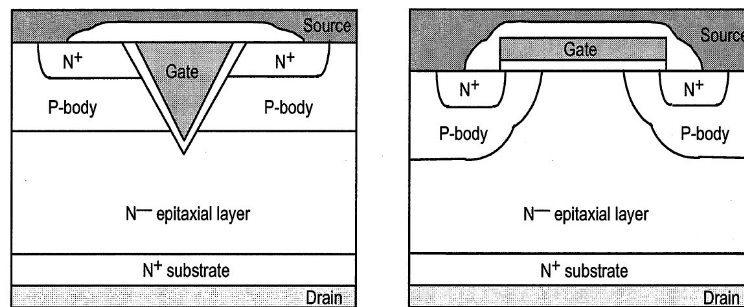

Figure 2.2 – VMOS (left) and DMOS (right) configurations

source to the accumulation layer. From there, they flow to the drain through the epitaxial layer.

Since VMOS structure has limited voltage capabilities, over the years it has been improved into a planar DMOS configuration (double diffused MOS), visible on the right of fig. 2.2. Its main advantage is a simpler building process, that allows an easier lead bonding for the source electrode, thus permitting a more efficient pack design for high power components [31]. DMOS principle is the same as in VMOS: the application of a potential V_{GS} to the gate electrode alters the conductivity of the adjacent channel region, thus allowing the current I_D to flow from source to drain, that are the device terminals to be controlled [71]. What is different, is that in DMOS the diffusion lines have no preferential directions as they do in VMOS. A typical example of DMOS design is the HEXFET structure developed by International Rectifier (IR) in the late 1970s. It is currently one of the most used MOSFET configurations, along with the "trench" structure. These two MOSFET configurations, shown in fig. 2.3, have been studied in this work with respect to their SEB sensitivity, and for this reason their geometry and technology are now presented.

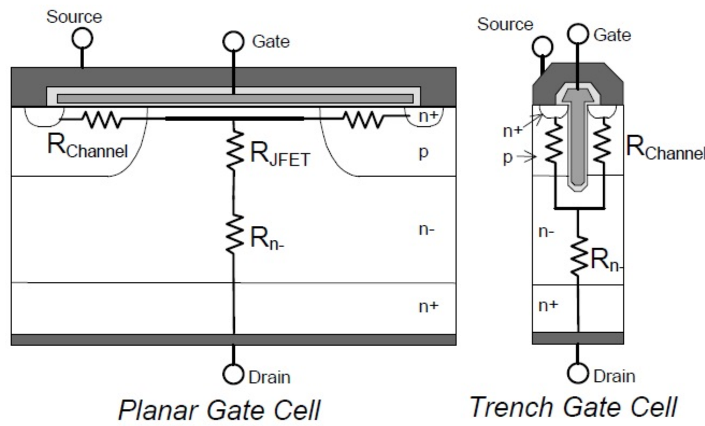

Figure 2.3 – Schematics of planar and trench MOSFET technologies [63]

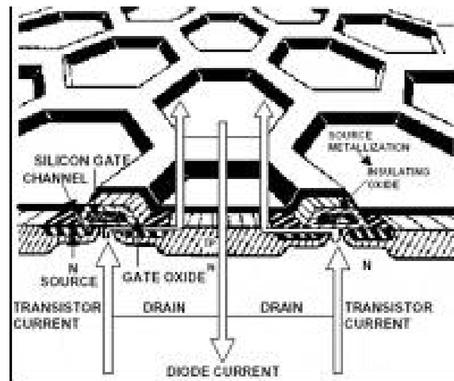

Figure 2.4 – HEXFET schematics

In general, power MOSFET has a multicellular organization: typically thousands of cells are connected in parallel to obtain large channel width while retaining the same channel length of the individual cell, in order to achieve large current and small resistance in ON state. In particular, in HEXFET configuration, diffusion lines trace out of a hexagonal grid pattern (fig. 2.4), visible on top of the die. Fig. 2.5 shows a typical HEXFET structure with its internal doping regions and dimensions.

For what concerns trench structures, they feature a vertical channel, which requires less area compared to the horizontal channel of planar structures. As a consequence, trench devices have greater cell density and lower ON resistance [63].

In this work, in addition to HEXFET, the second studied technology is a trench STRIPFET. Its top view is shown in fig. 2.6, where the striped technology is visible; fig. 2.7 shows a basic 3D trench structure, where the gate Polysilicon is evident with its elongated shape. Trench technology is especially used in power MOSFET for

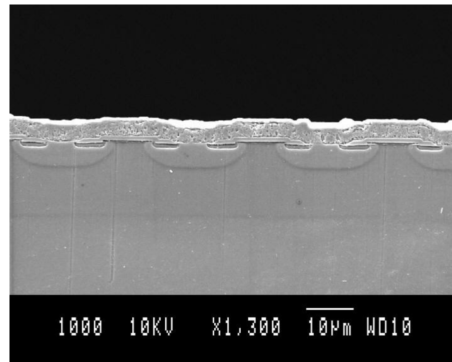

Figure 2.5 – Reverse engineering shows the internal HEXFET structure (courtesy of F. Darracq)

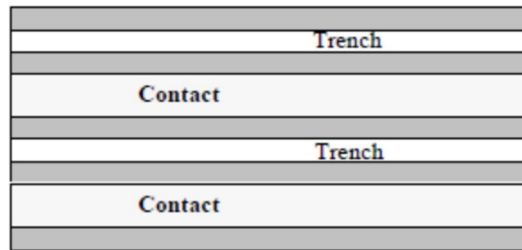

Figure 2.6 – Top view of a generic STRIPFET technology

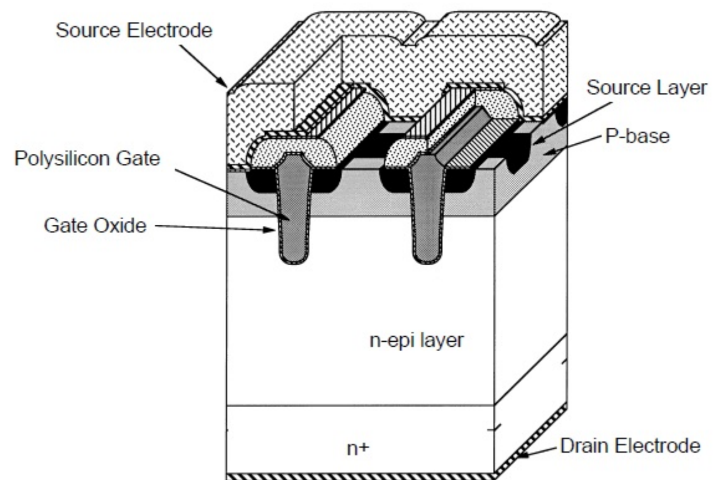

Figure 2.7 – Trench power MOSFET featuring the typical gate thrench structure [63]

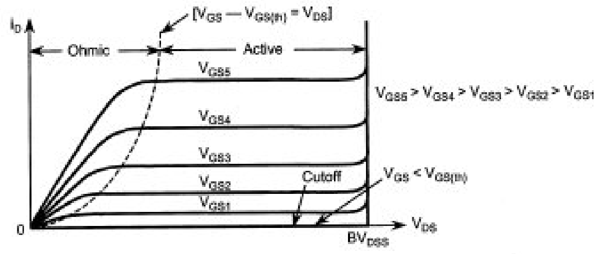

Figure 2.8 – Drain current characteristics versus drain to source bias voltage

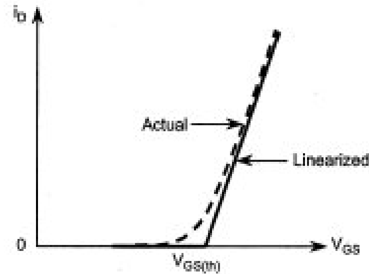

Figure 2.9 – Drain current characteristics versus gate to source voltage

low-voltage application devices.

As a general comparison between planar and trench components, one can remark that the minimal cell of trench technology is smaller than the one of planar devices (see fig. 2.3). This is going to be a key concept for the rest of the present study.

2.1.2 Power MOSFET characteristics

Because of MOSFET intrinsic technology structures previously discussed, power gain is very high and switching speeds are fast, so MOSFET is widely used in automotive and avionics power systems, among others. The typical parameters to choose a power MOSFET device in the design phase are the drain to source voltage V_{DS} and drain current I_D, represented in the transfer characteristics, as shown in fig. 2.8.

A minimum gate voltage V_{GSth} is required to establish the channel inside the device, and thus turn it to ON state (see fig. 2.9), according to the law

$$I_D = K(V_{GS} - VGSth)^2 \ , \tag{2.1}$$

where:

$$K = \mu_n C_{OX} \frac{W}{2L} \ . \tag{2.2}$$

μ_n is carrier mobility, C_{OX} is gate oxide capacitance per unit area, and W and L are respectively channel width and length. Common values for V_{GSth} are $2-4V$ for high voltage devices with thicker gate oxides, and $1-2V$ for lower voltage, logic-compatible devices with thinner gate oxides. Therefore, V_{GSth} value depends on gate oxide thickness and doping profile of the body region [84].

2.2 Natural radiation environment

When a power MOSFET works in the natural radiation environment, it undergoes its effects. In order to understand them, it is essential to know the environment itself. A first distinction can be made between space and atmospheric ones.

2.2.1 Space radiation environment

Space environment is characterized by several radiative phenomena which generate a wide range of particles [6]:

Sun activities Solar flares and coronal mass ejections (CMEs). Solar flares are seen as sudden brightenings in the photosphere near sunspots. Flares are intense releases of energy involving tearing and reconnection of strong magnetic field lines. In fact, they are the solar systems largest explosive events. Large increases in the solar wind density in interplanetary space are measured after solar flare occurrence because the energy released from the flare accelerates particles in the solar plasma to high energies. CMEs occur in the layer of the sun outside of the photosphere, the chromosphere. They release approximately 1017 *grams* of plasma into interplanetary space.

Solar wind The sun's outer atmosphere, the corona, extends several solar diameters into interplanetary space. The corona continuously emits a stream of protons (95%), electrons ($< 1\%$), doubly charged helium ions ($\sim 4\%$), and small amounts of other heavy ions ($< 1\%$), collectively called the solar wind.

Cosmic radiation The flux levels of the Galactic Cosmic Rays (GCRs) are hazardous to spacecraft electronics because their high energies make them extremely penetrating. The GCRs originate outside of the solar system. They are essentially isotropic outside of regions of space that are dominated by particles and fields of the sun. Galactic radiation consists of ions of all elements of the periodic table and are composed of about 83% protons, 13% alphas (^4He ions), 3% electrons, and about 1% heavier nuclei. The Earth's magnetic field provides some protection from the galactic particles by deflecting the particles as they impinge upon the magnetosphere.

Earth's magnetosphere The interaction of the solar wind and its associated magnetic field with the Earth's magnetic field defines the Earth's magnetosphere

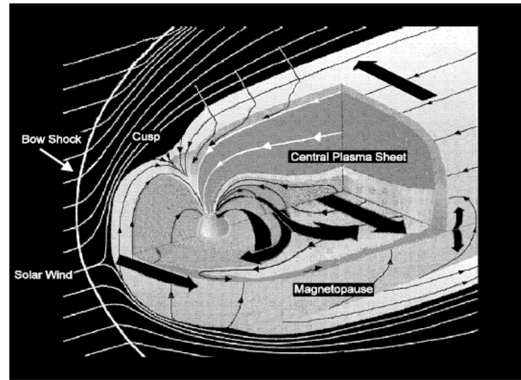

Figure 2.10 – Earth's magnetosphere, from [6]

(fig. 2.10). The lower boundary of the magnetosphere is the ionosphere and the upper boundary is the magnetopause. As the charged particles in the solar wind move around the Earth, some of the particles cross the Earth's magnetic field lines and leak into the magnetosphere. Others are trapped by the Earth's magnetic field and contribute to the formation of the Van Allen belts. Others collect in the magnetotail and create poles of opposite charge, producing a generator which transports particles along magnetic field lines at the poles. The particles trapped in the near-Earth environment are composed of energetic protons, electrons, and heavy ions. The trapped particles pose a significant radiation threat to electronic systems and humans. There is large variation in the level of hazard depending on the orbit of the spacecraft.

2.2.2 Atmospheric radiation environment

The atmosphere shields the Earth from a big part of space radiation [7]. As cosmic ray and solar particles enter the top of the Earth's atmosphere, they are in fact attenuated by interaction with nitrogen and oxygen atoms. The result is a shower of secondary particles and interactions created through the attenuation process (fig. 2.11). Products of the cosmic ray showers are protons, electrons, neutrons, heavy ions, muons, and pions. In terms of radiation in the atmosphere, the most important product of the cosmic ray showers is the neutrons. They are measurable at 330 km altitude, and their density increases with decreasing altitude until they reach a peak at about 20 km. At altitudes less than 20 km, the levels decrease: at the ground, the neutron density is 1/500 of the peak flux. Our knowledge of neutron levels comes from balloons, aircrafts, and ground based measurements. The energies of neutrons in the atmosphere reach energy levels of hundreds of MeV.

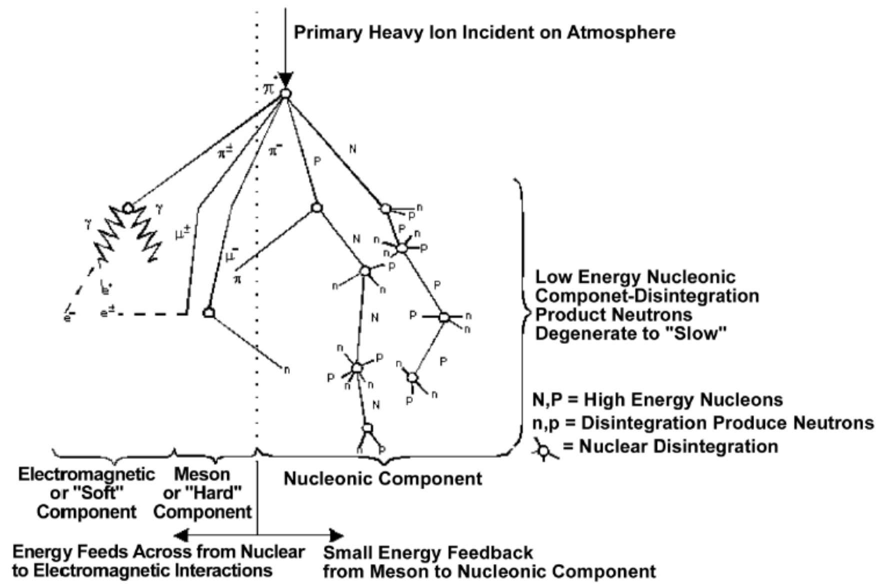

Figure 2.11 – Impact of cosmic rays on the atmosphere and generation of secondary particles [7]

2.3 Introduction of useful definitions

In order to understand and classify the effects of radiative environment on power electronics, it is necessary to first introduce some useful concepts and definitions. The principle of any radiative effect, is the fact that a particle before impact owns a certain amount of energy and in some cases an electrical charge. These two quantities define the nature of the particle itself and determine the kind of interactions it is going to have with the target material.

2.3.1 Cross section

Cross section can be defined at microscopic and macroscopic levels. In both cases it is the ratio of the number of radiative effects over the total radiative particle flux Φ. At a microscopic level (see fig. 2.12), the radiative effects are expressed as the number of scattering centres N, thus defining cross section as

$$\sigma_m = \frac{N}{\Phi} \ . \tag{2.3}$$

Microscopic cross section σ_m, also called nuclear cross section σ_N is measured in $barn = 10^{-24}\ cm^2$, because it is defined as $\sigma_N = \pi\rho^2$, where $\varrho = 10^{-12}\ m^2$ is the typical nuclei radius of the target material.

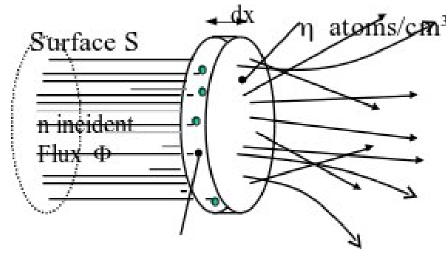

Figure 2.12 – Microscopic cross section

The multiplication of (2.3) by the number of atoms per unit volume η, gives the macroscopic cross section σ_M, which refers to the sample size and is usually expressed in cm^2.

2.3.2 Linear Energy Transfer

The first parameter to describe the interaction between particle and target is the rate of energy E exchange between them and along a certain linear track x

$$LET = \frac{1}{\rho}\frac{dE}{dx} \ . \tag{2.4}$$

It is called Linear Energy Transfer (LET) and it depends on both the nature of the particle and the density of the target ρ. It is in fact expressed in $pC/\mu m$ or in $MeVcm^2/mg$. Depending on the material, a conversion factor is calculated between the two units: for example, in silicon targets it is known that

$$1 \ pC/\mu m \approx 100 \ MeVcm^2/mg \ , \tag{2.5}$$

because to create an electron-hole pair inside silicon are necessary 3.6 eV.

A sure and complete reference to know LET values of all ions inside every target material is Ziegler table [97], which gives LET values for impact energies in the range $0,2 \div 1000 \ MeV/nucleon$.

A typical LET shape is shown in fig. 2.13, where it is visible that the energy loss has a maximum called *Bragg peak*; it also shows a tail called *Bremssthralung*, which depends on the interaction of electromagnetic radiation with matter and consists in fact of a gamma ray emission by interaction with electric field of the atom of the target. The concept of LET is strictly connected to the idea of stopping power $S(E)$, defined as

$$S(E) = \frac{dE}{dx} \ , \tag{2.6}$$

which accounts for the energy loss along the track and is measured in MeV/cm. A

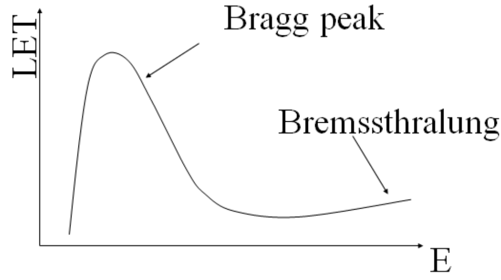

Figure 2.13 – A generic LET shape with respect to energy E [35]

more detailed expression of stopping power

$$\left.\frac{dE}{dx}\right|_{TOT} = \left.\frac{dE}{dx}\right|_{N} + \left.\frac{dE}{dx}\right|_{I} + \left.\frac{dE}{dx}\right|_{B} \tag{2.7}$$

introduces the different aspects of the interaction between particle and target material, detailed in § 2.4.

2.3.3 Range

According to particle initial energy and LET, the extension of its path, or range ζ, inside the target material varies. While it is not possible to calculate the range value, it is possible to estimate its mean value from the particle initial energy E and its energy loss per unit length

$$\zeta(E) = \int_E^0 \frac{dE}{\left.\frac{dE}{dx}\right|_{TOT}} \ . \tag{2.8}$$

According to particle nature there can be fluctuations around this mean value. Fig. 2.14 shows the small fluctuations of a 500 MeV magnesium ion (left), and the huge fluctuations of a 100 keV electron (right) inside a 500 μm silicon target. Heavier particles, such as ions, have in fact smaller fluctuations. The lighter the impact particle with respect to target nuclei, the bigger the deviations caused at each collision. In fact, other than depending on the particle, the range depends also on the density of the target: a denser target only allows for shorter ranges.

2.4 Interaction between particle and material

With respect to (2.7), different interactions occur when an energized particle impacts on a target material:

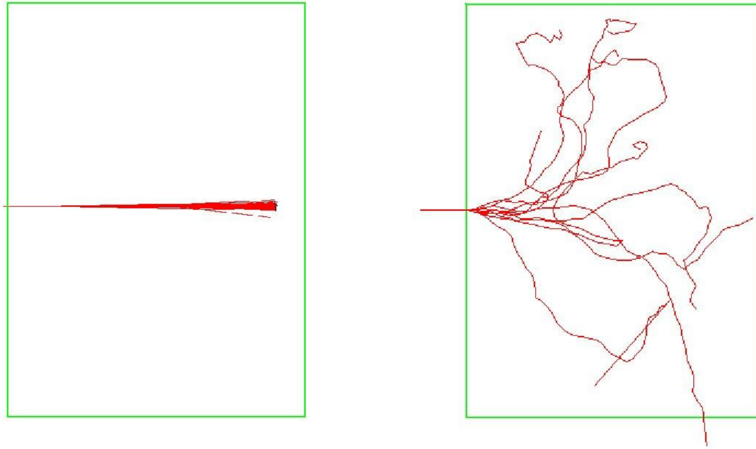

Figure 2.14 – Path of a magnesium ion, initial energy is 500 MeV (left) and of an electron, initial energy is 100 keV (right), inside a 500 μm silicon target

Nuclear interaction $\left.\frac{dE}{dx}\right|_N$ It happens for incident neutrons or protons; it might happen also for heavy ions, even though it is considered negligible unless at the end of the ion path [23]. The probability for an incident particle to encounter a nucleon is not null, so when they collide, there can be an elastic reaction (displacement) where there is conservation of kinetic energy and nature of particles; or an inelastic or non-elastic reaction

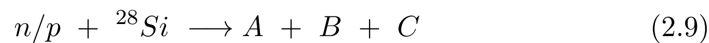

$$n/p \; + \; ^{28}Si \; \longrightarrow A \; + \; B \; + \; C \tag{2.9}$$

where there is no conservation of kinetic energy, because part of the energy is spent to modify the nucleon of the target material and thus create reaction products $A \, + \, B \, + \, C$. The nature of reaction products depends on the target material and it is relevant when studying neutron and proton secondary effects. For example, in this work proton-induced SEB is investigated, so knowing the nature of secondary generated ions is essential as a first step to determine component sensitivity to SEB. In detail, when a proton or a neutron impact on silicon, they can generate different possible ions, which go from hydrogen H to phosphorus P. Knowing the nature of the ions and of the target material, one can read ions' range and LET in Ziegler's tables [97], and thus know the characteristics of possible reactions. Still, this is not enough to predict the interaction, and a probabilistic approach is needed as a complement to the physics.

Ionizing interaction $\left.\frac{dE}{dx}\right|_I$ It happens when the incident particles are electrically

charged, like protons, electrons and heavy ions. In the lattice of target material, electron cloud acts like a viscous medium which slows down the impacting particle, whose energy is partially used to ionize lattice atoms, as described by LET. When the energy of the incident particle is in fact greater than the energy necessary to create an electron-hole pair (ehp) inside the target material, then there is ionization. Until the impacting particle has not exhausted its energy, it will continue its path inside the target material, thus creating a ionizing track. Since a heavy ion looses a very small energy in ionizing target atoms, the quantity of generated ehp is elevate and its track inside the target is quite long. As an example, alpha particles ^{4}He only loose 0.05% of their energy for every ehp created; this percentage is even smaller for heavier ions like ^{12}C (0.02%) or ^{52}Fe (0.005%). This means that heavy ions produce a long ionizing track inside the target, thus generating a great number of charges.

Bremssthralung $\left.\frac{dE}{dx}\right|_B$ This is also classified as a ionizing interaction, but it is generally negligible except in the case of energetic electrons impacting on a heavy material.

The interactions between incident particles and target material can be also classified according to their effects: there can be cumulated dose effects, or Single Event Effects (SEE).

2.4.1 Total Ionizing Dose

Dose is defined as the average energy deposited per unit mass

$$dose = \Phi \frac{1}{\rho} \frac{dE}{dx} \tag{2.10}$$

where Φ is the flux of incident particles.

Dose is measured in $rad = 10^{-2}\ J/kg$ or in Gray $1\ Gy = 1\ J/kg$, and is particularly important to evaluate for incident photons, protons and electrons. It consists of over time accumulation of charges in insulating materials, such as oxides, and the consequences can be as severe as the lost of a component because of permanent alteration of its electric characteristics.

2.4.2 Single Event Effects

Single Event Effects (SEE) are produced by a single particle interaction with the target semiconductor; they can be generated by direct ionization, in the case of heavy ions (and protons in a very limited measure), or secondary generation by proton or neutron impact, and thus secondary ionization.

All SEE trigger a perturbation on the device, and accordingly to the nature of their consequences at a component level, they can be divided in:

- Non destructive SEE. They generally consist of a transitory phenomenon and can thus be corrected. They are:

  Single Event Transient (SET) When charges are deposited inside the cell of an analogic component or a digital circuit, they cause the appearance of a temporary parasitic current, which can in turn alter the component response.

  Single Event Upset (SEU) It is typical in logic components, such as memories SRAM and SDRAM, and consists of one bit logic state upset inside a cell. The effect is totally correctable through rewriting of the concerned bit. SEU is becoming more and more relevant in the characterization of components based on logic MOS technology, because of their strong integration: with a single particle impact, several neighbours bits can be upset (Multiple Bit Upset: MBU) or even cells (Multiple Cell Upset: MCU).

- Destructive SEE. They consist of a permanent change of current or voltage level and can not be corrected, if not properly and very quickly handled. Their consequences might become critic at component, circuit or even system level. They are:

  Single Even Latch-up (SEL) It is a common phenomenon inside multicellular power components, especially with MOS and IGBT technologies. It consists of single particle that sets ON the parasite thyristor inside the device; since the thyristor has a low on-resistance, the generated currents can be quite high. This leads to high temperature and thus fusion of silicon or metallic parts at local level inside a single cell of the device, while total device current is still acceptable.

  Single Event Gate Rupture (SEGR) It appears in insulated gate devices. When there is a strong drain-source bias and a single heavy ion passes through silicon, the deposited charges tend to cumulate under gate oxide, thus inducing an image charge inside the gate electrode. The oxide can be destroyed if there is a sudden augmentation of electric field inside it [39]. SEGR can be recognized by the sudden augmentation of parasite gate current, and leads to the lost of the component.

  Single Event Burnout (SEB) It appears in power devices in their OFF state and biased with a drain to source voltage. A single ionizing particle is enough to trigger the parasite BJT transistor and if the electric field levels are high enough, there is the appearance of an avalanche phenomenon which becomes self sustained and leads to high current levels

Table 2.1 – Parameters which have an influence on SEB

Geometry	Electric	Particle	Environment
Injection location	Bias V_{DS}	LET	Space/atmospheric models
Injection angle	Doping profiles	Range	Temperature
Device technology			

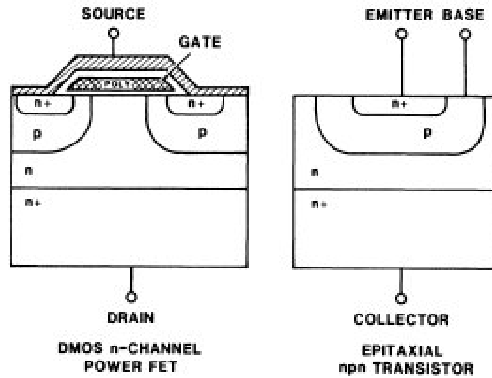

Figure 2.15 – Schematic diagram of the vertical cross sections of a DMOS (left) and the parasite *npn* transistor (right) [96]

inside the device, until silicon is melt. SEB is the phenomenon studied in this research, so it will be further detailed in the next section.

2.5 Single Event Burnout

SEB is triggered when a heavy ion impacts on a power MOSFET in the OFF state, that is when it is blocking a large voltage bias V_{DS}. In particular, after a heavy ion is injected in the structure, its possibility to trigger an SEB depends on the parameters listed in table 2.1.

2.5.1 Literature survey of SEB in power MOSFETs

SEB has been postulated for the first time in 1985 by T. Wrobel *et al.* [96]. They observed that devices could exhibit an avalanche breakdown at bias levels very much less than normal breakdown voltages. Because the avalanche mode followed a high current response, they postulated that the avalanche is a direct result of this high current, hence the name Current Induced Avalanche (CIA), i.e. second breakdown of the parasite *npn* structure (see fig. 2.15) caused by a ionizing particle. They

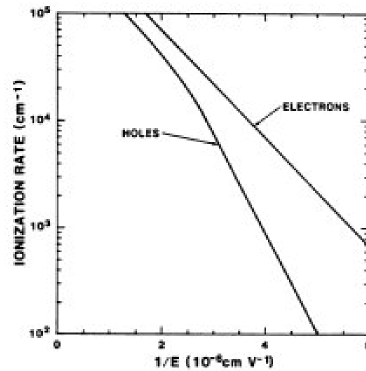

Figure 2.16 – Ionization rates for holes and electrons in silicon [84]

also explain why p-channel devices have not been observed to exhibit current induced avalanche. The reason for the CIA not being present in p-channel devices is attributed to the difference in ionization rates for holes and electrons, shown in fig. 2.16. As can be seen, the ionization rate (the number of impact ionizations produced per unit path length) for electrons is approximately three times that for holes at the same electric field intensity. Although this difference does not preclude CIA in p-type epitaxial layers, it does show that it is more difficult to induce.

It is Waskiewicz *et al.* in 1986, who first use the term Burnout to describe SEB, along with publishing the first experimental results of irradiation with Californium-252. They suggest also a physical explanation of SEB as a combination of the effects of BJT parasite transistor activation and avalanche, leading to thermal destruction of the device [93]. They identify three conditions to have SEB, corresponding to three phases of its dynamics:

1. the voltage generated by the collected charge from the particle track must be sufficient to turn ON the parasitic BJT;
2. the applied bias voltage must be greater than the breakdown voltage of the transistor;
3. the increase in charge crossing the junction must be sufficient to cause avalanche and burnout.

Among the firsts to study SEB physics, in 1987 Hohl and Galloway proposed a SEB analytical model, by which they showed the importance of electric field inside the epitaxial layer to determine SEB sensitivity [29], while in 1989 Hohl and Johnson analysed electric field intensity during SEB. They analytically show that its peak is located at the p/n junction at the beginning and because of current augmentation moves to the homo-junction between epitaxial layer and substrate further

on during SEB, thus causing the hole generation taking part to the self-sustained avalanche [30]. The role of the epi-substrate junction has been enlightened also by Lorfèvre *et al.* in 1998 for Vertical Intelligent Power (VIP) devices [54].

A temperature analysis has been made by Johnson *et al.* in 1992, showing that SEB susceptibility decreases with increasing temperature [36]. In 1993, Johnson *et al.* studied the turn ON of the parasitic BJT and defined a SEB criterion based on current: if the ion strike results in a current greater than critical current, then the transient currents inside the parasitic BJT will regeneratively increase until second breakdown sets [37]. The critical current is defined as the integration of parasitic collector electron current over MOSFET cell. Their model is coherent with CIA model.

In 1988, Keshavarz *et al.* have performed the first 2D computer simulation to study SEB sensitivity, and have confirmed breakdown immunity of p-channel devices [41]. In 1994, Roubaud *et al.* were the firsts to evaluate the effectiveness of 2D MEDICI simulations to describe SEB with respect to 3D ones: their conclusion has been a complete confirmation of 2D simulations as a reliable and less costly simulation approach. Also, they have simulated the effects of bias V_{DS}, impact position and angle, particle energy and external current limitations [75, 74]. According to their simulations, SEB occurrence increases proportionally to an increase of voltage bias or an increase of particle energy. They have also established deposited charge as a valid criterion to describe ion injection, considering that the ion's passage creates a charge column along its trajectory and that the carrier generation depends on particle LET, and on track radial and time distributions. All these concepts are going to be used in the 2D simulations presented in this work. On the other hand, Kuboyama *et al.* have used the same triggering criterion based on charge, and have defined a threshold charge to trigger an SEB, measured via pulse height measurement system. They have found that the critical charge depends only on physical and technological device design, and does not vary at different LET values and bias [48, 45, 44].

In 1994, Dachs *et al.* used again 2D MEDICI simulation tool to confirm the importance of the injection location on SEB sensitivity and identified the most sensitive region as the so called "neck", i.e. the inter-cellular region located under gate oxide and between cells channels [17]. The higher SEB sensitivity of the "neck" has been confirmed in 2009 by Darracq *et al.*, who also investigated the depth of SEB sensitive volume using 2D TCAD simulations and TPA laser testing [20], showing a strong dependency on MOSFET geometry, and further discussing the efficiency of TPA laser testing in 2011 [19, 18].

Several studies have enlightened the importance of epitaxial layer. For example, Stassinopoulos in 1992 identified the epitaxial layer as the sensitive volume for SEB, and postulated that charge distribution along the track as well as collected charge

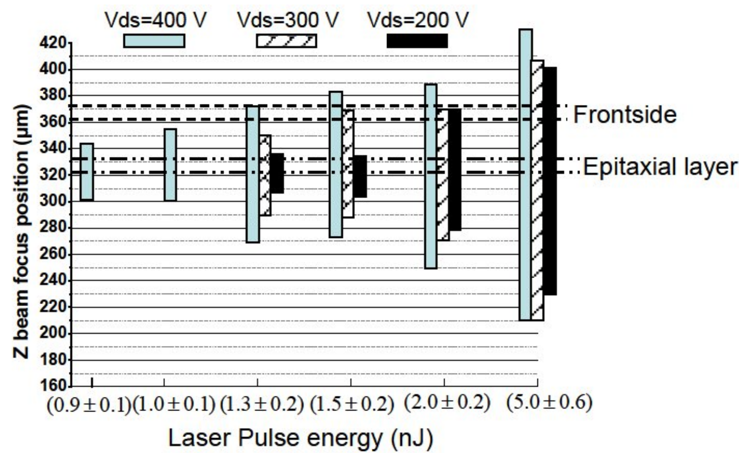

Figure 2.17 – Extent of sensitive volume at different laser energies and at different bias [19]

in epitaxial layer are the critical parameters to trigger an SEB [82]. Furthermore, in 2003 Velardi *et al.* studied the variations of electric field shapes inside epitaxial layer, depending on its thickness and doping [91]. Also, in 2010 Luu *et al.* used SILVACO 2D simulation to determine that the sensitive volume for SEB is the epitaxial layer and that the triggering criteria should be based on LET and range [55]. In 2011, Darracq *et al.* have showed the extent of the sensitive volume with TPA laser testing, illustrated in fig. 2.17. They thus confirmed the epitaxial layer as the key location for SEB dynamics. For what concerns physical models used in simulations, in 2001 Walker *et al.* demonstrated that it is not suitable to neglect temperature models among electrical models [92].

A few studies have been conducted to investigate SEB sensitivity for MOSFET in dynamic mode. A comparative study in 1991 by Calvel *et al.* [13] and in 1992 by Stassinopoulos *et al.* [82], showed that in dynamic mode the devices were less sensitive to SEB. On the other hand, in 1994 Stassinopoulos *et al.* and Tastet *et al.* concluded independently that SEB sensitivity is the same in case of static and dynamic operating modes [81, 87]. They used critical charge as a criterion to evaluate SEB sensitivity.

In 1999, J. Liu *et al.* proposed a circuit model for SEB [51], illustrated in fig. 2.18. In 2006, S. Liu *et al.* confirmed the necessity to have the combination of ion strike and high electric field to turn on parasitic BJT and thus trigger SEB, showing through quasi-stationary avalanche simulations that device's avalanche characteristics determine SEB sensitivity [52]. In 2011, S. Liu *et al.* used heavy ion tests to show that the average SEB failure voltage is strongly dependent on ion atomic number [53]. SEB has also been studied from a thermomechanical perspective by

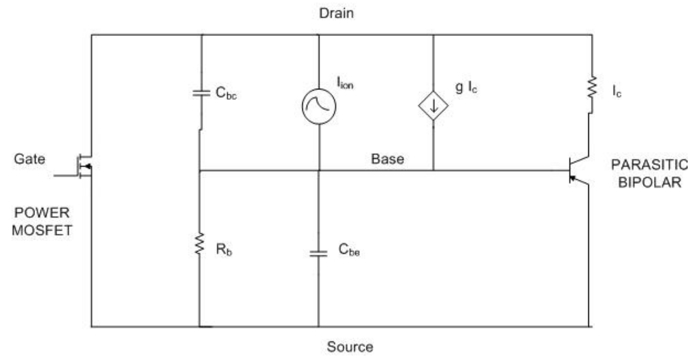

Figure 2.18 – Liu's circuit level model for SEB [51]

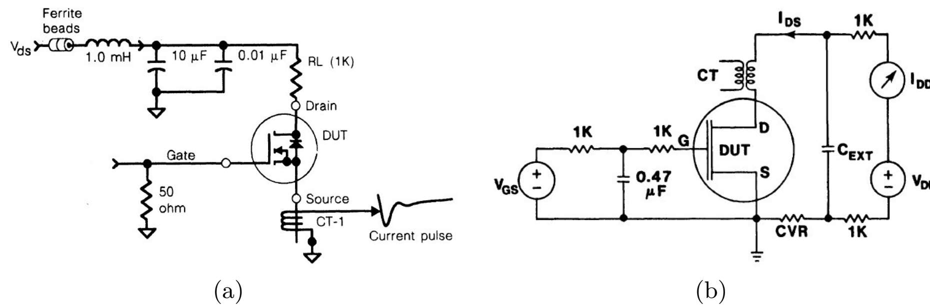

(a) (b)

Figure 2.19 – Schematics of non destructive test circuits from Oberg and Wert [69] (left), and from Fischer [25] (right)

Romero *et al.*, focusing on its time evolution to propose mitigation strategies [85, 73].

SEB experimental protocols have been defined since the very beginning [93]. One drawback of SEB testing is that Device Under Test (DUT) is completely destroyed during the test, and must consequently be replaced after each test. This leads to time consuming and expensive facilities, other than adding a further level of uncertainty in data treatment, because of the part-to-part variability. For these reasons it is extremely useful to have options for non destructive test procedures, like the one proposed in 1987 by Oberg and Wert. It is based on the presence of a 1 $k\Omega$ load resistor as a current limiter (see fig.2.19a) [69]. Starting from CIA model for SEB, in 1987 Fischer other than studying SEGR, proposed a non destructive experimental procedure for SEB based on the use of an external capacitance [25]. By controlling the external capacitor C_{EXT}, they controlled the appearance of SEB through the deposited energy inside the device.

Laser testing has been suggested as a complement to accelerators data already in 1996 by Buchner *et al.* [11, 12], and its advantage in mapping SEE has been proven by McMorrow *et al.* in 2003 [58, 59, 57]. In 2008, Luu *et al.* confirmed backside laser

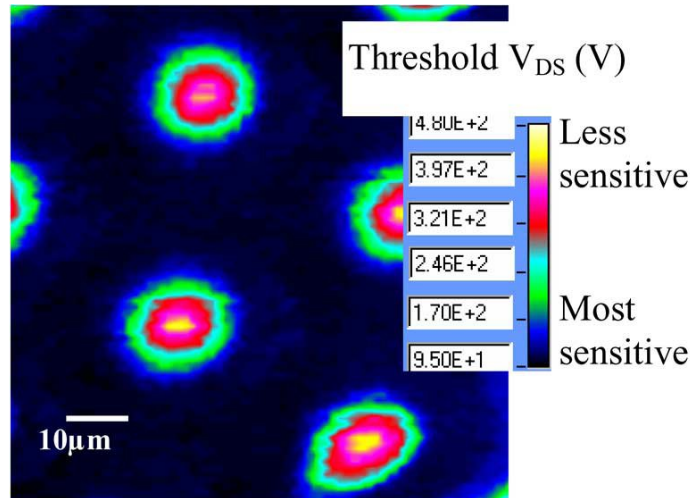

Figure 2.20 – Backside laser mapping of IRFU420 [56]

irradiations as a valid methodology to characterize devices to SEB [56]. Fig. 2.20 shows in fact a backside laser mapping of IRFU420 made by Luu. Cell structure is recognizable and the most sensitive zones are evident. In 2011, laser testing has been used by Miller *et al.* to validate a new non destructive test methodology [61].

In 2000, Huang [32] has studied SEB ang SEGR inside Super-Junction power MOSFETs. In 2004, Ikeda [34], compares the presumed lower sensitivity of S-J devices to standard MOSFETs, with a series of tests; the results show that there is not much difference between the two devices in SEB tolerance, even if S-J could have better SEB tolerance under specific technology conditions on die size and on-resistance.

The recent interest on Silicon Carbide (SiC) devices, has made SEB characterization an essential step, as for example in [4], where Asai *et al.* present evaluation results of neutron induced SEB in SiC power diodes; the same for Griffoni *et al.* [26].

In 1992, T. Wrobel and D. E. Beutler proposed hardening solutions to SEB, still using the Current Induced Avalanche (CIA) model [95].

In 1993, Johnson *et al.* suggested possible hardening solutions based on augmented collection capacity of the p^+ plug region; in 1995, Dachs *et al.* used 2D MEDICI simulation to state the same [16].

A relatively recent hardening proposal has been made by Barak *et al.*, who suggest to replace the single power MOSFET by two power MOSFETs connected in series and switched together, which protect one another from SEB [5].

The first experimental studies on SEB caused by proton and neutron impacts, were published by Waskiewicz in 1988 [94] and Oberg in 1996 [68]. In 1996 Normand

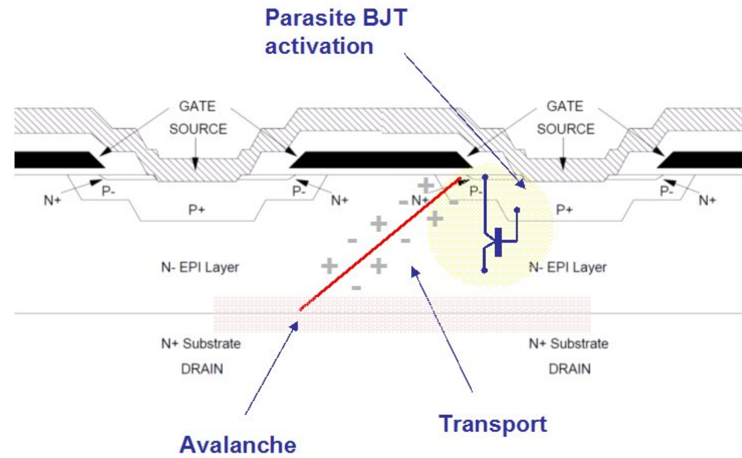

Figure 2.21 – Physics of SEB

confirmed the atmospheric environment as a source of SEU in SRAMs and DRAMs memories and also proves that neutrons can induce SEB [66]. In the same year, Adolphsen publishes data about proton induced SEB during CRUX experiment on APEX satellite [1]. This satellite crossed the radiation belts and was exposed to trapped protons with energies grater than 50 MeV and fluxes of 10^4 $particles/cm^2$.

In 2009, Bezerra *et al.* published the results of Latch-up and SEB on SRAM and power MOSFET, flying on the MEX experiment, induced by both heavy ions and protons [10]. This study is going to be used as an experimental reference to evaluate the DELPHY prediction model developed in the present work. In 2011, Hands *et al.* measured SEB cross sections on COTS MOSFETs exposed to atmospheric and thermal neutrons [27]. In 2012, the previously cited Asai *et al.* [4] and Griffoni *et al.* [26], studied neutron induced SEB on SiC components.

2.5.2 Summary of the state of the art

To conclude, SEB has been widely studied in the last thirty years, and the scientific community has now reached an agreement on its dynamics, resumed in fig. 2.21:

1. when a ionizing particle (primary particle or secondary effect of nuclear reactions) impacts on a n-channel power MOSFET, it deposes a charge column along its track, which leads to a current turning ON the parasitic BJT transistor. This creates a flux of electrons flowing down to the drain;

2. the intensity, shape and time evolution of electric field inside the epitaxial layer, determine ionization rates of electron and holes. When electric field peak moves from $p-n$ junction to $n_{epi}-n_{sub}$ junction, it causes holes generation;

3. if electric field intensity is high enough, the holes flux towards the BJT structure keeps it turned ON, thus creating a regenerative phenomenon;

4. the high level of currents thus established inside the device, lead to its meltdown an thus thermal destruction.

In the past years it has been shown that SEB sensitivity increases with voltage bias and particle energy, while decreases with temperature and epitaxial layer thickness. Based on these considerations, some hardening solutions have been proposed over the years, but none of them showed to totally avoid the appearance of SEB.

Several test protocols have also been defined, especially non destructive ones, in order to save facilities time and cost. They are either based on restraining the injected charge inside the component, or on facilitating current evacuation.

Thanks to non destructive tests, to 2D computer aided simulations and to laser mapping, component sensitivity characterization appears as an easy way to evaluate and try to predict the appearance of SEB in specific devices. However, there are other factors that must be taken into account, such as part-to-part variability, cost and time consumption of characterization itself. Most of all, none of the cited methods guarantees a complete and reliable estimation of SEB sensitivity for a given component. Still it appears to exist a lack of prediction models.

Chapter

3 Calculation of SEB triggering criteria via 2D TCAD simulation

All truths are easy to understand once they are discovered; the point is to discover them.

attributed to G. Galilei

In this chapter, Synopsys TCAD simulation is used to identify triggering criteria for SEB inside Power MOSFETs; in order to do that, a 2D component has been modelled, and the comparison of electrical characteristics between 2D and 3D configurations has been performed.

Once the component geometry is built, heavy ion injections are simulated in order to study SEB with respect to MOSFET topology, and with respect to injection location and tilt. Different sets of simulations are thus performed in order to obtain tendency curves of the minimum deposited charge inside the device that is necessary to trigger an SEB (i.e. critical charge), versus electric field inside the component.

Those tendency curves are plotted for each one of the topological and injection parameters above cited, in order to separate their singular influence on SEB phenomenon.

All those influences, are eventually synthesized in order to obtain an empirical mathematical expression that expresses the critical charge in terms of topological and injection characteristics, and electric field. This empirical law will be further used in the next chapter to predict the appearance of an SEB inside a power MOSFET.

3.1 Construction of an operational 2D MOSFET structure

The first step made has been the choice of the components to be studied. This choice was driven by the availability of reverse engineering data about the inner structure

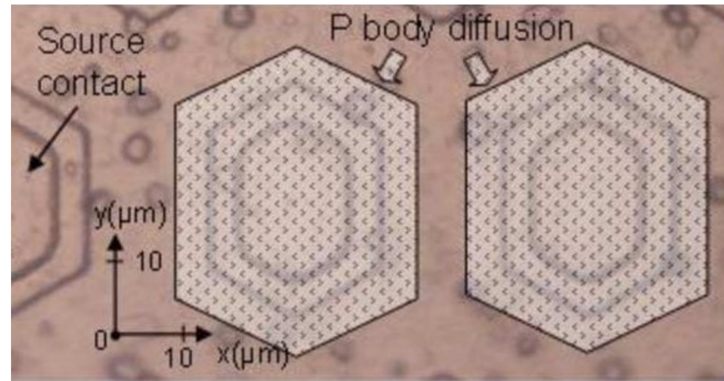

(a) *HEXFET, from [18]*

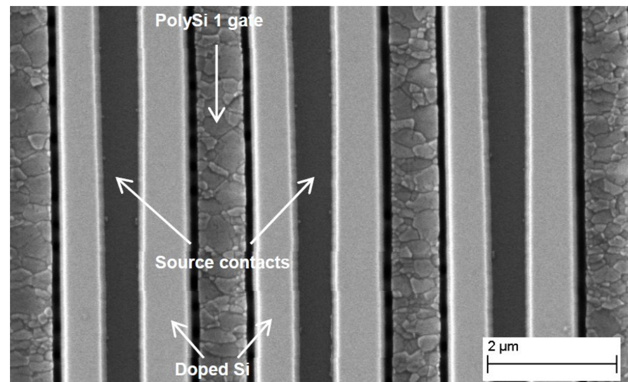

(b) *StripFET, from [88]*

Figure 3.1 – Detail and surface dimensions of the studied devices

and dimensions of the component, as well as irradiation data. For these reasons, two different components have been chosen, which are:

- A HEXFET structure, as shown in fig. 3.1a along with its surface dimensions; other internal dimensions, listed in table 3.1, have been taken from literature since no other sources were available [85].

- A StripFET structure, as shown in fig 3.1b. Internal dimensions are taken from a dedicated reverse engineering study made by Thales Communications & Security, for CERN [88], and they are listed in table 3.1.

For obvious reasons, the real component has been drastically simplified, in order to obtain a basic smart structure, actually usable in simulations.

A MOSFET is a multicellular device where a single cell structure is repeated several thousands of times. For this reason, it can be efficiently represented in

Table 3.1 – MOSFETs regions thicknesses

	Thickness (μm)	
Region	HEXFET [85]	STRIPFET [88]
Metal (aluminum)	5	5.57
Metal-gate insulator (silicon dioxide)	0.85	0.267
Gate-substrate insulator (silicon dioxide)	0.05	0.077
Gate (poly-silicon)	0.75	1.46
Substrate (silicon)	400	190
Epitaxial layer	40 [19]	3.98

simulations through one single cell, considering it totally identical to the other cells and thus permitting to apply the results in each single one of them.

For the hexagonal structure, a further simplification has been operated inside the cell itself, to adapt the study to 2D finite elements simulations: since the cell has a radial symmetry, there are no preferential planes along which the 2D section has to be cut, as shown by fig. 3.2, where it is visible that the simulated cell actually corresponds to any 2D section of the hexagonal cell. Darracq [20] suggests that the distance between cells (visible in the three sections of fig. 3.2) plays a role in SEB sensitivity, but this consideration has been neglected in the present work, which has to provide a first order model and is based on the replication of a single unity and not on a set of cells. HEXFET dimensions in fact are prohibitive when it comes to meshing the finite elements, and a simplification is needed in order to reduce calculation costs. The basic module which has been simulated, is shown in fig. 3.3, where its composition is visible, in terms of doping areas.

For the STRIPFET structure, the 2D section has been cut orthogonally to the striped pattern of the surface, in order to isolate the basic structure to be studied, as shown in fig. 2.7. Fig. 3.3 shows doping areas of the STRIPFET cell.

For both MOSFET configurations, the basic structure has been further simplified, because it is known from literature that the MOSFET areas involved in SEB do not include substrate [20], which is instead the biggest portion of the device, and also responsible of its valuable power properties. For this reason, the length of substrate along y axis has been shortened, in order to reduce simulation costs, and the final structure is presented in fig. 3.4. This change has proven to have no effects on the resulting drain current I_{DS} and in SEB triggering dynamics; therefore the resulting structure is the elementary module that has been studied in this work.

3.1.1 Introduction to simulated physical models

Technology Computer-Aided Design (TCAD) solves fundamental physical equations of semiconductors, such as Poisson's and continuity equations. The goal is to obtain

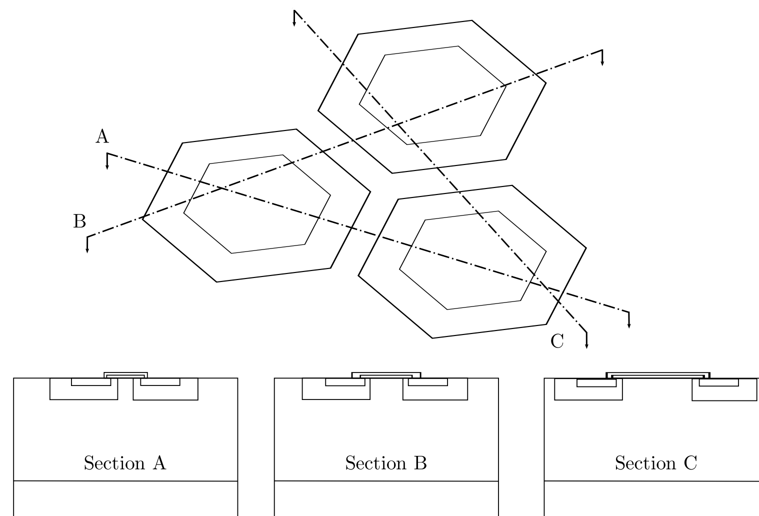

Figure 3.2 – Different 2D sections of MOSFET cell

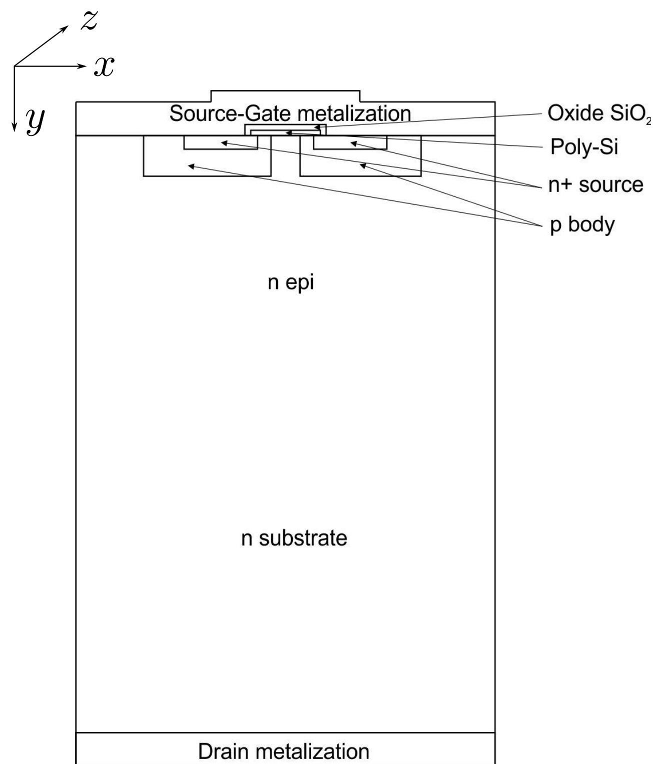

Figure 3.3 – Basic 2D MOSFET cell for TCAD simulations

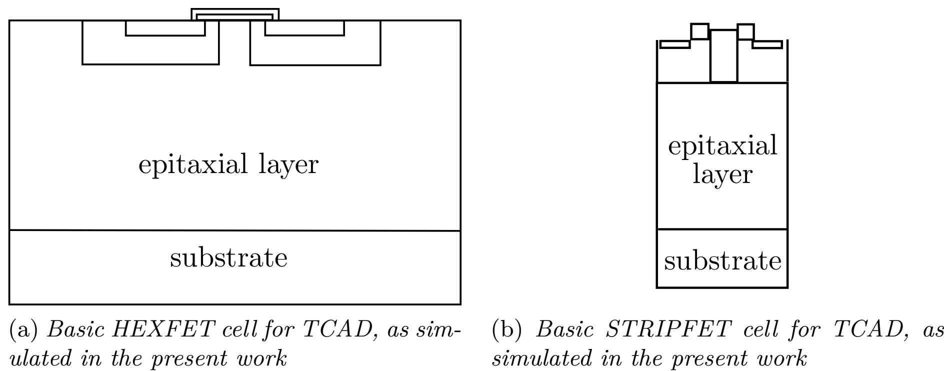

(a) *Basic HEXFET cell for TCAD, as simulated in the present work*

(b) *Basic STRIPFET cell for TCAD, as simulated in the present work*

Figure 3.4 – Detail and surface dimensions of the studied devices

electrical and physical values inside the component. In this work, version A-2007.12 has been used, under license from Synopsys, Inc.

Given that Poisson's equation and continuity equations for holes and electrons are differential and non linear, the Finite Elements Method (FEM) is used to solve them in a discrete way. The equations are in fact solved in each node, taking in consideration border conditions. The choice of the mesh nodes is thus a key step to obtain a consistent solution, because the smaller is the increment from one node to its adjacent, the more the solution is accurate in representing continuous physical values. In particular, node number has to be augmented in zones presenting higher gradients. To evaluate the precision of a mesh choice, the user has to check that the result does not change when augmenting node number. In this work, the mesh has been refined along the particle track and in the epitaxial layer, as shown in fig. 3.5.

Synopsys TCAD is composed of several utility tools, each one dedicated to a specific development of the simulated device. In this work, the used tools are Sentaurus Structure Editor and Sentaurus Device, hereby briefly presented. For further reference, Synopsys has released extensive software documentation [83].

Sentaurus Structure Editor is a 2D and 3D device structure editor based on CAD technology. User can define device structure, electrical contacts, doping concentration and mesh. Sentaurus Device is a tool for simulating, among others, electrical and thermal characteristics of silicon-based semiconductor devices. User can define physical model to be taken into account, mathematical solvers and their numerical strategy.

In this work, simulations are performed with SLIP90 mathematical solver, that is a linear algebra library containing several iterative methods for solving linear systems of equations.

Adopted physical models include electric field and doping concentration dependencies for mobility, bandgap narrowing, Shockley-Red-Hall and Auger models [83] for recombination, and electric field effects on avalanche recombination.

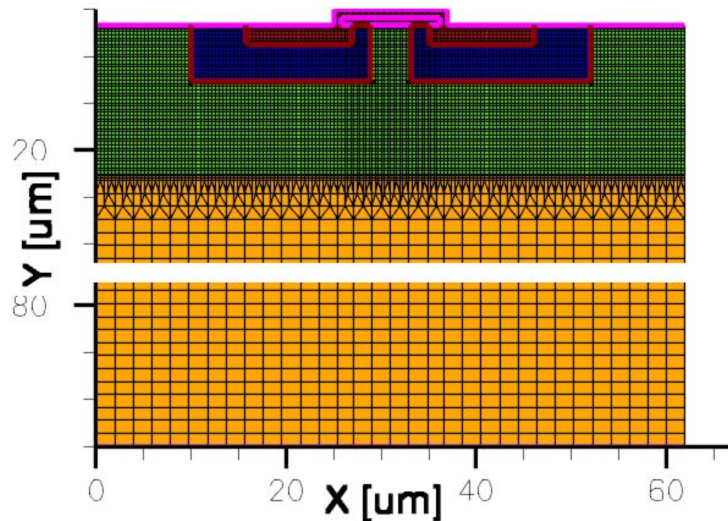

Figure 3.5 – Mesh used in TCAD simulations; it is refined inside the epitaxial layer

3.1.2 Comparison with component datasheet

Once the structures built, their respective electrical characteristics have been calculated and plotted, in order to determine the effective electrical behaviour of the simulated components, with respect to those listed in the respective datasheets from International Rectifier.

The first parameter that has been compared between 2D TCAD simulations and datasheet, is gate threshold voltage V_{GSth}: its value depends on gate oxide thickness and on doping level of the p body region [84]. Gate oxide thickness is fixed since it is known from reverse engineering, so controlling V_{GSth} allows for a fine tuning of p body doping inside the simulated structure, according to the following procedure:

- HEXFET datasheet indicates a gate threshold voltage V_{GSth} in the range of $2 \div 4\ V$, while literature predicates a 750 nm gate oxide thickness [85]. By iterating the simulations in order to comply to these requirements, a boron concentration of $1 \cdot 10^{+17}\ /cm^2$ has been calculated to be the necessary doping level in p body, and has thus been used in the further simulations.

- STRIPFET datasheet dictates $V_{GSth} = 2 \div 4\ V$, while gate oxide thickness is 1.46 μm according to reverse engineering data, so a boron concentration of $9 \cdot 10^{+16}\ /cm^2$ is necessary to comply to those requirements.

Secondly, drain current I_D from 2D TCAD simulations has been compared with transfer characteristics from datasheet. Fig. 3.6 shows that, while the shape of

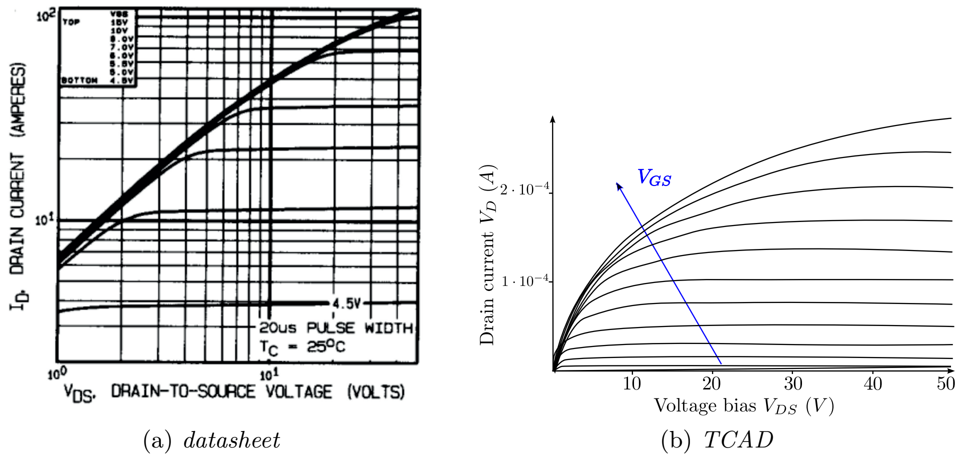

(a) *datasheet* (b) *TCAD*

Figure 3.6 – Drain current I_D comparison between datasheet and TCAD for HEXFET

the curves is the same, indicating a correct modelling of physical behaviour, the order of magnitude of datasheet drain current I_D^D is greater than I_D^T obtained with TCAD. The explanations for this difference are that TCAD simulations are only a 2D representation of reality, and that a MOSFET is composed of several cells in parallel, which thus form a wider effective channel.

3.1.3 Evaluation of scale factor between 3D component and its 2D simulation

To take into account the drain current difference in the further development of SEB prediction model, an equivalent third dimension z_{eq} has been calculated, which corresponds to the ideal length along z axis, of the cell represented in fig. 3.4. One has to know that 2D TCAD simulations assume that the 2D cell has an artificial third dimension of $z^T = 1\ \mu m$ [83]. For this reason, a scale factor λ_z is needed, which would theoretically give $z_{eq} = \lambda_z z^T$.

The coefficient λ_z is calculated according to

$$\lambda_z = \frac{I_D^D}{I_D^T} = \frac{I_{D_{3D}}}{I_{D_{2D}}} \ . \tag{3.1}$$

On the base of data presented in table 3.2, its value is thus $\lambda_z^H = 3.5 \cdot 10^{+5}$ for HEXFET, and $\lambda_z^S = 8 \cdot 10^{+5}$ for STRIPFET. The ratio between drain current from datasheet I_D^D and drain current from TCAD simulation I_D^T gives λ_z and thus z_{eq}: its physical meaning is the z dimension of a MOSFET built as in fig. 3.4, that would ideally be necessary to have a component equivalent respectively to a HEXFET or a STRIPFET in terms of drain current I_D; that is to say, z_{eq} is the channel width.

Table 3.2 – Drain current I_D values, from HEXFET datasheet and TCAD simulations

	46260 cells [10] HEXFET datasheet 3D	1 cell TCAD simulation 2D
V_{DS}	30 V	30 V
V_{GS}	9 V	9 V
I_D	70 A	$2 \cdot 10^{-4}\ A$

Table 3.3 – Drain current I_D values, from STRIPFET datasheet and TCAD simulations

	800 cells STRIPFET datasheet 3D	1 cell TCAD simulation 2D
V_{DS}	20 V	20 V
V_{GS}	8 V	8 V
I_D	80 A	$1 \cdot 10^{-4}\ A$

In the case of STRIPFET, reverse engineering data were available, and confirmed the value of λ. Indeed, channel width z^S_{eq} has been calculated also with a purely geometrical approach, multiplying the number of cells n^S_{cell} times the active chip area length L^S

$$\lambda^S_z = n^S_{cell} \cdot L^S \ . \tag{3.2}$$

The result is

$$z^S_{eq} = \lambda^S_z \cdot z^T = 82 \cdot 10^{+5} \cdot 1\ \mu m\ . \tag{3.3}$$

The estimation of the scale factor z_{eq} is not exhaustive as an appreciation of the difference between 2D and 3D when considering a complex phenomenon such as SEB. There are in fact physical phenomena whose profile is totally different in the two cases. As an example, it is now estimated the difference in diffusion.

3.1.4 Comparison of 2D and 3D diffusion phenomena

A further reflection on the difference between 3D and 2D SEB dynamics, is given by the calculation of the electron density in time, in both cases. As known, when a heavy ion is injected in a MOSFET, it generates a electron-hole pair (ehp) column around its track, and thus a concentration gradient that leads to a diffusion current. In a 3D scenario, diffusion happens along two directions (if the track is long enough

to have no gradient along its axis), while in a 2D scenario, only one direction is followed by the diffusion current.

Fig. 3.7 shows the simulations performed to study the diffusion difference between 2D and 3D configurations for HEXFET. A simple silicon block has been taken as a reference, and a track has been injected in its centre along the y direction, thus creating a carrier source. Track dimensions are 0.5 μm length and 0.1 μm maximal radial width. In the 2D configuration, injection is along the y direction, and located at the centre of the surface. In order to avoid border effects, the block and surface dimensions are large enough with respect to track dimensions: this ensures the existence of a concentration gradient. The silicon is doped as the epitaxial layer of HEXFET MOSFET, which is the location where heavy ions injections are situated in this study. Fig. 3.7a and 3.7b show the doped silicon structures, along with the 2D cut for the 3D configuration. Fig. 3.7a and 3.7b illustrate the electron concentration at time $t^{\star} = 1 \cdot 10^{-9}$ s, that is a reference time for SEB evolution (see further fig. 3.8), while fig. 3.7a and 3.7b show the space distribution of electron concentration at $t^{\star}$. Since 2D electron concentration after $1 \cdot 10^{-9}$ s is 68% higher than in the 3D configuration, one can conclude that the diffusion dynamics would not be the same in 2D and 3D TCAD MOSFETs. While this confrontation does not speak for other physical phenomena, such as conduction current, diffusion form the heavy ion track is considered to be the major reason for difference between 2D and 3D simulations.

Nevertheless, also simulation costs have to be taken into account in the trade-off, and 2D simulations of a power MOSFET are still more convenient than 3D ones, especially after one can quantify the effects of a 2D approach, and apply the necessary corrections.

Although this comparison of diffusion effects in 2D and 3D has been quantified, it is worth considering that the figure of 68% difference depends on the injection conditions used in this brief and non-exhaustive reflection. For example, it is dependent on track intensity and shape and should by no means be taken as an absolute estimation.

In addition, the present calculation is made only on diffusion, but for sure reflects the effects of other physical phenomena, which are all inter-connected and hardly decomposable.

3.2 Study of SEB physics by means of heavy ion injection

SEB phenomenon is of a complex nature, where several physics effects are interlaced: the advantage of studying it with TCAD simulations is the possibility to visualize the effects of one parameter at a time, controlling what is varying and thus permitting a better understanding of SEB dependencies from mentioned parameters, in order

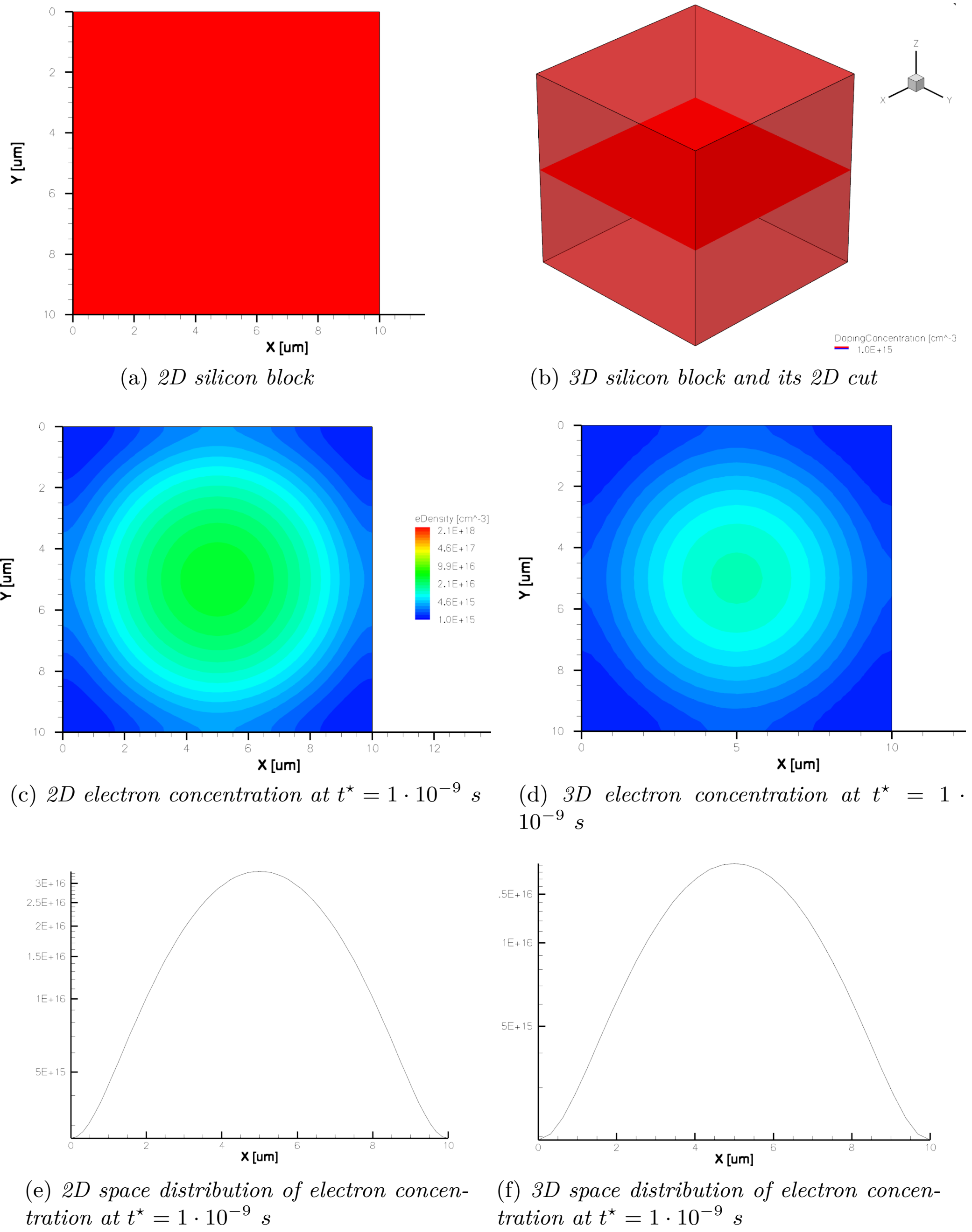

(a) *2D silicon block*

(b) *3D silicon block and its 2D cut*

(c) *2D electron concentration at* $t^{\star} = 1 \cdot 10^{-9}\ s$

(d) *3D electron concentration at* $t^{\star} = 1 \cdot 10^{-9}\ s$

(e) *2D space distribution of electron concentration at* $t^{\star} = 1 \cdot 10^{-9}\ s$

(f) *3D space distribution of electron concentration at* $t^{\star} = 1 \cdot 10^{-9}\ s$

Figure 3.7 – TCAD simulated diffusion in 2D (left) and 3D (right) for HEXFET

Table 3.4 – Selection of TCAD simulated parameters among all the variables which have an influence on SEB

Geometry	Electric	Particle
Injection location	Bias V_{DS}	LET
Injection angle	Doping levels	Range
Device technology		

to take them into account in the predictive model.

In order to simulate the injection of a heavy ion inside the 2D structure, the "heavy ion" package for Sentaurus Device has been used in TCAD. Adopted physical models include electric field and doping concentration dependencies for mobility, bandgap narrowing, Shockley-Red-Hall and Auger models for recombination, and electric field effects on avalanche recombination. For what concerns ion track characteristics, ion time evolution is Gaussian with a time constant of 2 ps; Gaussian is also track radial extension, while LET is assumed constant along the ion track. The choice of ion simulation parameters has been made after physical considerations on heavy ions tracks in power devices.

3.2.1 Proposition of study methodology and choice of SEB triggering criterion

To study and visualize relevant parameters for SEB, in this work the approach has been to find a threshold value for deposited charge inside the epitaxial layer, while simulating ion injection inside MOSFET. Then, similar sets of simulations have been performed, each time changing one particular parameter (such as impact location and so on); a complete list of the variables which have an influence on SEB is given at the end of chapter 2, while the studied parameters are listed in table 3.4. This approach has permitted the analysis of SEB physics, other than graphical visualization of the phenomenon inside MOSFET. In every configuration, the simulation objective has been the evaluation of the triggering criterion in terms of threshold charge q_{th} deposited inside epitaxial layer.

The choice of threshold charge as triggering criterion inside the epitaxial layer volume, comes from the bibliographic survey in § 2.5.1. In fact, the role of epitaxial layer as sensitive volume has been demonstrated, also given shape and intensity of electric field [82, 91, 55]. Also, SEB criteria based on deposited charge have already been used [48, 45, 44], since the ion's passage creates a charge column along its trajectory, depending on its LET [75, 74]. These considerations set a first step towards the building of a SEB prediction model.

In this work, threshold charge deposited inside the epitaxial layer is defined as

$$q_{th} = LET_{th}\frac{h_{epi}}{cos\theta}\ . \tag{3.4}$$

By this definition itself, threshold charge q_{th} is directly connected to technological parameters, such as epitaxial layer thickness h_{epi}; and threshold injection conditions, such as LET_{th}, which is the minimum particle LET that triggers a SEB in each TCAD simulation, and tilt θ.

The definition in (3.4) allows the explanation of the second main hypothesis used in this work: it is considered that relevant charge for SEB phenomenon is deposited inside epitaxial layer only. Longer particle tracks, which therefore deposit a certain amount of charge outside epitaxial layer, are thus truncated: their contribution to triggering SEB is evaluated only before they reach and pass trough the substrate.

3.2.2 SEB prints in terms of drain current and electric field

The previously described approach which involves the search for a triggering threshold charge, implies a clear recognition of SEB or noSEB inside the device. This has been accomplished by analyzing drain current I_D shape [25]. Fig. 3.8 shows three different cases of possible I_D shapes, which also identify the different physical phases of ion injection: parasitic BJT activation, transport and Kirk effect that leads to the decision of SEB or noSEB. Fig. 3.8 represents drain current I_D evolution in time, in the case of three different particle's LET: one can notice that for low LET values (curve 1), the generated ehp are not enough to turn on the parasitic BJT, while BJT activation and transport do not guarantee the triggering of a SEB, as in curve 2, since they do not generate a self-sustained phenomenon that results in a SEB. Indeed, only curve 3 is considered to be a SEB [20], while curves 1 and 2 result in transient phenomena. The same current patterns as a SEB printing are recognizable inside the device, as shown in fig. 3.9, where on the left is represented time evolution of current density in case of noSEB, with $LET = 10\ MeVcm^2/mg$; on the right instead, the same current density prints are shown in case of $LET = 15\ MeVcm^2/mg$, which leads to SEB.

A further way to have a SEB signature inside the device is given by time evolution of electric field averaged inside epitaxial layer, as shown in fig. 3.10. One can recognize a different pattern when the phenomenon is transient and leads to noSEB because of not enough carrier generation (case 1), and when a SEB is achieved (case 2 and 3). It is evident the similarity between SEB signatures in terms of current (fig. 3.8) and in terms of electric field (fig. 3.10). Since SEB happens when a voltage is blocking the device, i.e. MOSFET is in its OFF state, the electric field inside epitaxial layer represents the device condition before heavy ion injection. This concept had already been introduced in SEB literature [56] and has been further confirmed by this work, in particular via TCAD analysis. Electric field time evolution is therefore a valuable SEB signature.

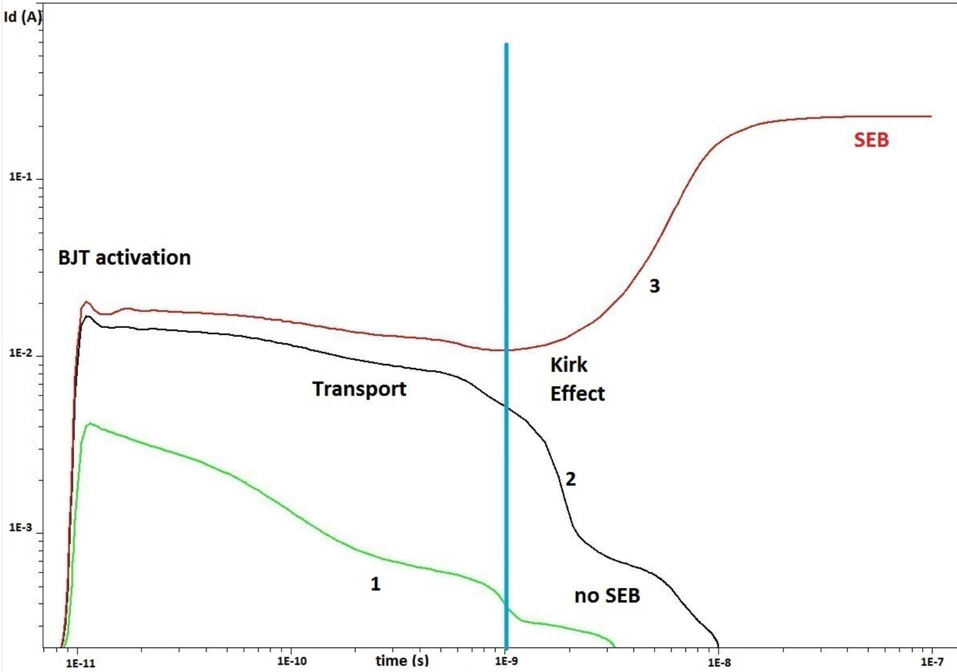

Figure 3.8 – Drain current I_D patterns plotted with time. Curve 3 is the SEB case, with $LET = 13\ MeV cm^2/mg$. Curves 1 and 2 are the noSEB case, respectively with $LET = 2\ MeV cm^2/mg$ and $LET = 10\ MeV cm^2/mg$

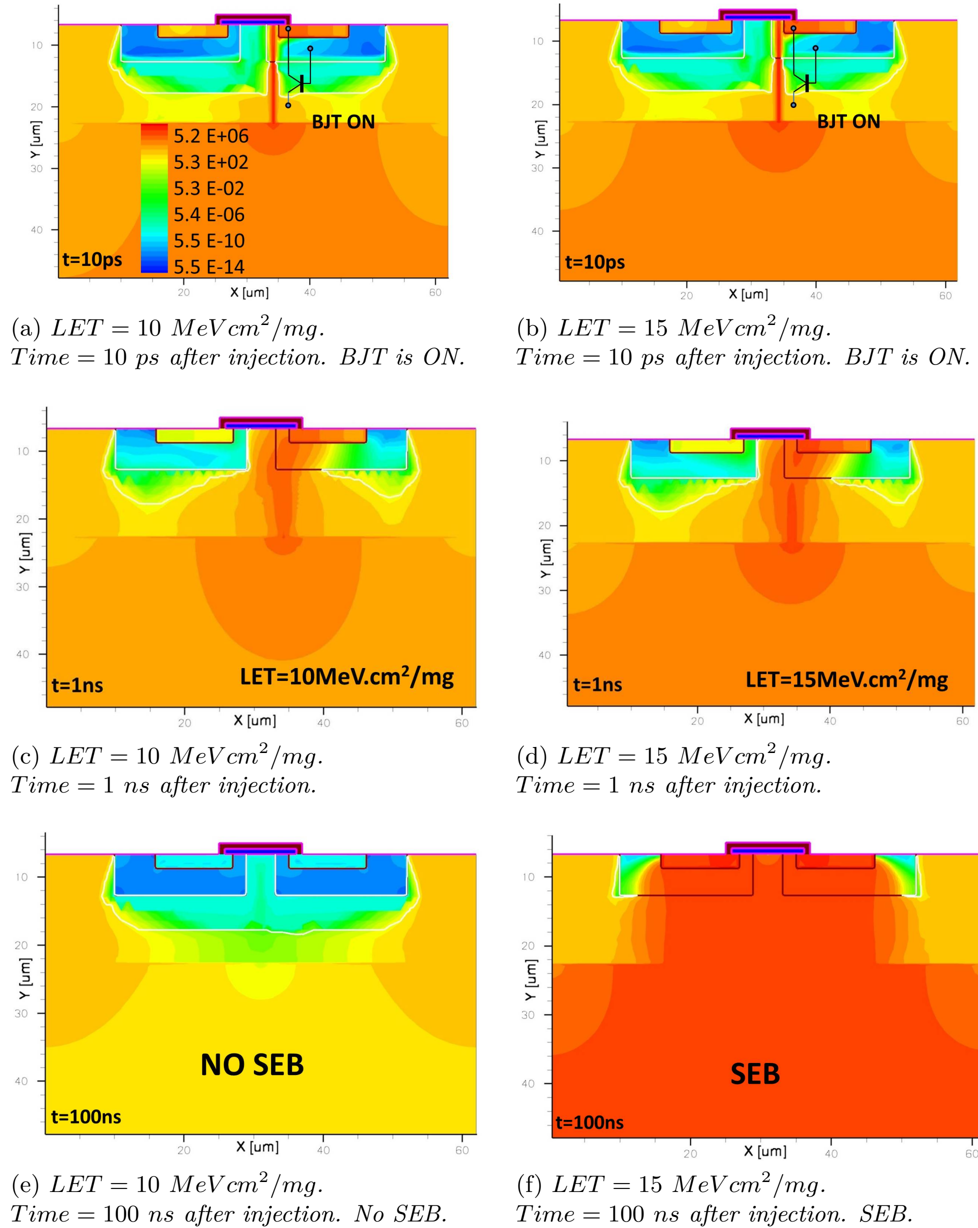

(a) $LET = 10\ MeV cm^2/mg$.
Time $= 10\ ps$ *after injection. BJT is ON.*

(b) $LET = 15\ MeV cm^2/mg$.
Time $= 10\ ps$ *after injection. BJT is ON.*

(c) $LET = 10\ MeV cm^2/mg$.
Time $= 1\ ns$ *after injection.*

(d) $LET = 15\ MeV cm^2/mg$.
Time $= 1\ ns$ *after injection.*

(e) $LET = 10\ MeV cm^2/mg$.
Time $= 100\ ns$ *after injection. No SEB.*

(f) $LET = 15\ MeV cm^2/mg$.
Time $= 100\ ns$ *after injection. SEB.*

Figure 3.9 – Current density prints inside MOSFET epitaxial layer, at significant times. On the left *(a, c, e)* is represented a transient phenomenon, while on the right *(b, d, f)* is represented a SEB. Current reference scale is provided in *(a)*

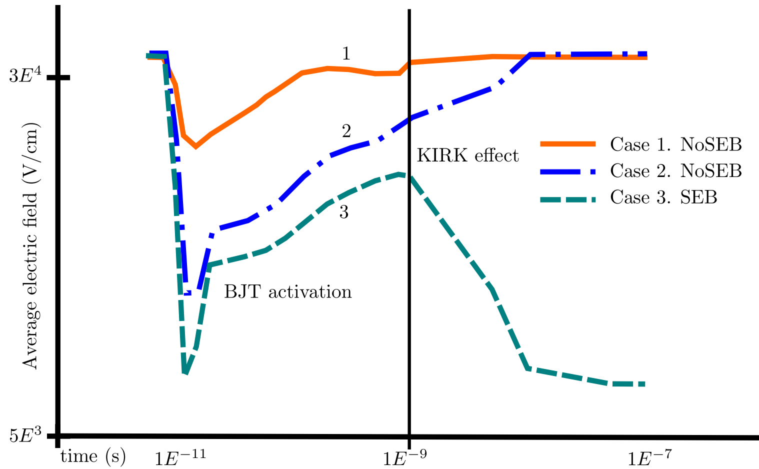

Figure 3.10 – Electric field plotted in time at different particle LET. Its value is averaged inside epitaxial layer. Curve 3 is the SEB case, with $LET = 13\ MeV cm^2/mg$. Curves 1 and 2 are the noSEB case, respectively with $LET = 2\ MeV cm^2/mg$ and $LET = 10\ MeV cm^2/mg$

Also, from curves 2 and 3 from figs. 3.8 and 3.10, it is visible the threshold effect on deposited charge: keeping identical simulation condition and only changing particle LET, leads to the triggering of SEB.

3.2.3 Determination of SEB threshold charge dependencies on physical parameters

Once defined how to clearly identify Burnout in a simulation, the following step has been to actually extract threshold charge. Every threshold charge value is obtained for a given polarization and depending on a specific physical parameter which has a direct influence on SEB triggering. The parameters chosen to be studied concern the impact geometry, like injection location and angle; the impact conditions, such as polarisation and particle LET; and the MOSFET geometry, like epitaxial layer thickness and doping.

Bias

A range of polarizations has been applied to the device, in order to simulate different working conditions and their effect on SEB triggering. Voltage bias V_{DS} is directly related to electric field inside the device, according to

$$EF = \frac{V_{DS}}{h_{epi}} \tag{3.5}$$

where h_{epi} is the epitaxial layer thickness, which is the active zone of MOSFET. Fig. 3.11 shows in fact that during SEB evolution, electric field is relevant only inside the epitaxial layer. The black solid curve is the representation of electric field before the injection of the ionizing particle, while red dotted curve is its representation at the end of SEB phenomenon. Studying voltage bias V_{DS} effect on SEB is as a way of understanding the evolution of electric field EF during the phenomenon. The considered bias values lie in the interval $(30 \div 120)\ V$ for HEXFET, which are relatively low with respect to its Safe Operating Area (fig. 3.12a). On the other hand, considered bias values for STRIPFET lie in the interval $(30 \div 55)\ V$, located in the higher part of its SOA. This allows to explore non conventional V_{DS} values and relatively wide component sensitivities to SEB triggering.

Impact location

Regardless of the component topology (HEXFET or STRIPFET), inside the elementary cell a heavy ion has been injected in three different impact locations, represented in fig. 3.13 as A, B, C. All other injection and device parameters (polarization, MOSFET geometry...) were kept constant in the three cases. The objective has been the search for the minimal charge deposited inside epitaxial layer that would trigger an SEB (threshold charge q_{th}), in order to accomplish the goal of SEB prediction.

The reason for the choice of these three impact locations is the number of $p - n$ junctions the heavy ion crosses when entering the device: no junctions, one or two. This criterion has been derived from [20]. All the other possible injection locations in the elementary cell, are comparable to the three already selected, at least for the number of junctions.

For a HEXFET, literature [20] suggests that the most sensitive zone should be the one under the "neck", indicated as A in the present work. The simulations have confirmed this trend, as shown in fig. 3.14, giving A as the most sensitive zone with lowest critical charge q_{th}, C as the less sensitive with highest q_{th} and B in the middle, while this trend is independent from voltage bias V_{DS}. Critical charge dependence on impact location is monotonic, suggesting a correlation with the number of junctions crossed by the heavy ion during the impact.

As for the STRIPFET technology, SEB threshold charge q_{th} has proven to be affected by impact location, but shows a non monotonic law, as illustrated in fig. 3.15 and also no direct relation with the number of junctions crossed by the heavy ion. Also, the trend independence from voltage bias V_{DS} is valid, but the impact location effect is quite limited in terms of critical charge values. This can be explained by the fact that all injections are quite close to each other, given the small cell characteristic dimension in STRIPFET technology.

To summarize (see table 3.5), the number of junctions crossed by the heavy ion appears to not have a direct influence on q_{th} in both HEXFET and STRIPFET technologies, as well as voltage bias. The effect of impact location A, B, C on

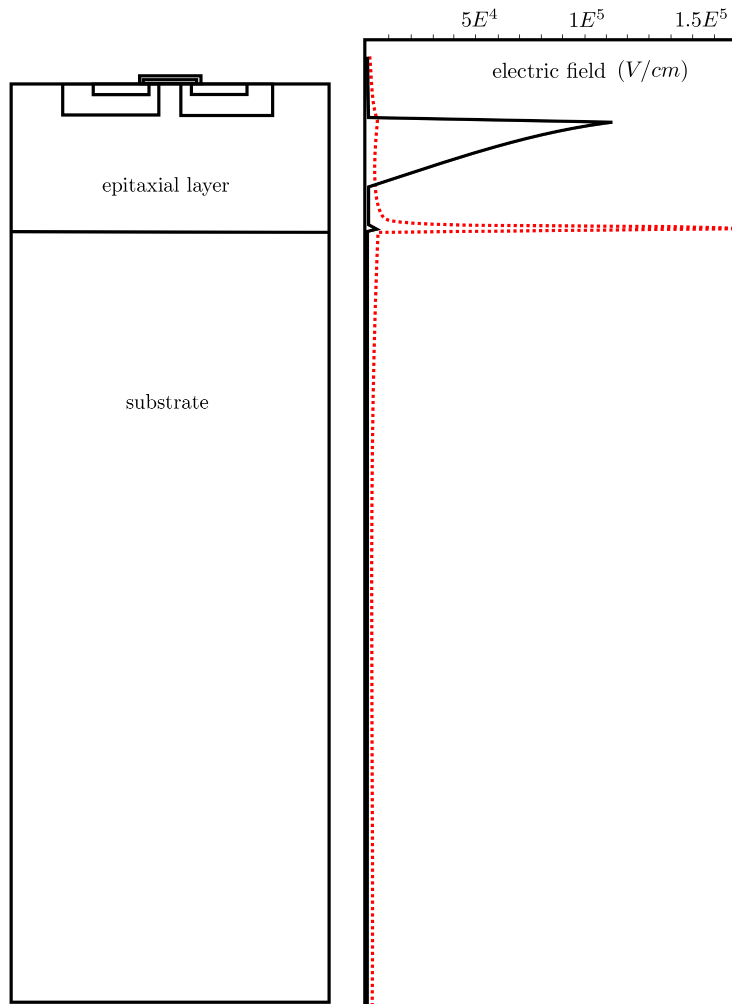

Figure 3.11 – Electric field inside HEXFET, as given by TCAD simulations, before injection of the ionizing particle (black solid curve), and at the end of SEB evolution (red dotted curve)

Table 3.5 – Impact location effect on SEB threshold charge $q_{th}(pC)$ in HEXFET and STRIPFET technologies. Voltage bias V_{DS} is 40 V

SEB Threshold charge (pC)			
Technology	Impact location		
	A	B	C
HEXFET	1.8	4.2	15
STRIPFET	0.32	0.28	0.39

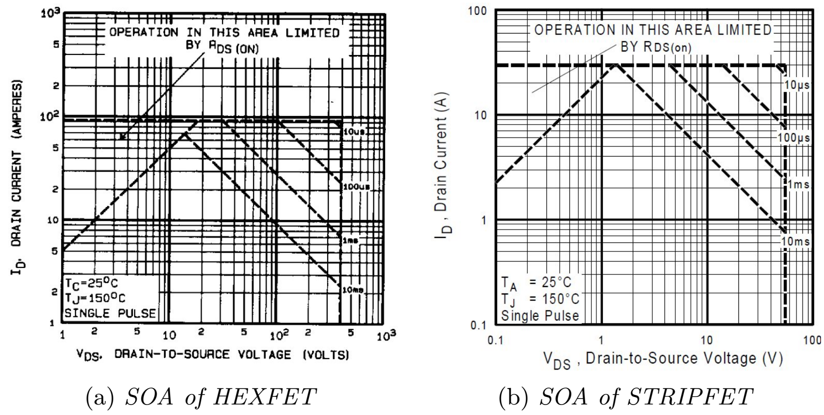

(a) *SOA of HEXFET* (b) *SOA of STRIPFET*

Figure 3.12 – Safe Operating Area of simulated components, according to respective datasheets

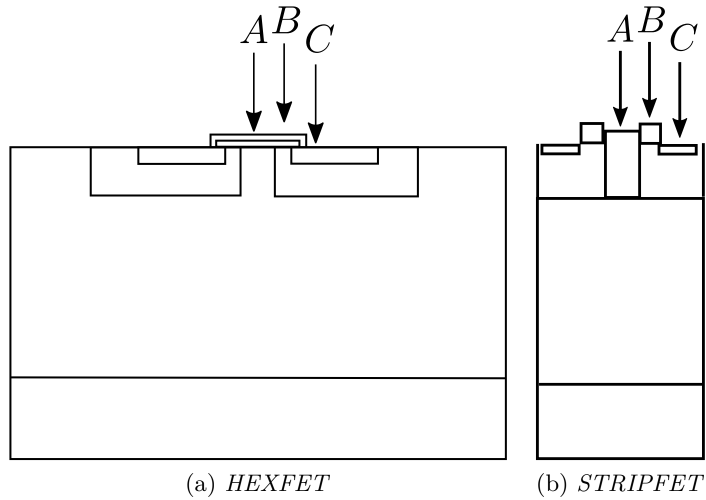

(a) *HEXFET* (b) *STRIPFET*

Figure 3.13 – A, B, C are the heavy ion impact locations studied inside the elementary cell

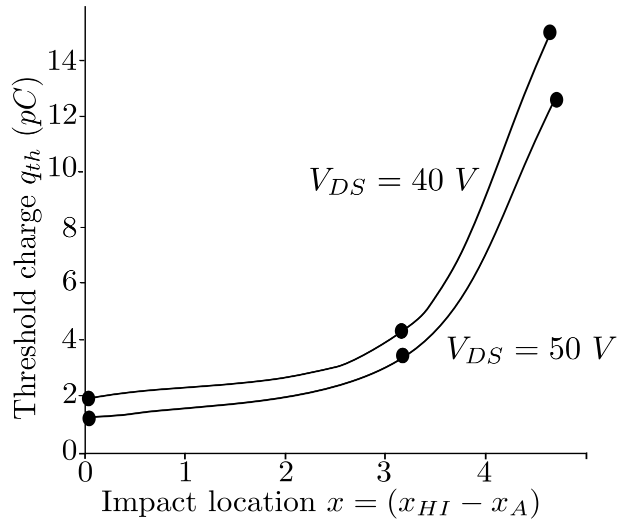

Figure 3.14 – Critical charge q_{th} as a function of impact location in a HEXFET cell. Epitaxial layer thickness h_{epi} is 30 μm and voltage bias V_{DS} is 40 V (upper curve) and 50 V (lower curve)

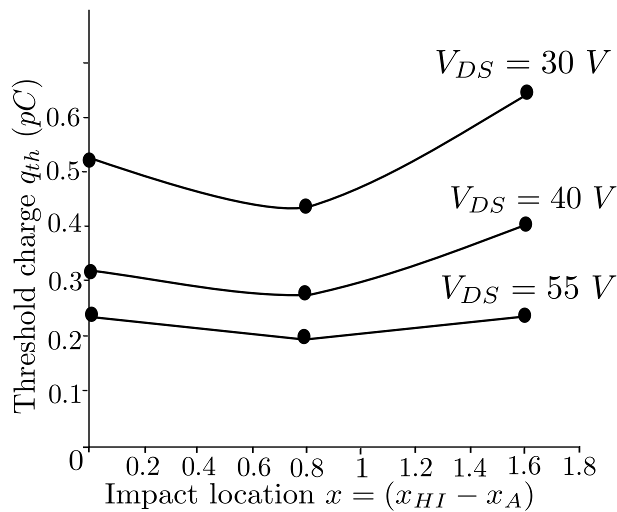

Figure 3.15 – Critical charge q_{th} as a function of impact location in a STRIPFET cell. Epitaxial layer thickness h_{epi} is 4 μm

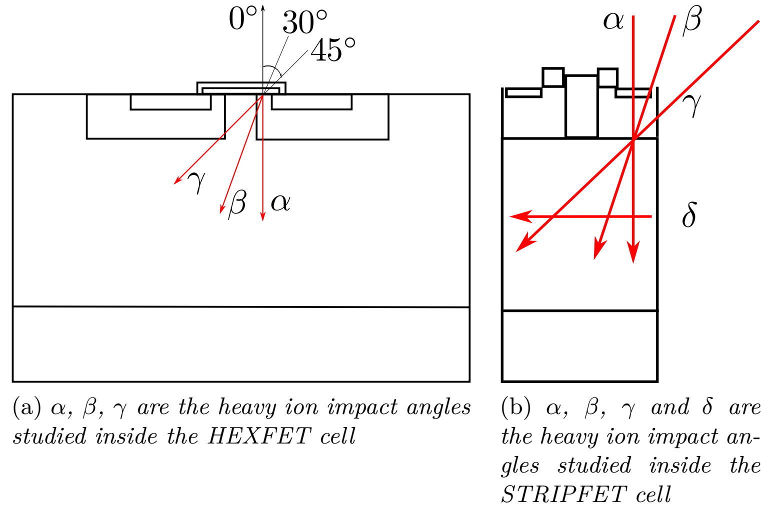

(a) *α, β, γ are the heavy ion impact angles studied inside the HEXFET cell*

(b) *α, β, γ and δ are the heavy ion impact angles studied inside the STRIPFET cell*

Figure 3.16 – α, β, γ and δ are the heavy ion impact angles studied inside the elementary cell

critical charge values seems to be larger in the case of HEXFET technology, while SEB sensitivity is up to 2 orders of magnitude higher in STRIPFETs (lower q_{th}). This difference in behaviour between the two technologies, can be explained by the fact that the STRIPFET is far more integrated than the HEXFET, so the same applied bias results in a higher average electric field inside epitaxial layer, resulting in an overall greater SEB sensitivity, but in a lower dependence on impact location.

Impact angle

Inside the simulated elementary cell, heavy ions have been injected with different impact angles, as shown in fig. 3.16. The tilt angle value is calculated with respect to the normal to the impact surface; in order to explore the physical effects of tilt, the simulated values are $\alpha = 0°$, $\beta = 30°$ and $\gamma = 45°$ in the HEXFET structure and $\alpha = 0°$, $\beta = 30°$, $\gamma = 45°$ and $\delta = 90°$ in the STRIPFET.

In the HEXFET structure, simulations have shown that the most sensitive case is $\alpha = 0°$, suggesting that a longer track of the heavy ion inside the epitaxial layer, helps mitigating injection effects. Also, the difference in terms of threshold charge in the 3 different angles α, β, and γ is relevant.

Similarly to the impact location case, in the STRIPFET the tilt effect does not produce a relevant difference in terms of threshold charge in the 4 different angles α, β, and γ, while for $\delta = 90°$ angle, there is a sensitive augmentation of threshold charge q_{th}, indicating a lower SEB sensitivity. The STRIPFET structure is thus confirmed to be more sensitive to SEB than the HEXFET, when polarized with the same voltage bias V_{DS} (see table 3.6).

Table 3.6 – Tilt effect on SEB threshold charge $q_{th}(pC)$ in HEXFET and STRIPFET technologies. Voltage bias V_{DS} is 30 V and threshold charge is calculated according to (3.4)

SEB Threshold charge (pC)				
Technology	Impact angle			
	α	β	γ	δ
HEXFET	3.1	19.5	66.3	–
STRIPFET	0.64	0.65	0.78	1.16

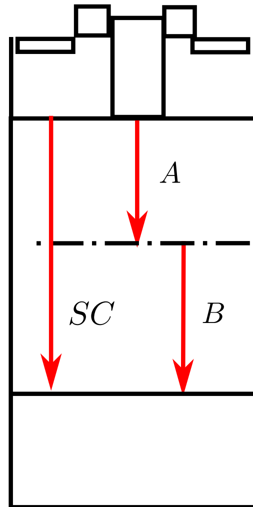

Figure 3.17 – A and B are the injection conditions studied with short track length. SC is the track length which short circuits the epitaxial layer

Short track length

In the STRIPFET device, a short track heavy ion has been injected at an identical position with three different bias conditions: 30 V, 40 V and 55 V. Short track length has been chosen as the half of the epitaxial layer thickness, and injected in its upper part and then in its lower part, as shown in fig. 3.17.

Simulations showed that the component is less sensitive when a heavy ion with a short track is injected, and the effects is greater at low bias. In particular, also injection position with respect to epitaxial layer has an effect on critical charge, as shown in table 3.7. A short track heavy ion depositing charge inside the lower part of epitaxial layer is the less sensitive configuration for SEB.

Table 3.7 – Effect of track length on threshold charge

SEB Threshold charge (pC)			
Bias V_{DS} (V)	Track length		
	SC	A	B
30	0.44	1.07	2.27
40	0.28	0.68	1.07
55	0.2	0.36	0.44

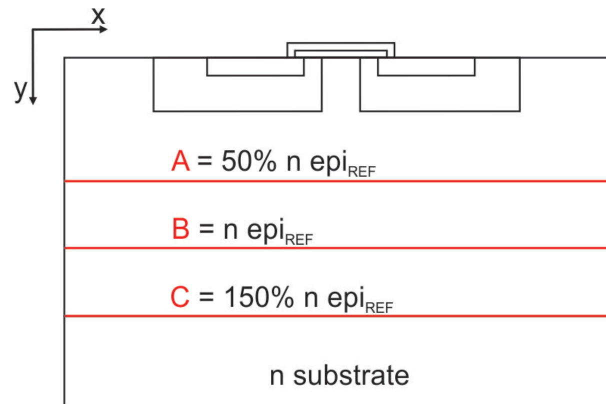

Figure 3.18 – A, B, C are the epitaxial layer thicknesses studied inside the HEXFET elementary cell

Epitaxial layer thickness

Knowing that the epitaxial layer is a key location for SEB dynamics, its thickness has been changed in order to study its influence on SEB triggering. To explore SEB physics, the applied values are 10 μm, 20 μm and 30 μm for the HEXFET structure. No variations have been studied for the STRIPFET topology, since reverse engineering data were made available by CERN for this work. Other parameters have been kept constant.

Simulations have shown that epitaxial layer thickness is inversely connected to SEB sensitivity: since polarisation is constant, an augmentation of epitaxial layer thickness, means a diminution of average electric field inside it, leading to higher critical charge q_{th} and thus lower SEB sensitivity, as shown in fig. 3.19.

Epitaxial layer doping level

In order to evaluate the effect of epitaxial layer doping on SEB, different epitaxial layer phosphorus concentrations have been implemented in the HEXFET structure,

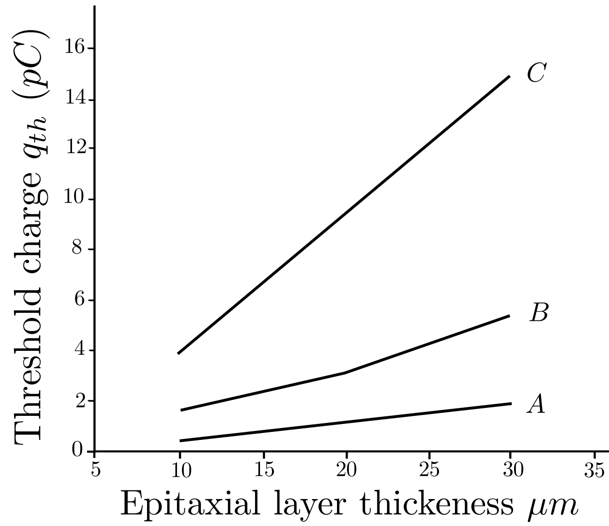

Figure 3.19 – Critical charge q_{th} as a function of epitaxial layer thickness, at $V_{DS} = 40\ V$ and in three impact locations A (low curve), B (middle curve) and C (high curve)

Table 3.8 – Epitaxial layer doping values studied via TCAD, at $V_{DS} = 30\ V$ and $LET = 13\ MeVcm^2/mg$

epitaxial doping level (at/cm^3)	$LET = 13\ MeVcm^2/mg$
$1 \cdot 10^{+15}$	SEB
$2 \cdot 10^{+15}$	SEB
$5 \cdot 10^{+15}$	NO SEB

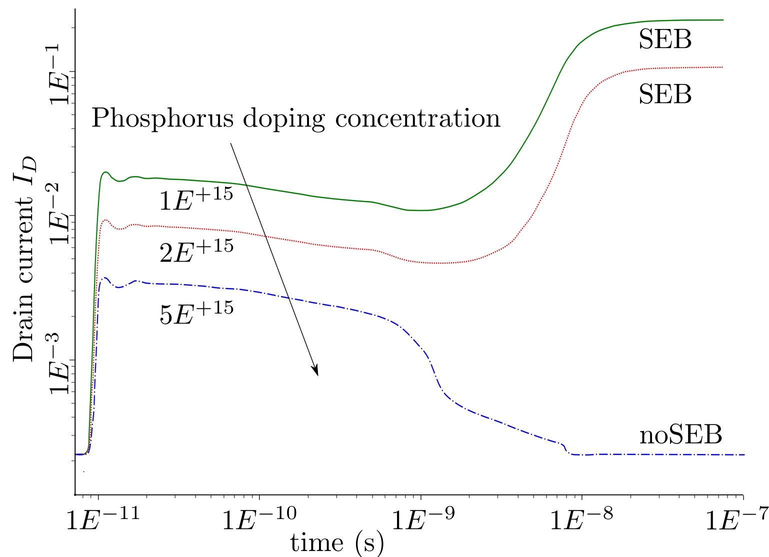

Figure 3.20 – Drain current I_D time evolutions at different epitaxial layer doping values, $V_{DS} = 30\ V$ and $LET = 13\ MeV cm^2/mg$

keeping constant all other injection and geometry parameters. No variations have been studied for the STRIPFET topology, since Secondary Ion Mass Spectrometry(SIMS) doping profile analysis data were made available by CERN for this work. Other parameters have been kept constant. With respect to standard epitaxial layer doping concentration values, actually used by power MOSFET manufacturers, relatively higher values have been studied, in order to define a behaviour tendency. The implemented values, however, still guarantee MOSFET working capabilities. The reference value is a phosphorus concentration of $1 \cdot 10^{+15}\ at/cm^3$ and all other studied values are listed in table 3.8, along with their results in terms of SEB triggering. Polarization is $V_{DS} = 30\ V$ and particle LET is 13 $MeV cm^2/mg$. Fig. 3.20 shows the respective drain current I_D time evolutions.

Fig. 3.20 and table 3.8 show that increasing epitaxial layer doping concentration is a way of contrasting SEB triggering. A higher doping profile in epitaxial layer is in fact responsible for a lower SEB sensitivity, as observed in literature for Super-Junction power MOSFETs [32, 34].

3.3 Extraction of a SEB triggering law based on deposited charge and electric field

After the analytical part so far described, a synthesis effort has been done, the aim of this work being to provide a SEB characterization for a given device: trigger-

ing sensitivities and current shapes have been processed and combined in order to produce a simple yet physically consistent law which takes into account physical influences of the different variables.

3.3.1 Synthesis of SEB physical parameters dependencies

To synthesize all TCAD simulations and their results in terms of SEB triggering, one can state that the most sensitive condition for a MOSFET to undergo a Burnout, is to have a heavy ion strike at normal incidence and neck location, while the component is relatively high polarized and presents a thin epitaxial layer (the combination of these two conditions means a high average electric field inside the device) which is also relatively low doped.

An overall synthesis of these dependencies is given in fig. 3.21 for HEXFET topology. Each of the figures presents some common characteristics:

- On the x axis, is plotted the value of electric field averaged inside epitaxial layer. By definition, this takes into account polarization and epitaxial layer thickness, i.e. technology and working conditions. In terms of SEB, it represents the state of a polarized component before it is reached by a particle.

- On the y axis, critical charge q_{th} is represented. It is the minimal quantity of charge to be deposited inside the epitaxial layer, that is required to produce an SEB inside the structure at a given electric field, i.e. for a given component and at a given polarization. In terms of SEB, its value takes into account the information about the injection (LET and impact location) and about SEB dynamics itself, because the way it is calculated.

- Every curve is composed by several branches, each one indicates the threshold charge values at different epitaxial layer thicknesses. The thicker is the epitaxial layer, the higher the charge required to trigger an SEB. The fact that different branches compose the same curve, removes SEB dependency from epitaxial layer thickness.

In order to eliminate the dependence from the impact location, a further synthesis is to read the previous three curves on the same scale, as shown in fig. 3.22. Location A is the most sensitive and thus has a lower q_{th}; at the same electric field (i.e. the same polarisation) for a given component, a heavy ion strike located in B or C needs to inject a higher level of charge inside epitaxial layer to trigger SEB.

An identical synthesis procedure has been applied to the STRIPFET technology, giving the representation of threshold charge q_{th} as a function of average electric field inside the epitaxial layer, as illustrated in fig. 3.23.

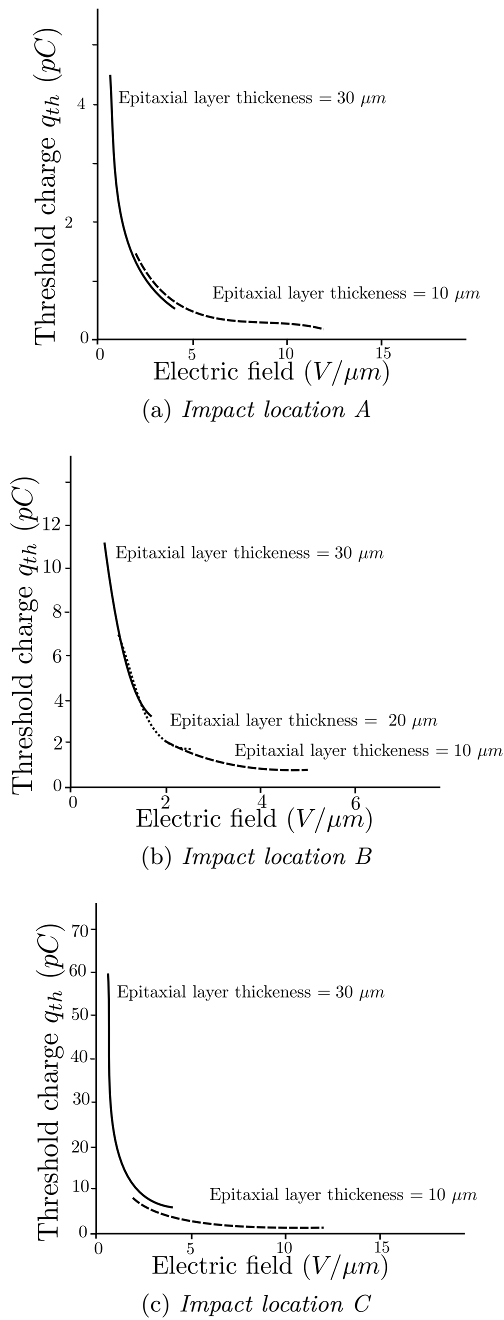

Figure 3.21 – Threshold charge versus average electric field at impact locations A, B, C inside the HEXFET structure. Each curve shows threshold charge for different values of epitaxial layer thickness

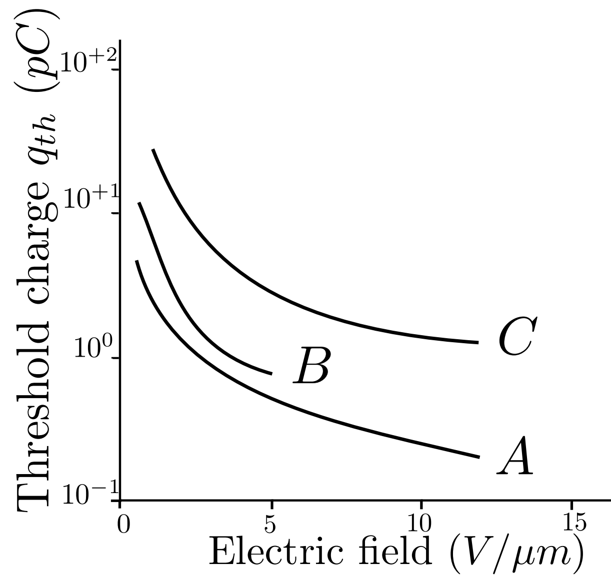

Figure 3.22 – Threshold charge as a function of average electric field inside the HEXFET topology. The 3 curves represents the three impact locations A, B, C

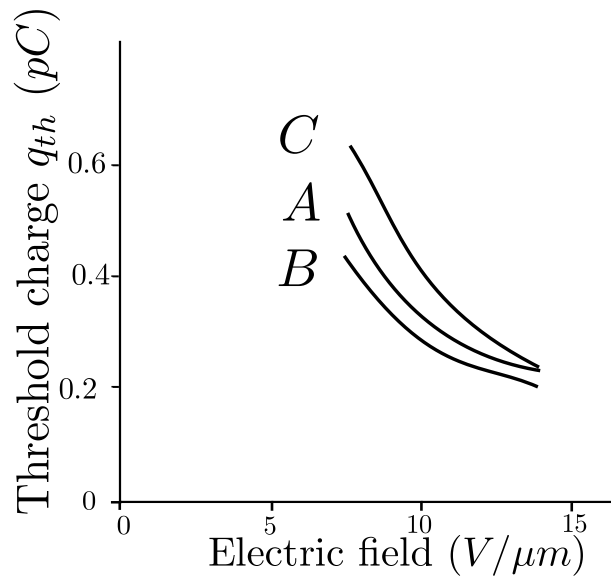

Figure 3.23 – Threshold charge as a function of average electric field inside the STRIPFET topology

Table 3.9 – HEXFET, values of k and z coefficients at different injection locations

	k	z
A	2.6577	1.05
B	6.4816	1.419
C	23.91	1.224

Table 3.10 – STRIPFET, values of k and z coefficients at different injection locations

	k	z
A	6.591	1.277
B	5.845	1.296
C	16.696	1.618

3.3.2 Choice of a mathematical representation of SEB physics

Since fig. 3.22 and fig. 3.23 are the base from which the prediction tool is issued, a necessary step to describe SEB phenomenology, has been its mathematical expression.

One can notice that, independently from the injection location and MOSFET technology, curves have a similar shape, as expected since they represent the same SEB dynamics. A fitting law has been chosen in order to better represent the curves

$$q_{th} = k\ EF^{-z} \tag{3.6}$$

where k and z are fitting coefficients, whose values depend on impact location and are listed in table 3.9 for HEXFET and in table 3.10 for STRIPFET technology.

This simple law contains SEB dependencies from polarization, epitaxial layer thickness and doping. The only explicit dependency is from impact location.

In this chapter, TCAD simulations have been used to identify and calculate triggering criteria for SEB inside Power MOSFETs, both in HEXFET and STRIPFET topologies. To do that, a 2D MOSFET structure has been built and compared to the datasheet of a 3D component, in order to evaluate a scale factor between the two configurations.

SEB has been studied by means of multiple sets of simulations of heavy ion injection, changing one physical parameter at a time, in order to better understand SEB dependencies on polarization, impact location and angle, epitaxial layer thickness and doping. At every simulation, critical charge has been evaluated.

Finally, all SEB dependencies have been synthesized plotting critical charge versus electric field, and a fitting law has been calculated in order to represent SEB

physics and its dependencies. This law is going to be the base of the predictive model developed in the next chapter.

Chapter

4 Construction of SEB rate prediction model based on deposited charge and electric field

The most effective way to do it
is to do it.

A. Earhart

In this chapter, DELPHY (Destructive effects prEdiction modeL based on PHysical analYsis) is developed as SEB rate prediction model, on the base of a criterion on deposited charge versus electric field inside MOSFET. First, TCAD simulation results are discussed in the optic of prediction, in order to determine inputs and outputs for DELPHY. This constitutes a general methodology for a transition from TCAD analysis to a prediction model of SEB generated by heavy ions.

Once the domain of the model is set, the above cited criterion on threshold charge is applied and DELPHY is developed around it. The model construction is thus detailed and leads to calculation of SEB cross sections. Also, the procedure is expanded to develop a prediction model for SEB generated by protons, taking into account differential probabilities of secondary ions generations inside a MOSFET structure.

4.1 Proposition of a methodology for transition from TCAD analysis to prediction model

In the previous chapter, an empirical law has been determined from TCAD simulations, which allows for calculating threshold charge inside the device, knowing electric field and impact location, regardless of the device topology. In this section, this law will be discussed and a methodology will be proposed to use it in order to build a SEB prediction model from it.

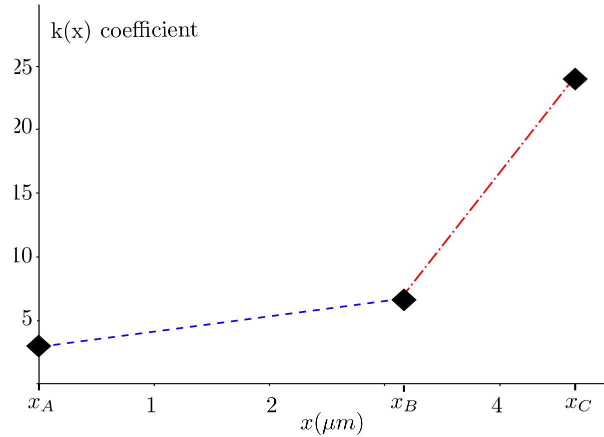

Figure 4.1 – $k(x)$ values versus heavy ion impact location, from TCAD simulations of a HEXFET structure, and piecewise linear law

4.1.1 Discussion of the empirical law for threshold charge

As seen in the previous chapter, TCAD simulations aided to perform a deep analysis of SEB dependencies from several parameters, and most of all to synthesize them using an empirical law for calculation of threshold charge q_{th} knowing electric field EF and impact location x

$$q_{th} = k(x)EF^{-z} \tag{4.1}$$

where $k(x)$ is a coefficient that changes accordingly to impact location x, defined as

$$x = x_{HI} - x_A \tag{4.2}$$

where x_{HI} is the generic heavy ion impact location. The definition of x takes into account the fact that the three values of x considered, come from the heavy ion impact locations studied with TCAD: x_A, x_B, x_C. In reality, a heavy ion can impact on any point of the MOSFET surface, so it is important to extend $k(x)$ to a larger domain which represents MOSFET area, as it is done with the definition of x itself in (4.2). Since now onwards in this manuscript, when referring to heavy ion impact location x_{HI}, it is the relative impact location x that is considered.

Fig. 4.1 shows $k(x)$ values versus impact location, as well as the studied piecewice linear law. The choice of coefficients is made to minimize the average error for all the three points to be fitted. The piecewise linear law requires to identify the angular point where the two linear curves overlap. This is easy to perform because it coincides exactly with impact location x_B, so its characteristics are well known in terms of threshold charge q_{th_B}.

As for the STRIPFET structure, a similar piecewise linear function law for $k(x)$ has been calculated, with the shape illustrated in fig. 4.2.

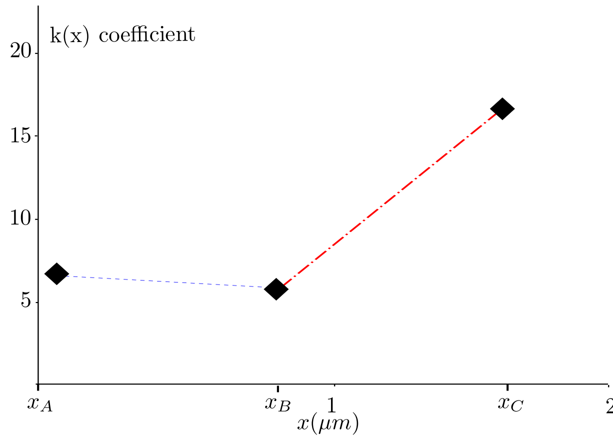

Figure 4.2 – Piecewise linear law to express $k(x)$ in the STRIPFET structure

Once $k(x)$ piecewise linear law extracted, the expression (4.1) is known and detailed in every part as a function of x, and thus ready to be used as the key of SEB prediction model.

4.1.2 Definition of SEB prediction criterion

Starting from the expression of threshold charge versus electric field, one can define the physical criterion on which DELPHY is based

$$q_{epi} \geqslant q_{th} \Longrightarrow SEB \tag{4.3}$$

where q_{epi} is the charge deposited inside the epitaxial layer by the heavy ion, and q_{th} is the threshold charge. Taking into account (4.1), the criterion becomes

$$q_{epi} \geqslant k(x)EF^{-z} \Longrightarrow SEB\ . \tag{4.4}$$

From a physical point of view, it means that when the heavy ion impacting in a certain location of MOSFET surface, deposes inside the epitaxial layer a charge that equals or is greater than threshold charge at that location, then the device will undergo a Single Event Burnout.

4.1.3 Derivation of model INPUTs and OUTPUTs

From the definition of the operational criterion on which stands the prediction, also INPUTs and OUTPUTs of the model are defined: in order to calculate average electric field inside the epitaxial layer, one has to know MOSFET polarization and epitaxial layer thickness. Particle LET and impact location have to be known, as well as coefficient description for $k(x)$, and z, and MOSFET cell characteristic dimension.

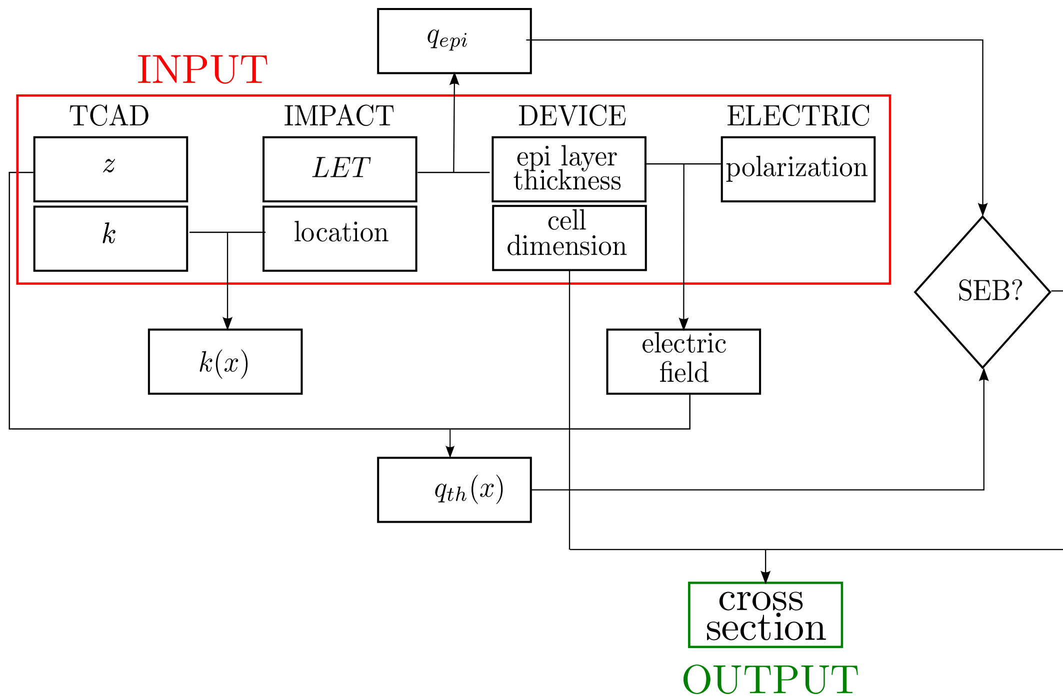

Figure 4.3 – INPUTs and OUTPUTs of DELPHY

In return, the model DELPHY will calculate SEB cross section for a MOSFET cell, and if the number of cells is known, also for the device. An overall vision of model INPUTs and OUTPUTs in given in fig. 4.3.

4.2 Development of DELPHY for SEB generated by heavy ions

Once INPUTs and OUTPUTs defined, the model has been built around the criterion, through geometry considerations.

DELPHY development has been inspired by the Rectangular Parallelepiped (RPP) concept, very popular in SEE prediction. RPP models rely on the principle of defining a sensitive structure inside the component (a rectangular parallelepiped indeed), and evaluate the deposited charge inside it with respect to a threshold charge to trigger the Single Event Effect. In the case of a SEB inside a power MOSFET, this basic concept of modelling has to be refined in order to take into account the peculiarity of SEB and most of all its dependencies from the variety of physical parameters previously described. Also, a rectangular parallelepiped becomes insufficient to describe SEB sensitive area inside a HEXFET or a STRIPFET. For these reasons, the choice of the geometric sensitive volume has to be further improved.

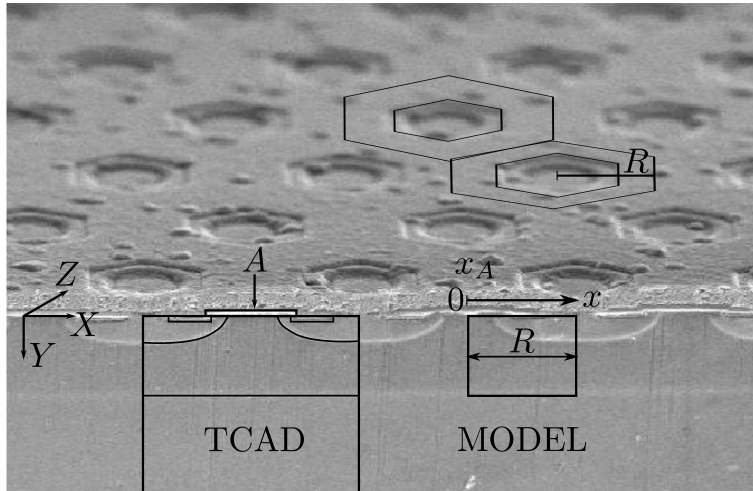

Figure 4.4 – Transition from TCAD geometry to model geometry for a HEXFET structure

4.2.1 DELPHY geometry for HEXFET topology

In order to build the prediction model, all considerations on the choice of threshold charge have been made from a TCAD simulated MOSFET cell. When using the subsequent results to build the model, a similar geometric structure has to be implemented in order to ensure continuity, while on the other hand a maximum of simplification is desirable, as well as easy to implement, taking into account cell intrinsic symmetry.

Knowing the device geometry has permitted to apply the triggering law inside it and calculating Single Event Burnout cross sections. The foundation of this procedure is the identification of modular structures inside the device, such as elementary hexagonal cells for a HEXFET topology. The cross section is calculated as the sensitive surface inside a single cell, which is likely to trigger an SEB under a heavy particle impact. It has a hexagonal annulus shape, whose width is determined by the triggering criterion on threshold charge with respect to electric field inside the epitaxial layer. Fig. 4.4 illustrates the transition from TCAD geometry to model geometry, and introduces the used symbolism. R is the total width of the model cell along x axis. It corresponds to the apothem of the considered hexagon, which includes source contact and the surrounding gate metallization, in order to have a replicable unit that covers all MOSFET surface (see fig. 4.4). The origin of the x axis is in x_A, where A is the impact location studied in the TCAD analysis. The width of a minimum TCAD cell is double the width of a minimum model cell, because in TCAD simulations all physics aspects are taken into account, while the model itself only uses the resulting threshold charge criterion and applies to the simplest

geometry possible.

Another difference between TCAD and model geometries, is the thickness of the studied area: the former has been detailed in the previous chapter and includes epitaxial layer and substrate; the latter instead, only includes epitaxial layer, since it is the zone where electric field has relevant values and where deposited charge is evaluated.

Both the TCAD and model geometries are 2D on the $< XY >$ plane; nevertheless, since the model output is a cross section σ, i.e. a SEB sensitive surface on the $< XZ >$ plane, a further step has to be made to achieve this plane transition. The parameter that connects the two planes is R, which is the width of the rectangular sensitive area of the model, and hexagon apothem.

4.2.2 DELPHY geometry for STRIPFET topology

Analogue geometric considerations have been made for the STRIPFET topology: a geometric frame has been implemented in DELPHY, whose characteristics reflect those of the TCAD simulated MOSFET cell. The identified modular structures inside the device are elementary striped cells for a STRIPFET topology. The cross section is calculated as the sensitive surface inside a single cell, which is likely to trigger an SEB under a heavy particle impact. It has a rectangular shape, whose width is determined by the triggering criterion on threshold charge with respect to electric field inside the epitaxial layer, and whose height comes from reverse engineering measurement of the device active surface. Transition from TCAD geometry to model geometry for a STRIPFET structure is illustrated in fig. 4.5. R is the total width of the model cell along x axis. It corresponds to the width of the considered strip, which includes source contact and the surrounding gate metallization, in order to have a replicable unit that covers all MOSFET surface (see fig. 4.5). The origin of the x axis is in x_A, where A is the impact location studied in the TCAD analysis. The width of a minimum TCAD cell is double the width of a minimum model cell, because in TCAD simulations all physics aspects are taken into account, while the model itself only uses the resulting threshold charge criterion and applies to the simplest geometry possible.

Another difference between TCAD geometry and model geometry, is the thickness of the studied area: the former has been detailed in the previous chapter and includes epitaxial layer and substrate; the latter instead, only includes epitaxial layer, since it is the zone where electric field has relevant values and where deposited charge is evaluated.

Both the TCAD geometry and model geometry are 2D on the $< XY >$ plane; nevertheless, since the model output is a cross section σ, i.e. a SEB sensitive surface on the $< XZ >$ plane, a further step has to be made to achieve this plane transition. The parameter that connects the two planes is R, which is in turns the width of the rectangular sensitive area of the model, and the width of the elementary strip.

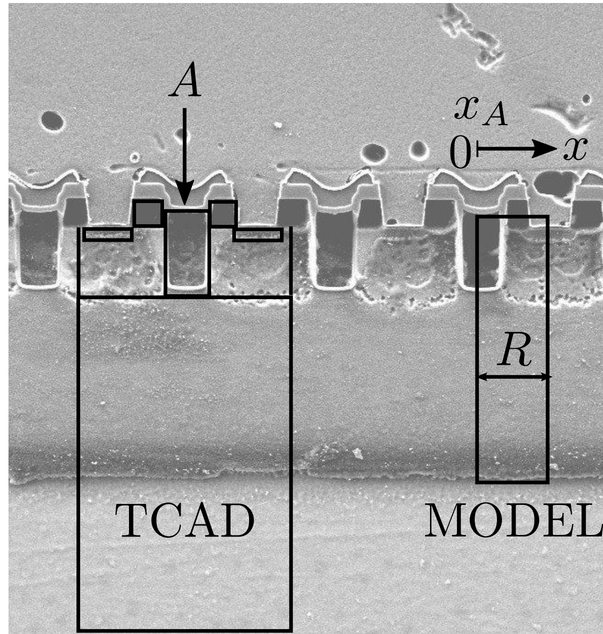

Figure 4.5 – Transition from TCAD geometry to model geometry for a STRIPFET structure

4.2.3 Implementation of the threshold charge criterion

Once all aspects of the geometry are clearly defined for each topology, the implementation of SEB criterion inside geometry makes the model. Referring to fig. 4.3 and to (4.4), the considered SEB criterion evaluates the deposited charge inside epitaxial layer with respect to the threshold charge at a certain location and bias condition, whose value comes from TCAD results and mathematical fitting. Fig. 4.6 illustrates the concept from a geometric point of view, and introduces $\xi = (R - r)$, i.e. the coordinate along x axis of the point where deposited charge equals threshold charge.

The definition of ξ is essential to implement the criterion, because the impact location of the heavy ion can not be calculated nor determined beforehand, leaving x as an unknown INPUT, with respect to fig. 4.3. From (4.3), ξ is defined as

$$q_{epi} = q_{th}(x) \mid_{x=\xi} \tag{4.5}$$

and taking (4.4) into account, it becomes

$$q_{epi} = k(\xi) E F^{-z} \ . \tag{4.6}$$

Solving (4.6) gives the value of ξ and thus of $r = (R - \xi)$, which is going to be implemented to calculate SEB cross section.

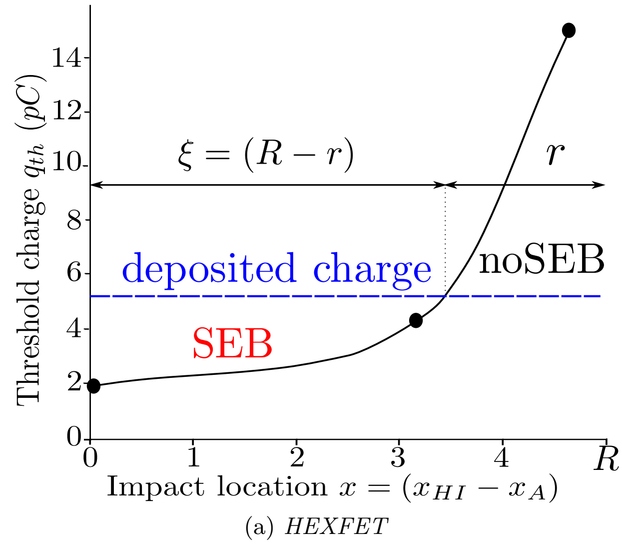

(a) *HEXFET*

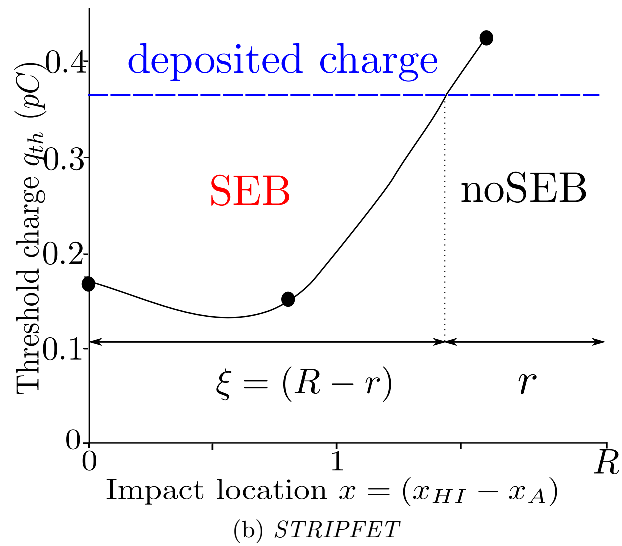

(b) *STRIPFET*

Figure 4.6 – Geometrical illustration of SEB criterion used in this work for HEXFET ans STRIPFET topologies

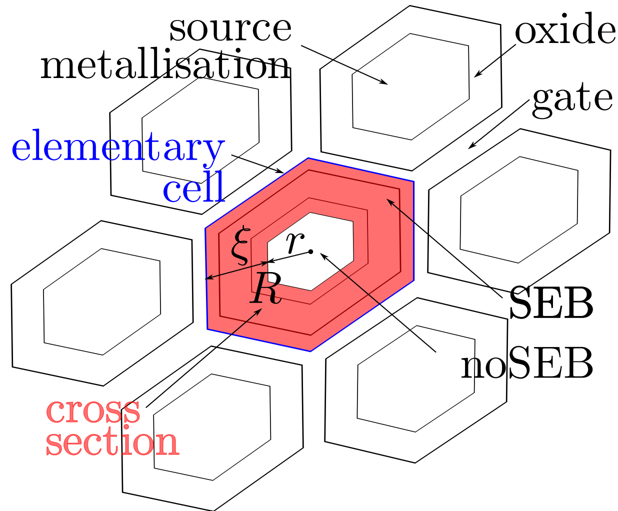

Figure 4.7 – Elementary cell and hexagon annulus as visual representation of SEB cross section σ_{HI} in HEXFET technology

4.2.4 Cross section calculation for heavy ion generated SEB

The definition and calculation of ξ is a key step to determine SEB cross section σ_{HI}. By definition, a SEB cross section is the portion of component surface that is sensitive to Burnout: when a heavy ion hits this sensitive surface, it is likely to trigger a SEB, while no SEB will be triggered when the heavy ion hits the non sensitive portion of the surface. Intuitively, the larger is the cross section σ_{HI}, the higher is the probability of a heavy ion to trigger a SEB. In the present model, since the component surface has been divided in single cells, σ_{HI} will be calculated with respect to total reference cell surface.

For the HEXFET configuration, each reference cell has a hexagonal shape, thus cross section has the shape of a hexagonal annulus (see fig. 4.7). In literature and in the previous chapter, the hexagon center has been demonstrated to be the less sensitive area of the surface, so the hexagonal annulus tends to become a full hexagon in the case of high SEB sensitivity. In order to calculate SEB cross section, the area of the hexagonal annulus has been calculated as a difference between the hexagonal area of apothem R and the one with apothem r. This procedure, illustrated in fig. 4.8, has the advantage to take into account SEB physics and heavy ion characteristics: the curve of threshold charge $q_{th}(x)$ comes from TCAD analysis and thus accounts for injection location, MOSFET bias, doping and geometry, while deposited charge depends on particle LET. To calculate SEB cross section for the entire device, it is sufficient to multiply the cell cross section by the number of cells.

In the case of a STRIPFET topology, each reference cell has a strip shape, thus the cross section has the shape of a rectangle (see fig. 4.9). The higher is the

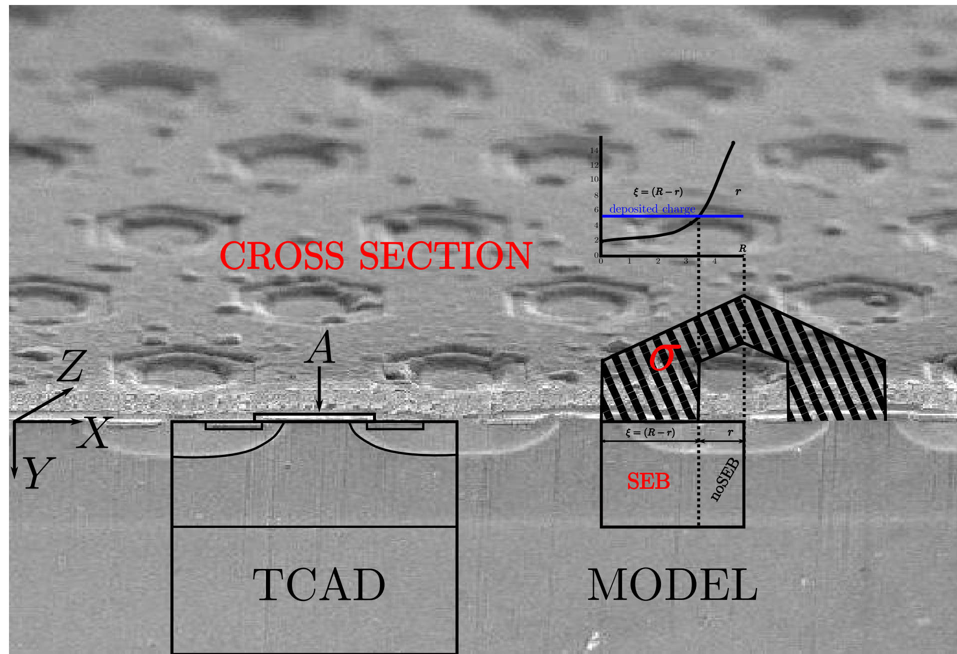

Figure 4.8 – Transition from TCAD and model geometries to σ_{HI} cross section calculation in HEXFET technology

device sensitivity to SEB, the larger is the surface of cross section, whose limit is the total strip cell surface. Fig. 4.10 shows MOSFET geometrical entities used for the calculation of SEB cross section: ξ is the rectangle width coming from the implementation of the criterion on threshold charge (see fig. 4.6b), while Λ is the strip length, whose value has been found through reverse engineering; for the studied STRIPFET component, $\Lambda = 1.029\ mm$. By multiplying cell cross section for the number of cells, device cross section is obtained.

In both HEXFET and STRIPFET topologies, the implementation of threshold charge criterion allows for calculating the cell and device cross section at a given particle LET. Indeed, if this simple procedure is iterated for different LET values, a σ_{HI} versus LET curve is issued as in fig. 4.11, and it is comparable to irradiation data available in the literature. The iteration over a LET range completes the procedure for a didactic approach to SEB prediction.

DELPHY model also provides heavy ion SEB cartographies, as shown in fig. 4.12 for the HEXFET configuration.

In the next section, its results in terms of cross section curves are evaluated and compared to experimental data, and a coefficient is calculated and suggested to convert the didactic model into an operational one.

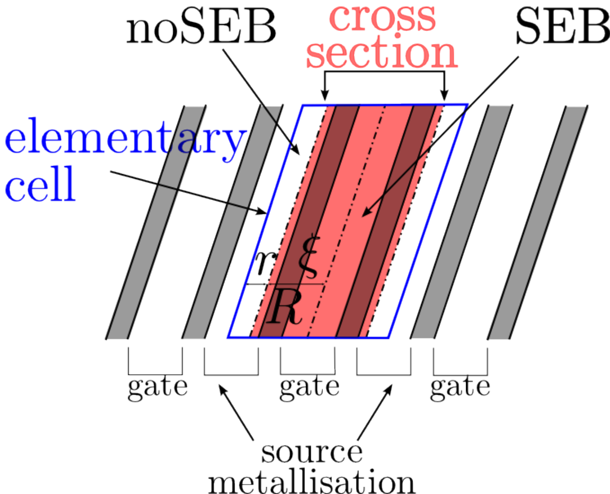

Figure 4.9 – Elementary cell and rectangle as visual representation of SEB cross section σ_{HI} in STRIPFET technology

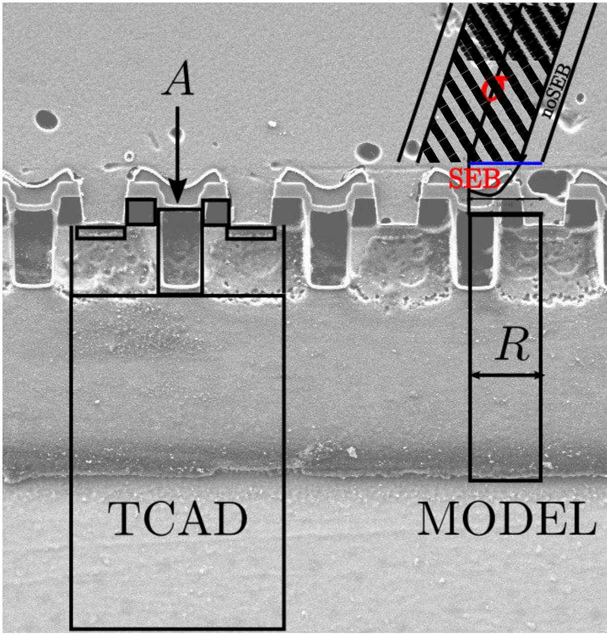

Figure 4.10 – Transition from TCAD and model geometries to σ_{HI} cross section calculation in STRIPFET technology

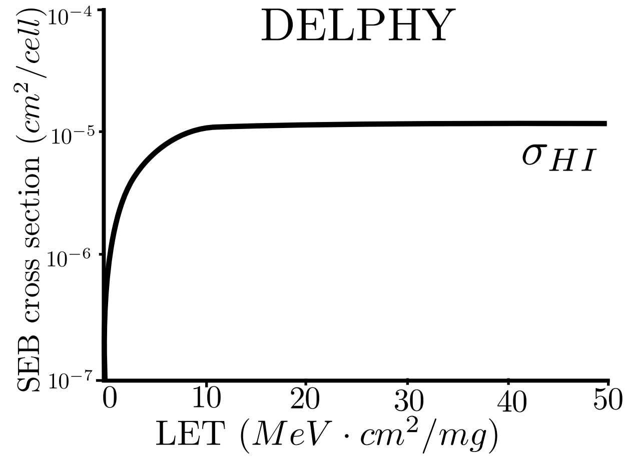

Figure 4.11 – σ_{HI} cross section per cell versus LET

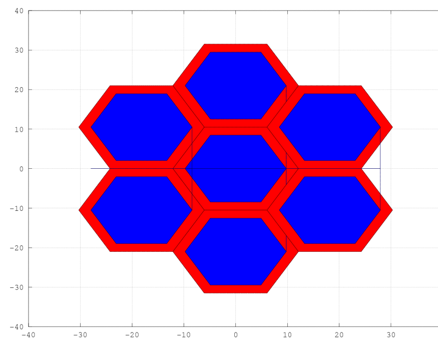

(a) $V_{DS} = 200\ V$

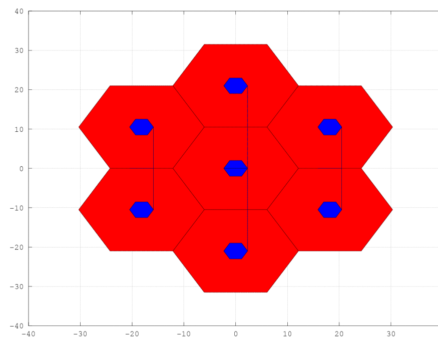

(b) $V_{DS} = 320\ V$

Figure 4.12 – Heavy ion SEB cartographies for the HEXFET component, calculated by DELPHY. Red area is SEB sensitive

Table 4.1 – Linear and piecewise linear laws to describe $k(x)$ in the STRIPFET structure

Ion	$LET(MeV cm^2/mg)$	Range (μm)
Kr	34	43
Ni	20.6	98
Ar	10.1	119
Ne	3.3	199
C	1.2	266

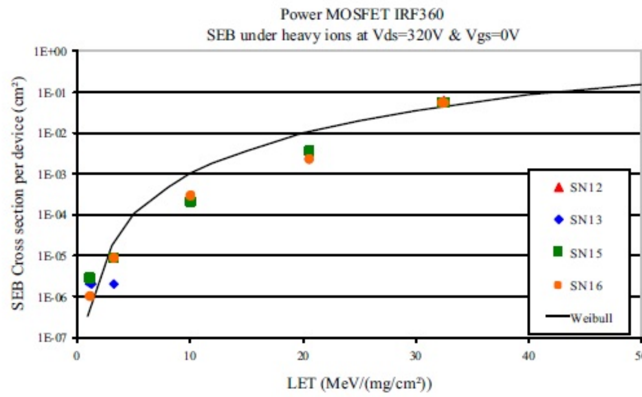

Figure 4.13 – Heavy ion irradiation data from [10]

4.3 Comparison with heavy ion irradiation data

The methodology to calculate heavy ion SEB cross section through DELPHY, has been applied to the case of a real HEXFET component: IRF360, whose heavy ion SEB characterization was published in [10].

4.3.1 Test configuration

Heavy ions tests have been performed by CNES on samples from CARMEN2-MEX flight-lot procured by THALES ALENIA SPACE ETCA. Tests were run by TRAD on their power MOSFET test system. Heavy ions tests took place at UCL. Gate and source were short-circuited to 0 V and the applied bias was $V_{DS} = 320\ V$. Table 4.1 shows the characteristics of the heavy ions used. More test details are available in [10], while test results are illustrated in fig. 4.13.

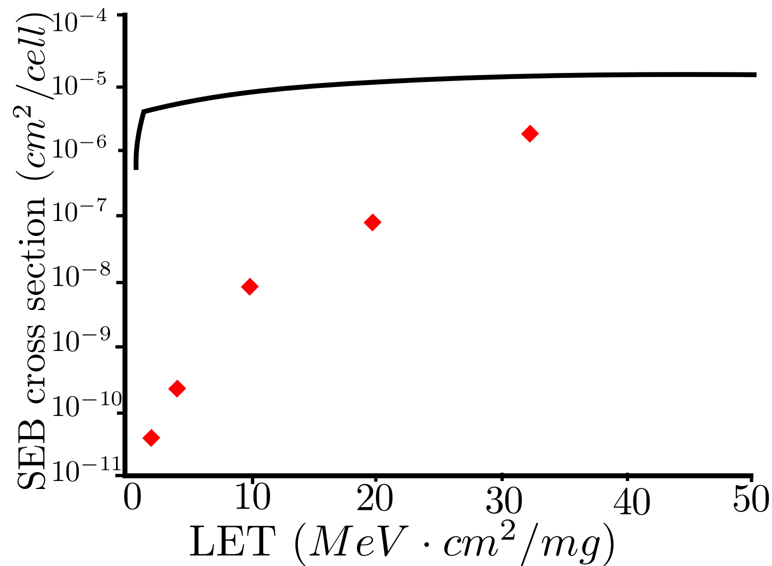

Figure 4.14 – σ_{HI} cross section per cell versus LET: black continuous curve is calculated with prediction model, while red dots are from [10]

4.3.2 Comparison

Fig. 4.14 shows the comparison between the calculated σ_{HI} and irradiation data published in [10]: it is evident that a calibration is needed to predict SEB in a real component.

The prediction model overestimates SEB risk with respect to irradiation data. The reasons for this difference of cross section values reside in the procedure and the approximations used to build the model itself, which will now be discussed.

4.3.3 Effect of mathematical fitting of $k(x)$

As shown in fig. 4.1, a piecewise linear fitting law for $k(x)$ has been determined. It is now discussed how this choice has an influence on cross section curve.

A way to improve model prediction for cross section, would be a better description of $k(x)$ coefficient, featuring a larger number of points in the curve, with a consequent calculation a a new fitting law. From a physical point of view, this would mean the investigation of SEB threshold charge in more than three impact locations.

4.3.4 Effect of 2D/3D diffusion

A further reason why predicted SEB cross section does not coincide with irradiation data, is the fact that it is based on a criterion defined from 2D TCAD analyses, which are not at all comparable to a real MOSFET. This difference has been explained

and quantified in § 3.1.4, both from geometrical and physical point of view: it has been calculated that 2D simulations tend to overestimate electron concentration over time, because they can not model 3D diffusion phenomena (see fig. 3.7). Indeed, the presence of a 68% higher electron concentration makes the 2D structure more sensitive to SEB, thus diminishing SEB threshold charge q_{th}: this is believed to be a cause of higher cross section values. A correction of 68% has thus been applied to the TCAD calculated threshold charge, but does not lead to a significant improvement of the prediction.

4.4 Cross section calculation for proton generated SEB

Once heavy ion cross section is calculated, DELPHY takes into account secondary heavy ion generation rate to compute proton cross section as a function of impacting proton energy.

4.4.1 Secondary heavy ion generation by proton impact

When a proton impacts on a target material, it generates secondary particles according to the nature of the material itself and its chemical structure. In the case of a MOSFET, the proton is impacting on a silicon block, thus the possible secondary particle which are generated are ions from hydrogen to phosphorus (see § 2.4).

According to proton energy, secondary generation rates change, and a nuclear cross section σ_N is defined to take into account this dependency. It is measured in $barn = E^{-24}\ m^2$, because it is defined as $\sigma_N = \pi\rho^2$, where $\rho = E^{-12}\ m^2$ is the typical nuclei radius of the target material. Fig. 4.15 shows the microscopic nuclear

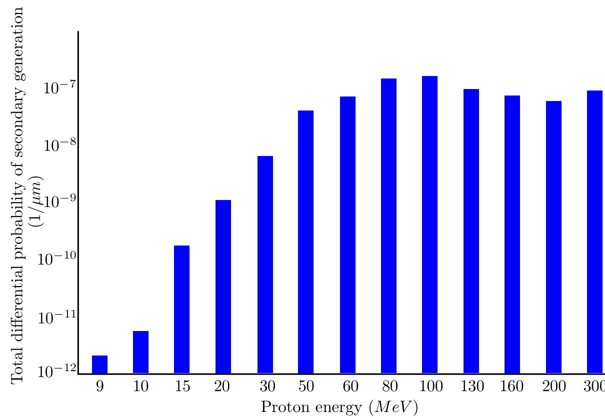

Figure 4.15 – Total differential probability per μm to generate a heavy ion by proton impact, versus proton energy.

cross section as a function of impacting proton energy. Since there is no deterministic

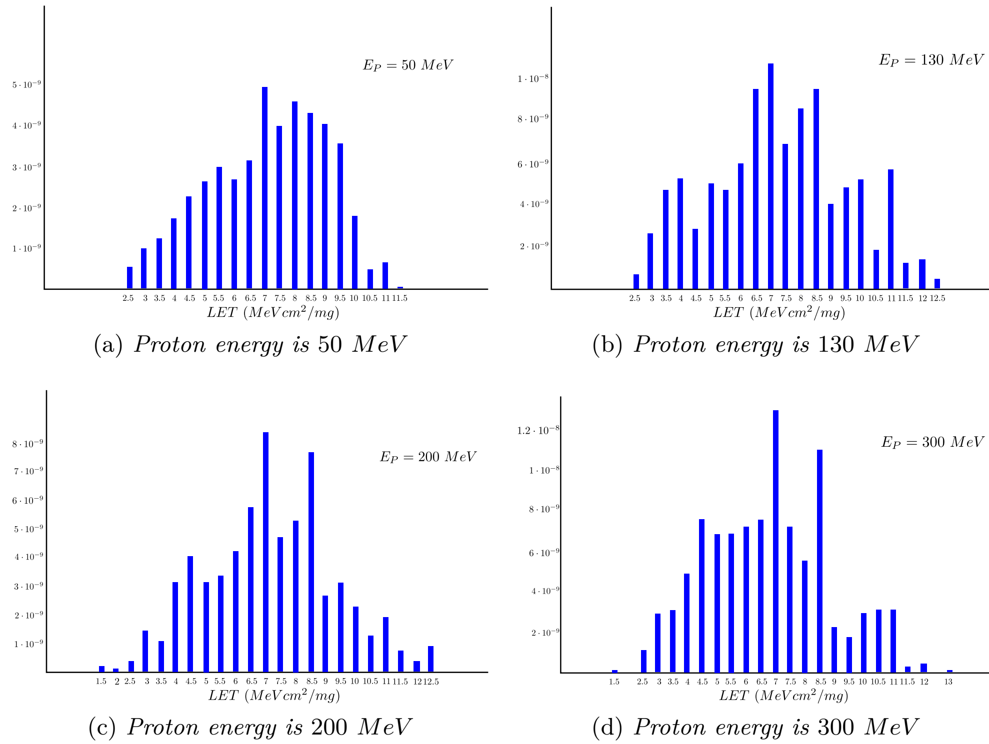

(a) *Proton energy is* 50 MeV (b) *Proton energy is* 130 MeV

(c) *Proton energy is* 200 MeV (d) *Proton energy is* 300 MeV

Figure 4.16 – LET spectra of secondary ions generation differential probability, as a function of proton energy

law to predict the nature of the reaction between proton and the target material, the secondary reaction can not be predicted in terms of generated particles and their energy characterization. For this reason, a probabilistic approach is needed when treating secondary generation.

ONERA disposes of a statistically significant database of nuclear reactions, created through GEANT 4 simulator. In order to be used for the specific calculation of the DELPHY model, this rough database has been filtered according to the specificities of this study. Two main filtering criteria were used:

- the atomic number Z of the secondary particle is selected to be greater than 4, in order to exclude all the lighter particles as alphas and light ions; they have in fact long ranges inside the target material but low relevance for SEB triggering as they deposit low energy along the track;
- the track length is set to be lower or equal to the epitaxial layer thickness of the considered MOSFET, in order to be coherent with DELPHY geometry settings.

By means of these criteria, it has been possible to calculate the differential probability of secondary ions generation inside the studied power MOSFETs, as a function of the impacting proton energy. Furthermore, proton energy has an influence not only on the total nuclear cross section as shown in fig. 4.15, but also on its LET spectrum, as illustrated in fig. 4.16. In fact, a secondary ion of a given LET has different probabilities of being generated by impact of protons with different energies. Also, fig. 4.16 shows that there is no deterministic law to predict secondary LET generation as a function of the impacting proton energy, thus making the probabilistic way the only possible approach. Another fact to be noticed is the physical coherence of LET values, which do not go over 15 $MeV cm^2/mg$, as illustrated by Ziegler's tables [97] and explained in § 2.4.

4.4.2 Proton SEB cross section calculation

Once the database of secondary generation filtered, and the probabilistic generation rates extracted which are pertinent with the structures studied in this work, they have been coupled with the heavy ion SEB cross sections σ_{HI}. In fact, proton SEB cross section σ_P is defined as

$$\sigma_P = \int h_{epi} \frac{dc_{LET}}{dLET} \sigma_{HI}(LET) \, dLET \tag{4.7}$$

where h_{epi} is the epitaxial layer thickness, and $\frac{dc_{LET}}{dLET}$ is the differential secondary ions generation probability, discussed in § 4.4.1.

A simple way of calculating the integral in (4.7) is to represent the differential generation probability $\frac{dc_{LET}}{dLET}$ as a (m, n) matrix

$$C = \begin{bmatrix} c_{11} & c_{12} & \cdots & c_{1n} \\ c_{21} & c_{22} & \cdots & c_{2n} \\ \vdots & \vdots & \ddots & \vdots \\ c_{m1} & c_{m2} & \cdots & c_{mn} \end{bmatrix} \tag{4.8}$$

which describes m possible proton energies generating n possible heavy ion LET with a probability of $c_{m,n}$.

Defining H as the $(n, 1)$ vector of heavy ion SEB cross sections, calculated at n LET values, and P as the $(m, 1)$ vector of proton SEB cross sections, calculated at m proton energies

$$H = \begin{bmatrix} h_1 \\ \vdots \\ h_n \end{bmatrix} \qquad P = \begin{bmatrix} p_1 \\ \vdots \\ p_m \end{bmatrix} , \tag{4.9}$$

allows to rewrite (4.7) as

$$C \cdot H = P \, . \tag{4.10}$$

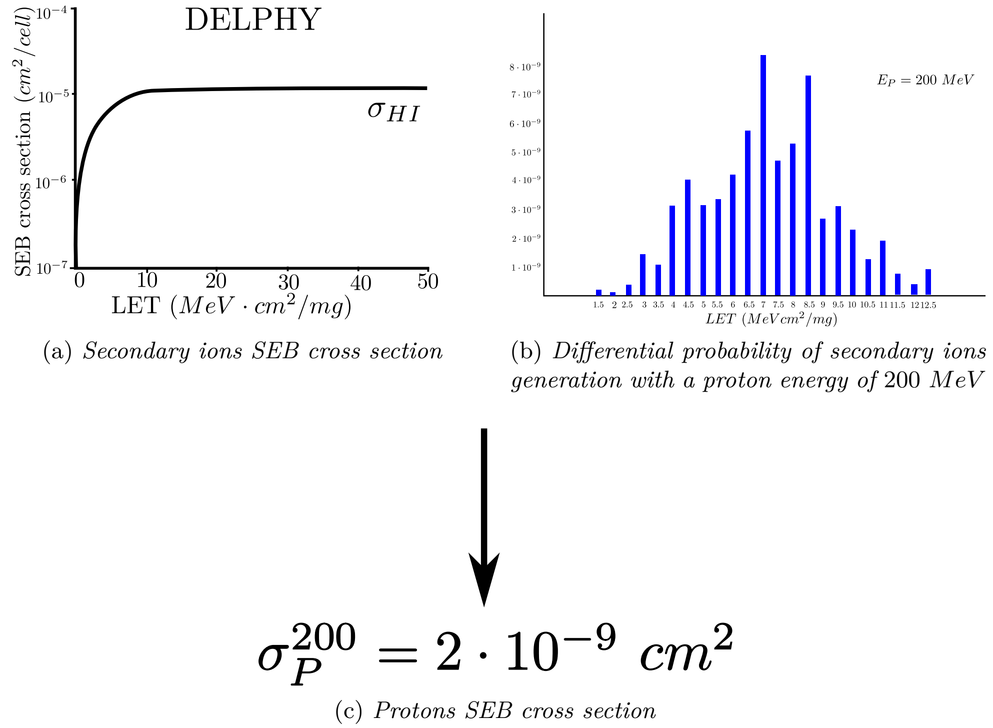

(a) *Secondary ions SEB cross section*

(b) *Differential probability of secondary ions generation with a proton energy of* 200 MeV

(c) *Protons SEB cross section*

Figure 4.17 – Calculation of protons SEB cross section by convolution of secondary ions SEB cross section and secondary ions generation probability. Proton energy is 200 MeV

Then, solving the linear system of equations in (4.10), gives proton SEB cross sections at m proton energies.

Fig. 4.17 gives a visual representation of the approach. SEB cross section σ_P is in fact calculated for an impacting proton energy of 200 MeV, by convolution of heavy ion SEB cross section σ_{HI} (fig. 4.17a) with differential heavy ion generation rate at a proton energy of 200 MeV (fig. 4.17b). The same convolution procedure can be repeated at different proton energies; the total result is the proton cross section curve visible in fig. 4.18.

4.5 Comparison with proton irradiation data of STRIPFET

The proton SEB cross section calculated with DELPHY has been compared to irradiation data on a STRIPFET device performed by CERN at the PSI (Paul Scherrer Institute) [14]. The frame of this comparison is a study conducted together by CERN and ONERA, in order to evaluate SEB sensitivity to proton irradiation for

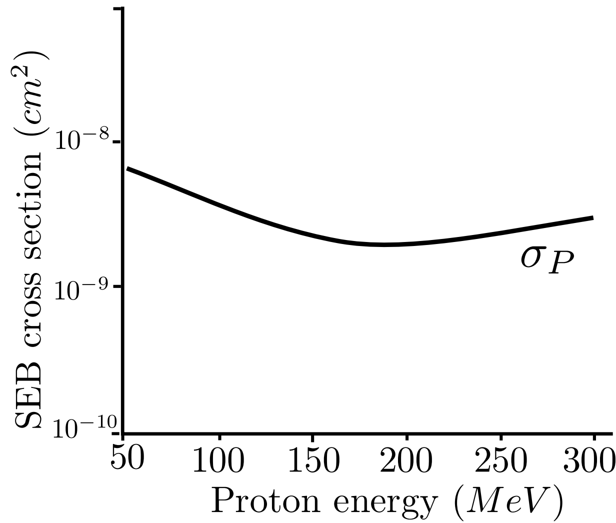

Figure 4.18 – Proton SEB cross section versus proton energy

the devices that could be used in the next generation of the LHC (Large Hadron Collider) power converters.

4.5.1 Test configuration

Devices have been irradiated with 230 MeV protons in a static configuration, when they are more vulnerable. For this reason, the gate and source have been short-circuited to keep the DUT in the OFF state, and drain source bias $V_{DS} = 30\ V,\ 40\ V,\ 55\ V$ was applied.

A non destructive test procedure was applied according to method 1080 in the MIL-STD-750E, in order to achieve high amounts of SEB events without damaging the devices. A more detailed description of test procedure and results is given in [14].

4.5.2 Comparison

Even though a non destructive test configuration was applied, devices were subjected to destructive SEB events. While a deep analysis of the effectiveness of test methodology is given in [70], the necessity arose for a physical evaluation of the phenomenon through DELPHY prediction model.

DELPHY calcluations have been performed using the methodology so far described, that is to say: first evaluating heavy ion SEB cross section through TCAD analysis and the criterion on threshold charge, and then applying (4.10) to calculate proton SEB cross section at a proton energy of 230 MeV.

Table 4.2 – Proton SEB cross section by CERN and by DELPHY

	Cross section (cm^2)
CERN	$8.39E^{-10} < 9.46E^{-10} < 1.05E^{-9}$
DELPHY	$2.5E^{-9}$

The comparison showed an agreement in the order of magnitude of SEB rates, as presented in table 4.2. Also, an explanation of the relatively high SEB sensitivity of the device has been given, taking into account the deep physical analysis performed in § 3.

The present work has shown that the STRIPFET structure is more sensitive to SEB than the HEXFET. The difference between the two topologies lies not only in their elementary geometrical shape, but also in their dimensions, resulting in a much more integrated technology for the STRIPFET. The different order of magnitude of the two structures (see table 3.1) is believed to be responsible for the higher SEB sensitivity of the STRIPFET, regardless of secondary generation conditions in terms of location and tilt inside the epitaxial layer.

In this chapter, DELPHY (Destructive effects prEdiction modeL based on PHysical analYsis) has been developed to predict SEB rate, on the base of a criterion on deposited charge versus electric field inside MOSFET. First, TCAD simulation results have been discussed to determine INPUTs and OUTPUTs for DELPHY.

Secondly, the application of the criterion on threshold charge has determined the construction of DELPHY model. Heavy ion SEB cross section has been calculated and compared to characterization performed by CNES for the HEXFET device IRF360. The comparison shows the need of a calibration, since DELPHY overestimates SEB sensitivity. Several explanations of the overestimation have been given and some enhancements have been made.

A further step has been to take into account differential probabilities of secondary ions generations inside a MOSFET structure, in order to develop a prediction model for proton generated SEB. The calculated proton SEB cross sections are compared with experimental data in the frame of a joint ONERA-CERN study on STRIPFET devices characterization, and the comparison shows a good agreement in the order of magnitude. Also, a reflection has been made on the difference between the two prediction cases of HEXFET and STRIPFET.

Chapter

5 Extension of SEB cross section calculation from irradiation data

Fatto trenta, facciamo trentuno.
(In for a penny, in for a pound.)

Proverb

This chapter presents an extension of DELPHY capabilities: the prediction model is used to calculate proton SEB sensitivity based on heavy ion irradiation data, and vice versa. In fact, INPUT heavy ion cross section does not come from SEB modelling, but from irradiation data instead.

The methodology is applied to IRF360, a component whose SEB characterization had been published in [10], both in terms of heavy ion and proton cross section.

Proton SEB cross section has been calculated from heavy ion SEB cross section, and taking into account differential probability of secondary ion generation by proton impact inside the device. The calculated proton SEB sensitivity is compared to published heavy ion cross section.

In the second part of this chapter, the reverse procedure is applied, in order to calculate heavy ion SEB cross section from proton SEB cross section. The calculated heavy ion SEB sensitivity is then compared to published cross section, thus enlightening advantages and limitations of the methodology.

5.1 Motivation of SEB sensitivity calculation from irradiation data

Before going into details of calculation methodology and comparison of cross section, a few words have to be spent on the interest of this procedure.

In the frame of the present work, cross section calculation from irradiation data marks quite the difference with respect to SEB prediction from TCAD modelling. As seen in chapters 4 and 3, in order to predict SEB cross section, DELPHY performs a TCAD investigation to extract threshold charge q_{th} to be used as a criterion

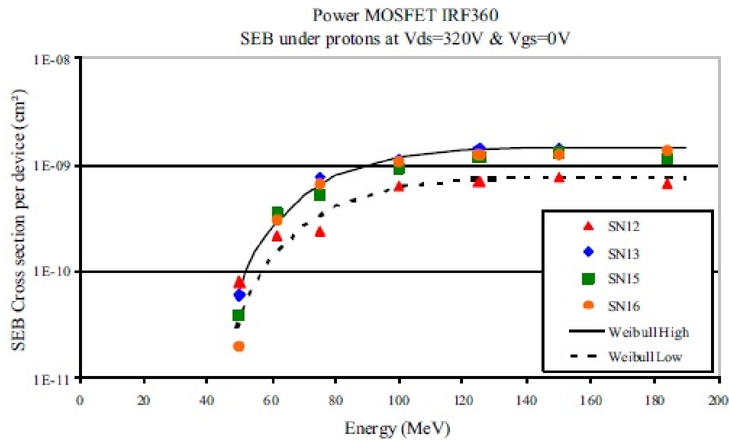

Figure 5.1 – Proton irradiation data from [10]

inside the geometry defined according to device technology. This represents a reasonable amount of information and work to be performed in order to characterize a component with respect to SEB sensitivity.

Sometimes, however, irradiation data might already be available, either in literature or following dedicated tests. The procedure presented in the present chapter, thus comes handy in these cases, as is in the published work that has been chosen to validate this work.

5.2 Test configuration and results for IRF360

The extension of DELPHY presented in this chapter, needs to be validated with irradiation data for both heavy ions and protons. For this reason, the same published work from Bezerra *et al.* [10] used in chapter 4, has proven to be useful also as a general evaluation of the method illustrated in § 4.4.2.

While heavy ion test configurations and results have already been presented in § 4.3.1, proton tests are now presented. Proton irradiation tests were performed by CNES at KVI, at proton energies of 50 MeV, 62 MeV, 75 MeV, 100 MeV, 125 MeV, 150 MeV, 184 MeV. Characterization under protons has been performed with both counting and verification modes. The results using counting mode are given on fig. 5.1, while fig. 5.2 shows the visible effects of a proton generated SEB. More details are available in [10].

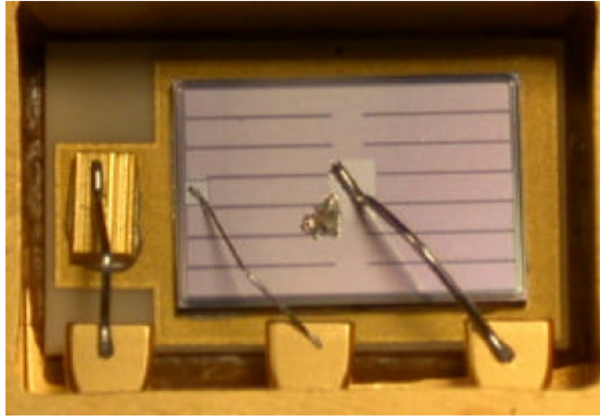

Figure 5.2 – Picture of proton induced SEB in a IRF360 ($V_{DS} = 320\ V$ and $V_{GS} = 0\ V$), from [10]

5.3 Calculation of proton cross section

Proton SEB cross section calculations by DELPHY have thus been compared to proton irradiation data published in [10].

In order to calculate proton cross section, in the previous chapter the INPUT heavy ion cross section σ_{HI}, represented by the $(n, 1)$ vector H in (4.10), has been obtained by DELPHY prediction model. In this chapter instead, it comes from irradiation data.

The calculation is based on (4.10), where C is the (m, n) matrix of differential generation probability $\dfrac{dc_{LET}}{dLET}$.

For this reason, heavy ion irradiation data (as in fig. 4.13) have been used as an entry in

$$C \cdot H = P \tag{5.1}$$

in order to calculate proton SEB cross section σ_P in the form of the vector P.

The solution of the linear system in (5.1) gives the curve illustrated in dotted black in fig. 5.3.

The comparison of the curves from irradiation and from the calculations shows a good SEB prediction performed by DELPHY. The overall estimation of SEB cross section has the same order of magnitude of the experimental curve.

Nevertheless, there is room for improvement in terms of threshold LET and saturated cross section. A possible way to enhance SEB prediction is in the filtering criteria of rough GEANT 4 data; this would lead to a coefficient matrix C more adequate to device geometry and to specificity of secondary generation inside the studied device.

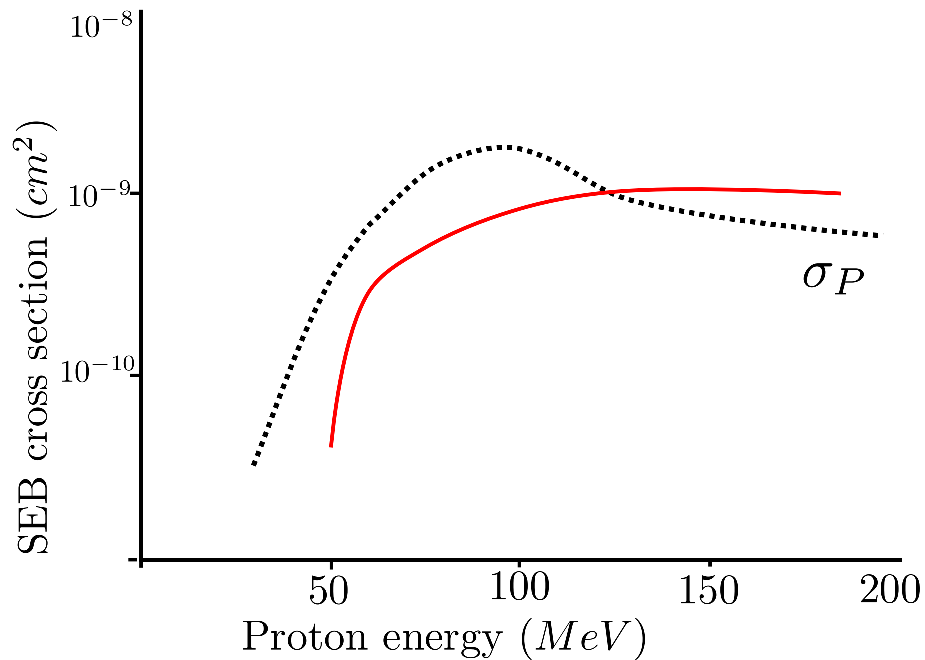

Figure 5.3 – Proton SEB calculation (dotted black line) compared with proton irradiation data from [10] (solid red line)

5.4 Calculation of heavy ion cross section

After the first validation of the coefficient matrix C to calculate proton SEB cross section, the reverse methodology has been used to predict heavy ion SEB cross section.

The idea comes from the fact that performing experimental proton characterization is far more convenient than the heavy ion characterization, because protons are more penetrating and there is no need to pre-treat DUTs before irradiation.

The procedure is founded on the same equation (4.10); only this time experimental proton cross section P are used as an entry, and predicted heavy ion SEB cross section H are calculated according to

$$C \cdot H = P \, . \tag{5.2}$$

The solution of the linear system in (5.2) gives the $(n, 1)$ vector H, represented as black dots in fig. 5.4. The heavy ion SEB experimental data are taken from [10] and are indeed well predicted by DELPHY in terms of order of magnitude.

The intrinsic limitation of this methodology is given by the fact that no secondary particles with $LET > 15 \ MeV cm^2/mg$ are generated by a proton inside a silicon target. For this reason, no cross section is predicted at higher LET values.

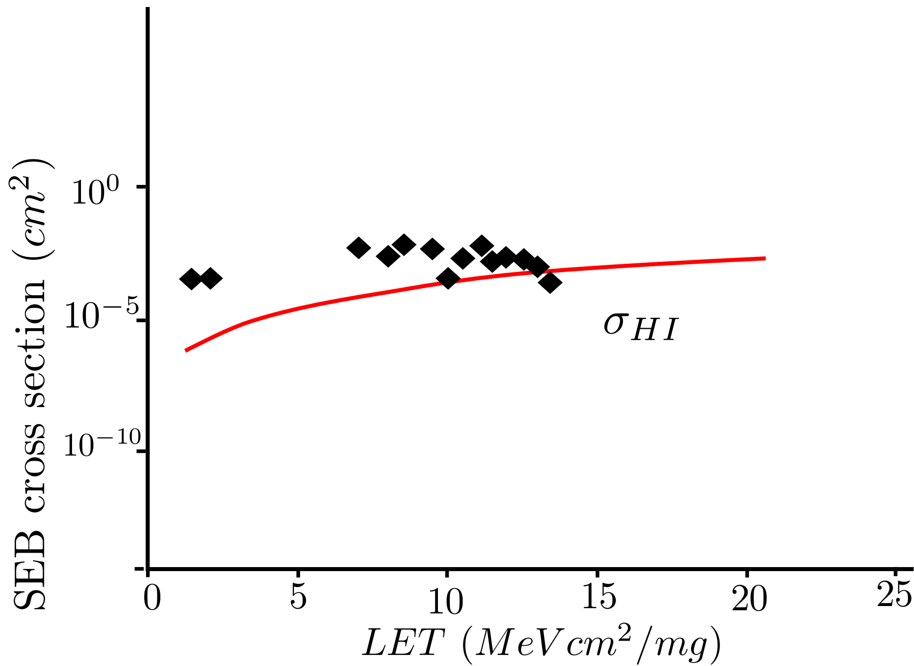

Figure 5.4 – Heavy ion SEB calculation by DELPHY(dots), compared with heavy ion irradiation data from [10] (solid line)

The general methodology is resumed in fig. 5.5. As a general conclusion, the overall agreement between predicted and experimental cross sections, validates DELPHY methodology of using irradiation data to predict complementary SEB sensitivities. The methodology is based on proton secondary effects inside the device, and thus implies a database of nuclear reactions and an accurate and physical coherent filtering of rough data.

It is in the filtering itself that might be the key to improve predicted cross sections: filtering criteria on atomic number and range should be applied to better describe SEB physics inside the studied component. A different target material, or a different device topology and dimension, lead to different nuclear reactions, and thus to different secondary products in terms of particle nature, range and LET [97], as seen in § 2.4.

On the same principle of well though filtering of nuclear database, one could extend the same methodology to other components, like IGBTs, or CMOS memories; and other SEE, such as LATCH-UP or SEU: with an adequate C matrix of differential generation probability $\frac{dc_{LET}}{dLET}$, the physics of secondary generation is adequately represented and usable.

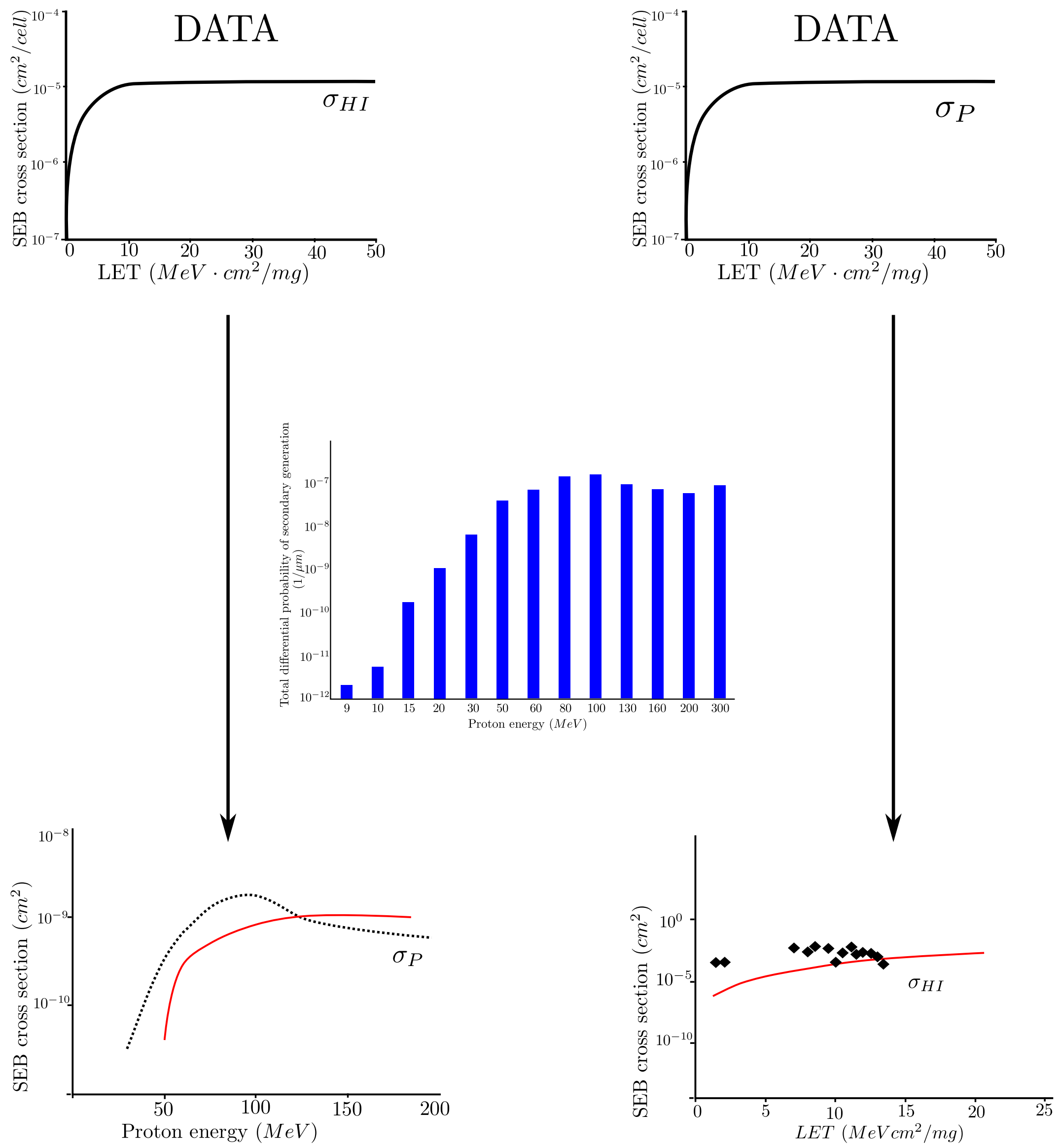

Figure 5.5 – Overview of the methodology: SEB prediction (bottom row) is achieved from experimental data (top row), through differential probability of secondary ions generation

In this chapter, proton SEB cross section has been calculated from heavy ion SEB cross section, and taking into account differential probability of secondary ion generation by proton impact inside the device. The calculated proton SEB sensitivity is compared to published heavy ion cross section.

In the second part of this chapter, the reverse procedure is applied, in order to calculate heavy ion SEB cross section from proton SEB cross section. The calculated heavy ion SEB sensitivity is then compared to published cross section, thus enlightening advantages and limitations of the methodology.

In both cases, calculated cross sections agreed with the experimental ones, showing a a prediction in the same order of magnitude than experimental SEB sensitivity. Nevertheless, there is room for improvement in terms of threshold LET and saturated cross section. A possible way to enhance SEB prediction is in the filtering criteria of rough GEANT 4 data; this would lead to a coefficient matrix C more adequate to device geometry and to specificity of secondary generation inside the studied device. Also, SEE prediction in other devices could also be made possible by the same principle.

Chapter

6 Discussion

> Read not to contradict and confute; nor to believe and take for granted; nor to find talk and discourse; but to weigh and consider.
>
> F. Bacon

This chapter discusses the present work, reviewing the main choices that have been made, in order to show its strong points and its limitations.

This study composes itself of two main parts and one extension: 2D TCAD analysis to extract a SEB triggering law, application of the law to build a prediction model for heavy ion and proton induced SEB, and extension of the proton sEB calculation to the case when INPUT data are experimental.

6.1 Choice of 2D simulations

For HEXFET and STRIPFET technologies, a basic 2D MOSFET cell has been identified and simulated, verifying its electrical functionality by confrontation to device datasheets. The comparison has lead to estimate an equivalent third dimension, as the ratio of drain current from datasheet and drain current from 2D TCAD.

Although literature has shown that 2D simulations are enough to reasonably describe SEB physics, there are many physical phenomena whose dynamics is affected by the fact that the simulation is 2D or 3D.

In this work, a brief example is given with diffusion. Its dynamics has been studied in the two configurations, showing a 68% gap after $1 \cdot 10^{-9}$ s. This figure of merit has no intention to be exhaustive in evaluating 2D/3D difference, since there are other phenomena involved, which can not be easily separated one from another. Also, diffusion phenomenon depends on track intensity and shape and should by no means be taken as an absolute estimation of 2D/3D difference.

However, the costs of a 3D simulation would have been not suitable for this work, because a high number of simulations has been run, so that the 2D configuration has been used for the rest of the study, expecting to see the consequences of this choice in the predicted SEB sensitivity.

Indeed, the overall overestimation of SEB sensitivity calculated by DELPHY, might be caused by the difference between 2D and 3D configurations. This work has shown in fact, that electron concentration is 68% higher in 2D. Even if the exact quantification is neglected, the idea remains of a greater electron concentration in 2D, because diffusion from the track follows only one direction, instead of following two gradients as in 3D simulations. As it is known, greater electron current leads to greater holes generation at the $n_{epi} - n_{sub}$ junction, thus worsening the self-sustained avalanche and parasitic BJT conduction which create a SEB.

It would be interesting to verify this concept by running in parallel two of the same simulations, one in 2D and one in 3D, in order to check if the SEB sensitivity is actually less in the 3D case.

6.2 Choice of triggering criterion

In order to study SEB, a preliminary choice of triggering criterion has been made and elected threshold charge: it is the minimal deposited charge inside the epitaxial layer necessary to trigger an SEB.

The choice of threshold charge as triggering criterion inside the epitaxial layer volume, comes from the bibliographic survey in § 2.5.1. In fact, the role of epitaxial layer as sensitive volume has been demonstrated, also given shape and intensity of electric field [82, 91, 55]. Also, SEB criteria based on deposited charge have already been used, since the ion's passage creates a charge column along its trajectory, depending on its LET [75, 74].

A few works [48, 45, 44] have identified critical charge as SEB criterion, but claiming that its value only depends on technology, and does not change with particle LET. The present work shows the opposite, defining a critical charge that accounts for particle LET and track.

6.3 Choice of simulated physical models

A few words should be spent on the choice of physical laws simulated in order to describe SEB. Other than Poisson's and continuity equations, adopted physical models include electric field and doping concentration dependencies for mobility, bandgap narrowing, Shockley-Red-Hall and Auger models for recombination, and electric field effects on avalanche recombination. These are the models used by previous works.

This study, however, does not investigate temperature dependence of SEB, thus the specific model has not been activated in TCAD. Previous works had done so [18], and others had recommended not to neglect temperature models [92]. The overall overestimation of calculated heavy ion cross section might be caused to this particular choice, since it is known that SEB sensitivity decreases with rising temperature. Thus the simulated SEB in this work is not mitigated by the local augmentation of temperature inside the device when the Burnout is ON. This idea would be interesting to demonstrate with some twin simulations, whose only difference is the activation of the temperature physical model.

6.4 Confirmation of SEB trends

SEB studies over the years have demonstrated that several parameters have an effect on SEB triggering, so TCAD has been useful in studying the influence of each single one of them: even though it is known that they are inter-dependent, a SEB sensitivity variation has been extracted for every parameter. This is a standard procedure which has already been followed with previous simulators, such as MEDICI [17] and SILVACO [55].

In this work, injection location and tilt, epitaxial layer thickness and doping, voltage bias and track length have been studied, and all simulations aimed to determine the variation of the triggering criterion as a function of these parameters. These simulations have coherently reproduced SEB physics as presented by previous works, thus confirming the qualitative validity of the used physical models. They have shown SEB sensitivity augmentation with voltage bias and particle LET, diminution with injection angle and dependence on injection location.

6.5 Identification of triggering law

Previous studies have demonstrated the key role of electric field and the thickness of epitaxial layer as the sensitive volume for SEB. For this reason, all simulation results have been summarized with an empirical triggering law, which states that threshold charge depends on the average electric field inside the epitaxial layer through a coefficient that describes the injection location effect. This law is particularly useful because it includes voltage bias and epitaxial layer thickness (trough electric field), particle characteristics as LET and injection conditions, and thus gives a practical yet non refined instrument for prediction.

It would be interesting to run some 3D simulations and evaluate the difference in the law coefficients. That would be costy but could offer an appreciation of the 2D/3D difference on the triggering law. Also, the two studied MOSFET topologies were very different in terms of structure and characteristic dimensions, and yet they showed the same behaviour; the investigation on a third structure would indeed give

a wider perspective on SEB evaluation and confirm the validity of the triggering law while underlying the topology effects.

The empirical law has been exploited through basic mathematical fitting, and the triggering criterion has been determined as a comparison between deposited charge and threshold charge. A way to improve model prediction for cross section, would be a better mathematical description, thus featuring a larger number of points in the curve, with a consequent calculation a a new fitting law. From a physical point of view, this would mean the investigation of SEB threshold charge in more than three impact locations.

6.6 Discussion of RPP methodology

This work predicts SEB with an adapted use of RPP methodology, which is based on a sensitive volume and a triggering criterion. In this case it represents an extreme simplification of SEB, taking into account that the phenomenon depends on many interlaced parameters and takes place in relatively big structures as are power MOSFETs.

In fact, after running DELPHY prediction model, the calculated cross sections better agreed with experimental results in the case of STRIPFET technology which is indeed more integrated than the HEXFET, thus making RPP approach a better description of reality in a smaller device. This confirms the idea of running the same procedure on other component topologies and, by comparative analysis, trying to identify possible ameliorations of DELPHY.

6.7 Proton induced SEB

Proton induced SEB has been evaluated inside a quite small structure (STRIPFET), thus making the RPP approach and the triggering law a more accurate prediction tool. The order of magnitude of the predicted SEB cross section corresponds in fact to the experimental one given by CERN, with only a slight overestimation.

It is a fact that DELPHY model overestimates SEB sensitivity, but the evidence that the estimation error is reduced in the case of a smaller structure, confirms the discussion previously made about the necessity of a more detailed physical description of SEB inside bigger structures, and demonstrates that SEB prediction is possible with DELPHY, given a few improvements to be done.

It would be a natural follow-up of this work, to extract neutron differential secondary generation probabilities and use them to calculate neutron induced SEB cross section, very interesting in evaluating SEB sensitivity of devices working in the atmospheric environment.

6.8 SEB calculation from experimental data

The overall agreement between predicted and experimental cross sections, validates DELPHY methodology of using irradiation data to predict complementary SEB sensitivities. The methodology is based on proton secondary effects inside the device, and thus implies a database of nuclear reactions and an accurate and physical coherent filtering of rough data.

It is in the filtering itself that might be the key to improve predicted cross sections: filtering criteria on atomic number and range should be applied to better describe SEB physics inside the studied component. A different target material, or a different device topology and dimension, lead to different nuclear reactions, and thus to different secondary products in terms of particle nature, range and *LET* [97], as seen in § 2.4.

On the same principle of well though filtering of nuclear database, one can extend the same methodology to other components, like IGBTs, or CMOS memories; and other SEE, such as LATCH-UP or SEU: with an adequate matrix of differential generation probability, the physics of secondary generation is adequately represented and usable.

Chapter

7 Conclusions

It always seems impossible until it's done.

N. Mandela

Power MOSFETs are widely used electronic devices capable of delivering high power levels. They are also subject to severe failures caused by the impact of a radiative particle on them. Among the possible radiation effects, this work addresses Single Event Burnout (SEB), which is caused by one single particle depositing charge inside the device and thus switching ON the parasitic BJT structure. This leads to an electron current which activates the epitaxial/substrate junction and thus generates a hole current if a high electric field is present. The phenomenon is self-sustained and leads to thermal destruction of the device.

It is in this frame that the present work has its reasons to be performed, its goal being to define a SEB prediction model taking into account physics and technology. The model development has moved from a wide TCAD analysis, followed by a synthesis of SEB dependencies and definition of a triggering criterion. DELPHY prediction model has been built this way.

By means of TCAD simulation tool, two different MOSFET topologies have been studied, a HEXFET and a STRIPFET, in order to determine technology effect on SEB dynamics.

Electrical performances of both configurations have been compared to the respective datasheets, confirming an exhaustive choice of simulated physical models, and then heavy ions injection has been simulated. SEB trends from literature have been confirmed by the simulation of this study, showing SEB sensitivity dependence from technological and injection parameters.

These dependencies have been summarized in newly defined triggering law, which calculates the necessary charge to be deposited inside epitaxial layer to trigger a SEB, from electric field. This law has proven to be valid in the two studied MOSFET configurations at at different tilt values.

The empirical law has then been exploited through basic mathematical fitting, and the triggering criterion has been determined as a comparison between deposited charge and threshold charge. They both refer to the epitaxial layer as the sensitive volume.

Through an RPP approach, the application of the triggering criterion inside the sensitive volume, constitutes the core of DELPHY prediction model, which has calculated heavy ion SEB cross section. It gives an overestimation of SEB sensitivity but leads the way as a first SEB prediction tool. A few improvement suggestions have also been identified.

In the occasion of a dedicated joint study ONERA-CERN, in order to characterize power MOSFETs for the future generation of power converters inside the Large Hadron Collider, proton induced SEB sensitivity has been calculated int he STRIPFET structure, showing agreement with the irradiation data.

The concept used to predict proton induced SEB has been extended to the calculation of heavy ion SEB sensitivity from proton SEB test data, and its reciprocal: in both cases, the predicted heavy ion cross section agrees in the order of magnitude to the experimental one, thus establishing the validity of the procedure.

The overall results of DELPHY prediction are encouraging to continue its development for other MOSFET topologies, and for different SEB cases.

Also, the fact that a quite complex physics as in SEB has been reduced to a charge deposition inside a sensitive volume, opens the way to apply DELPHY predictive approach to more confined Single Event Destructive Effects in other devices.

To resume, this study has filled the existing gap of SEB prediction models, creating a simple yet working predictive tool. DELPHY being the first step made towards SEB prediction, it also leaves room for many improvements and enrichments, in terms of TCAD better simulations, more accurate mathematical description, more power devices technologies to be studied and more radiative environments effects to be taken into account.

References

[1] Adolphsen, J., Barth, J., and Gee, G. B. G. First observation of proton induced power MOSFET burnout in space: the CRUX experiment on APEX. *IEEE Transactions on Nuclear Science 43*, 6 (1996), 2921–2926.

[2] Albadri, A. M., and Schrimpf, R. D. Coupled electro-thermal simulations of single event burnout in power diodes. *IEEE Transactions on Nuclear Science 52*, 6 (2005), 2194–2199.

[3] Artola, L., Hubert, G., Duzellier, S., and Bezerra, F. Collected Charge Analysis for a New Transient Model by TCAD Simulation in 90 nm Technology. *IEEE Transactions on Nuclear Science 57*, 4 (Aug. 2010), 1869–1875.

[4] Asai, H., Sugimoto, K., Nashiyama, I., Iide, Y., Shiba, K., Matsuda, M., and Miyazaki, Y. Terrestrial Neutron-Induced Single-Event Burnout in SiC Power Diodes. *IEEE Transactions on Nuclear Science 59*, 4 (Aug. 2012), 880–885.

[5] Barak, J., Haran, A., David, D., and Rapaport, S. A Double-Power-MOSFET Circuit for Protection From Single Event Burnout. *IEEE Transactions on Nuclear Science 55*, 6 (Dec. 2008), 3467–3472.

[6] Barth, J. Applying computer simulation tools to radiation effects problems. In *IEEE NSREC conference* (1997).

[7] Barth, J. Space, atmospheric, and terrestrial radiation environments. *IEEE Transactions on Nuclear Science 50*, 3 (2003), 466–482.

[8] Barth, J., Adolphsen, J., and Gee, G. Single event effects on commercial SRAMs and power MOSFETs: final results of the CRUX flight experiment on APEX. In *IEEE NSREC conference* (1998), IEEE, pp. 1–10.

[9] Barth, J., LaBel, K., and Poivey, C. Radiation assurance for the space environment. *IEEE ICICDT conference* (2004), 323–333.

[10] Bezerra, F., Lorfevre, E., Ecoffet, R., Peyre, D., Binois, C., Duzellier, S., Falguere, D., Nuns, T., Melotte, M., Calvel, P., Marec, R., Chatry, N., Falo, W., and Deneau, C. In flight observation of proton induced destructive single event phenomena. In *IEEE RADECS conference* (Sept. 2009), IEEE, pp. 126–132.

[11] Buchner, S., and McMorrow, D. Laboratory tests for single-event effects. *IEEE Transactions on Nuclear Science 43*, 2 (1996), 678–686.

[12] Buchner, S., Tran, L., and Mann, J. Single-event effects in resolver-to-digital converters. *IEEE Transactions on Nuclear Science 46*, 6 (1999).

[13] Calvel, P., and Peyrotte, C. Comparison of experimental measurements of power MOSFET SEBs in dynamic and static modes. *IEEE Transactions on Nuclear Science 38*, 6 (1991), 1310–1314.

[14] CERN. Radiation Test Report. Tech. rep., 2013.

[15] Coss, J., Swift, G., and Selva, L. Compendium of single event failures in power MOSFETs. *IEEE RADECS conference* (1998).

[16] Dachs, C., and Roubaud, F. Simulation aided hardening of N-channel power MOSFETs to prevent single event burnout. *IEEE Transactions on Nuclear Science 42*, 6 (1995), 1935–1939.

[17] Dachs, C., Roubaud, F., Palau, J.-M., Bruguier, G., Gasiot, J., and Tastet, P. Evidence of the ion's impact position effect on SEB in N-channel power MOSFETs. *IEEE Transactions on Nuclear Science 41*, 6 (Dec. 1994), 2167–2171.

[18] Darracq, F., Mbaye, N., Azzopardi, S., Pouget, V., Lorfevre, E., Bezerra, F., and Lewis, D. Investigation on the Single Event Burnout Sensitive Volume Using Two-Photon Absorption Laser Testing. *IEEE Transactions on Nuclear Science 59*, 4 (2012), 999–1006.

[19] Darracq, F., Mbaye, N., Larue, C., Pouget, V., Azzopardi, S., Lorfevre, E., Bezerra, F., and Lewis, D. Imaging the Single Event Burnout sensitive volume of vertical power MOSFETs using the laser Two-Photon Absorption technique. *IEEE RADECS conference* (Sept. 2011), 434–441.

[20] Darracq, F., Pouget, V., Lewis, D., Fouillat, P., Lorfevre, E., Ecoffet, R., and Bezerra, F. Investigation of single event burnout sensitive depth in power MOSFETS. *IEEE RADECS conference 1* (Sept. 2009), 106–111.

[21] Delepaut, C., Siconolfi, S., Mourra, O., and Tonicello, F. MOSFET gate open failure analysis in power electronics. In *IEEE APEC conference* (2013).

[22] Demarco, G., Romero, E., and Peretti, G. THERMAL MODELING OF SINGLE EVENT PROCESSES. *iberchip.net* (2005).

[23] Enge, H. A. *Introduction à la physique nucléaire*. Masson et Cie, 1972.

[24] Fairchild Semiconductor. Application Note 9010: MOSFET Basics. Tech. rep., 2000.

[25] Fischer, T. Heavy-ion-induced, gate-rupture in power MOSFETs. *IEEE Transactions on Nuclear Science*, 6 (1987), 1786–1791.

[26] Griffoni, A., van Duivenbode, J., Linten, D., Simoen, E., Rech, P., Dilillo, L., Wrobel, F., Verbist, P., and Groeseneken, G. Neutron-Induced Failure in Silicon IGBTs, Silicon Super-Junction and SiC MOSFETs. *IEEE Transactions on Nuclear Science 59*, 4 (Aug. 2012), 866–871.

[27] Hands, A., Morris, P., Ryden, K., Dyer, C., Truscott, P., Chugg, A., and Parker, S. Single Event Effects in Power MOSFETs Due to Atmospheric and Thermal Neutrons. *IEEE Transactions on Nuclear Science 58*, 6 (Dec. 2011), 2687–2694.

[28] Haran, A., Barak, J., David, D., Refaeli, N., Fischer, B. E., Voss, K.-O., Du, G., and Heiss, M. Mapping of Single Event Burnout in Power MOSFETs. *IEEE Transactions on Nuclear Science 54*, 6 (Dec. 2007), 2488–2494.

[29] Hohl, J., and Galloway, K. Analytical model for single event burnout of power MOSFETs. *IEEE Transactions on Nuclear Science 00*, 6 (1987), 1275–1280.

[30] Hohl, J., and Johnnson, G. Features of the triggering mechanism for single event burnout of power MOSFETs. *IEEE Transactions on Nuclear Science 36*, 6 (1989), 2260–2266.

[31] Hu, C. A Parametric Study of Power MOSFETs. In *IEEE PESC conference* (1979), pp. 385–395.

[32] Huang, S., Amaratunga, G., and Udrea, F. Analysis of SEB and SEGR in super-junction MOSFETs. *IEEE Transactions on Nuclear Science 47*, 6 (2000), 2640–2647.

[33] Hubert, G., Palau, J.-M., Castellani-Coulié, K., Calvet, M.-C., and Fourtine, S. Detailed Analysis of Secondary Ions' Effect for the Calculation of Neutron-Induced SER in SRAMs. *IEEE Transactions on Nuclear Science 48*, 6 (2001), 1953–1959.

[34] Ikeda, N., Kuboyama, S., and Matsuda, S. Single-event burnout of Super-junction power MOSFETs. *IEEE Transactions on Nuclear Science 51*, 6 (Dec. 2004), 3332–3335.

[35] Inguimbert, C. Radiation interaction with matter. In *SREC* (2004).

[36] Johnson, G. Temperature dependence of single-event burnout in n-channel power MOSFETs. *IEEE Transactions on Nuclear Science 39*, 6 (1992).

[37] Johnson, G., Brews, J., Schrimpf, R., and Galloway, K. Analysis of the time-dependent turn-on mechanism for single-event burnout of n-channel power MOSFETs. *IEEE RADECS conference*, 441–445.

[38] Johnson, G., and Hohl, J. Simulating single-event burnout of n-channel power MOSFET's. *IEEE Transactions on Nuclear Science*, 5 (1993).

[39] Johnson, G. H., Palau, J.-M., Dachs, C., Galloway, K. F., and Schrimpf, R. D. A review of the techniques used for modeling single-event effects in power MOSFETs. *IEEE Transactions on Nuclear Science 43*, 2 (1996), 546 – 560.

[40] Johnston, A. Charge generation and collection in p-n junctions excited with pulsed infrared lasers. *IEEE Transactions on Nuclear Science 40*, 6 (1993), 1694–1702.

[41] Keshavarz, A. Computer simulation of ionizing radiation burnout in power MOSFETs. *IEEE Transactions on Nuclear Science 35*, 6 (1988), 1422–1427.

[42] Kirk, C. A theory of transistor cutoff frequency falloff at high current densities. *IRE Transactions on Electron Devices*, 42 (1962), 164–174.

[43] Koga, R., and Katz, N. Bevalac ion beam characterizations for single event phenomena. *IEEE Transactions on Nuclear Science* (1990), 1923–1928.

[44] Kuboyama, S., and Ikeda, N. Enhanced avalanche multiplication factor and single-event burnout. *IEEE Transactions on Nuclear Science 50*, 6 (2003), 2233–2238.

[45] Kuboyama, S., Ikeda, N., Hirao, T., and Matsuda, S. Improved model for single-event burnout mechanism. *IEEE Transactions on Nuclear Science 51*, 6 (Dec. 2004), 3336–3341.

[46] Kuboyama, S., Maru, A., and Ikeda, N. Characterization of microdose damage caused by single heavy ion observed in trench type power MOSFETs. *IEEE Transactions on Nuclear Science 57*, 6 (2010), 3257–3261.

[47] Kuboyama, S., and Matsuda, S. Mechanism for single-event burnout of power MOSFETs and its characterization technique. *IEEE Transactions on Nuclear Science 39*, 6 (1992).

[48] Kuboyama, S., and Matsuda, S. Numerical analysis of single event burnout of power MOSFETs. *IEEE Transactions on Nuclear Science 40*, 6 (1993), 1872–1879.

[49] Kuboyama, S., Matsuda, S., Kanno, T., and Hirose, T. Single event burnout of power MOSFETs caused by nuclear reactions with heavy ions. *IEEE Transactions on Nuclear Science 41*, 6 (Dec. 1994), 2210–2215.

[50] Langworthy, J. Depletion region geometry analysis applied to single event sensitivity. *IEEE Transactions on Nuclear Science 36*, 6 (1989), 2427–2434.

[51] Liu, J., and Schrimpf, R. Circuit-level model for single-event burnout in N-channel power MOSFET's. *IEEE RADECS conference* (1999).

[52] Liu, S., and Boden, M. Single-event burnout and avalanche characteristics of power DMOSFETs. *IEEE Transactions on Nuclear Science 53*, 6 (2006), 3379–3385.

[53] Liu, S., Lauenstein, J.-M., Ferlet-Cavrois, V., Marec, R., Hernandez, F., Scheick, L., Bezerra, F., Muschitiello, M., Poivey, C., Sukhaseum, N., Coquelet, L., Cao, H., Carrier, D., Brisebois, M. A., Mangeret, R., Ecoffet, R., LaBel, K., Zafrani, M., and Sherman, P. Effects of Ion Species on SEB Failure Voltage of Power DMOSFET. *IEEE Transactions on Nuclear Science 58*, 6 (Dec. 2011), 2991–2997.

[54] Lorfevre, E., Sudre, C., Dachs, C., Detcheverry, C., Palau, J.-M., Gasiot, J., Calvet, M.-C., Garnie, J., and Ecoffet, R. SEB occurrence in a VIP: Influence of the epi-substrate junction. *IEEE Transactions on Nuclear Science 45*, 3 (June 1998), 1624–1627.

[55] Luu, A., Austin, P., Miller, F., Buard, N., Carriere, T., Poirot, P., Gailla, R., Bafleur, M., and Sarrabayrouse, G. Sensitive Volume and Triggering Criteria of SEB in Classic Planar VDMOS. *IEEE Transactions on Nuclear Science 57*, 4 (Aug. 2010), 1900–1907.

[56] Luu, A., Miller, F., and Poirot, P. SEB characterisation of commercial power MOSFETs with backside laser and heavy ions of different ranges. *IEEE RADECS conference 55*, 4 (2007), 2166–2173.

[57] McMorrow, D., and Buchner, S. Demonstration of single-event effects induced by through-wafer two-photon absorption. *IEEE Transactions on Nuclear Science 51*, 6 (2004), 3553–3557.

[58] McMorrow, D., and Lotshaw, W. Subbandgap laser-induced single event effects: Carrier generation via two-photon absorption. *IEEE Transactions on Nuclear Science 49*, 6 (2002), 3002–3008.

[59] McMorrow, D., and Lotshaw, W. Three-dimensional mapping of single-event effects using two photon absorption. *IEEE Transactions on Nuclear Science 50*, 6 (2003), 2199–2207.

[60] Miller, F., Luu, A., Prud, F., Poirot, P., Gaillard, R., Buard, N., and Carrière, T. Characterization of Single-Event Burnout in Power MOSFET Using Backside Laser Testing. *IEEE Transactions on Nuclear Science 53*, 6 (2006), 3145–3152.

[61] Miller, F., Morand, S., and Douin, A. Laser validation of a non-destructive test methodology for the radiation sensitivity assessment of power devices. *Nuclear Science, ... 58*, 3 (2011), 813–819.

[62] Morand, S. Validation par l'outil laser d'une méthodologie de test non-destructif pour la caractérisation de sensibilité aux radiations des composants de puissance.

[63] Motto, E. Trench-Gate Technology for The Next Generation of MOS Power Devices. In *IEEE APEC conference* (1999).

[64] Musseau, O., Toitbs, A., Campbell, A. B., Buchner, S., Fischer, B., Schlog, M., and Briand, P. Medium-energy heavy-ion single-event-burnout imaging of power MOSFETs. *IEEE Transactions on Nuclear Science 46*, 6 (1999), 1415–1420.

[65] Nichols, D., McCarty, K., Coss, J., Waskiewicz, A., Groninger, J., Oberg, D., Wert, J., Majewski, P., and Koga, R. Observations of single event failure in power MOSFETs. *Workshop Record. 1994 IEEE Radiation Effects Data Workshop* (1994), 41–54.

[66] Normand, E. Single-Event Effects in Avionics. *IEEE Transactions on Nuclear ScienceE 43*, 2 (1996), 461–474.

[67] Normand, E., Wert, J. J., Oberg, D., Majewski, P., Voss, P., and Wender, S. Neutron-induced single event burnout in high voltage electronics. *Nuclear Science, ... 44*, 6 (1997), 2358–2366.

[68] Oberg, D., Wert, J., Normand, E., Majewski, P., and Wender, S. First observations of power MOSFET burnout with high energy neutrons. *IEEE Transactions on Nuclear Science 43*, 6 (1996), 2913–2920.

[69] Oberg, D. L., and Wert, J. L. First nondestructive measurements of power MOSFET single event burnout cross sections. *Nuclear Science, IEEE Transactions on*, 6 (1987), 1736–1741.

[70] Oser, P., Mekki, J., Spiezia, G., Fadakis, E., Foucard, G., Peronnard, P., Masi, A., and Gaillard, R. Effectiveness Analysis of a Non-Destructive Single Event Burnout Test Methodology. In *IEEE RADECS conference* (2013).

[71] Renesas. Application Note: Power MOSFET. Tech. rep., 2004.

[72] Richter, a. K., and Arimura, I. Simulation of Heavy Charged Particle Tracks Using Focused Laser Beams. *IEEE Transactions on Nuclear Science 34*, 6 (1987), 1234–1239.

[73] Romero, E., Demarco, G. L., and Tais, C. E. Time Evolution of Single-Event Burnout in Vertical Power MOSFETs and Implications for Mitigation Strategies. *IEEE Transactions on Device and Materials Reliability 11*, 1 (Mar. 2011), 171–178.

[74] Roubaud, F., and Dachs, C. Use of 2D simulations to study parameters influence on SEB occurrence in n-channel MOSFETs. In *Radiation Effects* (1994), pp. 446–451.

[75] Roubaud, F., Dachs, C., Palau, J.-M., Gasiot, J., and Tastet, P. Experimental and 2D simulation study of the single-event burnout in N-channel power MOSFETs. *IEEE Transactions on Nuclear Science 40*, 6 (1993), 1952–1958.

[76] Scheick, L., and Selva, L. Sensitivity to LET and Test Conditions for SEE Testing of Power MOSFETs. In *2009 IEEE Radiation Effects Data Workshop* (July 2009), IEEE, pp. 82–93.

[77] Selva, L. E., Ikeda, N., and Scheick, L. Z. SEGR/SEB Test Results on Emerging Hi-Rel Power MOSFETs. *2009 IEEE Radiation Effects Data Workshop* (July 2009), 76–81.

[78] Sexton, F. Destructive single-event effects in semiconductor devices and ICs. *Nuclear Science, IEEE Transactions on 50*, 3 (2003), 603–621.

[79] Siconolfi, S., Hubert, G., Artola, L., Darracq, F., and David, J.-P. A Physical Prediction Model Issued from TCAD Investigations for Single Event Burnout in Power MOSFETs. In *IEEE RADECS conference* (2013).

[80] Stapor, W. W., McDonald, P. P., Knudson, A., Campbell, A., and Glagola, B. Charge collection in silicon for ions of different energy but same linear energy transfer (LET). *Nuclear Science, ... 35*, 6 (1988), 1585–1590.

[81] Stassinopoulos, E. Dependence of power MOSFET static burnout on charge distribution in the active region of IRF15O. *Radiation and its ...* (1993), 458–461.

[82] Stassinopoulos, E., Brucker, G., Calvel, P., Baiget, A., Peyrotte, C., and Gaillard, R. Charge generation by heavy ions in power MOSFETs, burnout space predictions and dynamic SEB sensitivity. *IEEE Transactions on Nuclear Science 39*, 6 (1992), 1704–1711.

[83] Synopsys. TCAD User Guide. Tech. rep., 2007.

[84] Sze, S. M. *Physics of Semiconductor Devices.* John Wiley and Sons, 1981.

[85] Tais, C. E., Romero, E., and Demarco, G. L. Thermomechanical Stresses Analysis of a Single Event Burnout Process. *Nuclear Science, IEEE Transactions on 56*, 3 (June 2009), 1521–1530.

[86] Takahashi, Y., Fugane, M., Imagawa, R., and Ohnishi, K. Heavy-Ion induced Gate Current in MOSFET. pp. 438–441.

[87] Tastet, P., and Garnier, J. Burnout sensitivity of power MOSFETs operating in a switching converter. *Nuclear Science, IEEE ... 41*, 3 (1994).

[88] TCS. Reverse Engineering Report. Tech. rep., 2014.

[89] Titus, J., and Wheatley, C. Experimental studies of single-event gate rupture and burnout in vertical power MOSFETs. *Nuclear Science, IEEE Transactions on 43*, 2 (1996).

[90] Titus, J. L. An Updated Perspective of Single Event Gate Rupture and Single Event Burnout in Power MOSFETs. *IEEE Transactions on Nuclear Science 60*, 3 (June 2013), 1912–1928.

[91] Velardi, F., Iannuzzo, F., and Busatto, G. Reliability of Medium Blocking Voltage Power VDMOSFET in Radiation Environment. *... Reliability* (2003).

[92] Walker, D., Fisher, T., Liu, J., and Schrimpf, R. Thermal modeling of single event burnout failure in semiconductor power devices. *Microelectronics Reliability 41*, 4 (Apr. 2001), 571–578.

[93] Waskiewicz, A. Burnout of power MOS transistors with heavy ions of Californium-252. *Nuclear Science, ...*, 6 (1986), 1710–1713.

[94] Waskiewicz, A., and Groninger, J. Burnout Thresholds and Cross Section of Power MOS Transistors with Heavy Ions.

[95] Wrobel, T., and Beutler, D. Solutions to heavy ion induced avalanche burnout in power devices. *IEEE Transactions on Nuclear Science 39*, 6 (1992), 1636–1641.

[96] Wrobel, T. F., Coppage, F. N., Hash, G. L., and Smith, A. J. Current Induced Avalanche in Epitaxial Structures. *IEEE Transactions on Nuclear Science 32*, 6 (1985), 3991–3995.

[97] Ziegler, J. F., Biersack, J. P., and Littmark, U. *The Stopping and Range of Ions in Matter*. Pergamon Press, 1985.

General abstract

The natural radiation environment has proved to be particularly harsh on power electronics devices. It is characterized by electrically charged particles such as heavy ions and protons among others. In particular, inside the atmosphere it has now become essential to estimate the effects of these particles: power MOSFETs in fact are widely used because of their appealing electrical characteristics and costs, thus making the prediction of destructive effects one of the fundamental parts of the project. This work focuses on the prediction of Single Event Burnout (SEB) inside power MOSFETs: based on physical analysis through TCAD simulations, the prediction model DELPHY is built in order to calculate occurrence rates of heavy ion and proton induced SEB.

SEB consists of a charge generation inside the device, which evolves into a high and self-sustained current, whose main consequence is the thermal destruction of the component. SEB has been deeply studied in several aspects: it is now established that it depends on multiple factors, such as component geometry, doping and bias; particle nature and Linear Energy Transfer, impact location and angle. A power electronics designer does not have control over all the cited parameters, and the trade-off between cost and functionality limits the application of hardness measures at circuit and device level. For this reason, a SEB rate prediction model is needed and represents the object of this work.

DELPHY model moves from physical analysis of SEB, performed with TCAD 2D simulations, in order to control the aforementioned factors which are relevant for the phenomenon. Two different MOSFET topologies have been studied (HEXFET and STRIPFET). Starting from this analysis, an empirical triggering law has been calculated and a SEB criterion based on electric field and charge deposition inside the epitaxial layer has been defined. SEB cross sections have then been calculated for heavy ion impacts. Taking into account the differential probability of secondary generation by proton impact, a SEB rate has been predicted also for proton induced SEB.

All the calculated cross sections have been successfully compared to experimental

data: firstly from a device characterization published by CNES; and secondly in the frame of a dedicated joint study ONERA-CERN to characterize next generation of Large Hadron Collider power converters. As a general conclusion, DELPHY model leads the way as a valid SEB prediction tool and opens new roads for enhancement of SEB rates estimation.

Keywords

power MOSFET; HEXFET; STRIPFET; SEB; TCAD simulation; prediction; heavy ion; proton

Résumé français

1 Introduction

Les MOSFETs (Metal Oxide Semiconductor Field Effect Transistor) sont des composants électroniques très utilisés, capables de délivrer hauts niveaux de puissance. Ils sont sujets à des défaillances causées par l'impact des particules radiatives. En fait, le sévère environnement radiatif est parmi les aspects fondamentaux à prendre en considération pendant la phase de projet.

Parmi les possibles effets des radiations, ces travaux traitent le Single Event Burnout (SEB), qui est causé par une particule qui dépose de la charge dans le composant et ainsi met en conduction la structure BJT parasite. Cela mène à un courant d'électrons qui active la jonction épitaxié/substrat, générant donc un courant de trous en présence d'un fort champ électrique. Le phénomène est auto-alimenté et conduit à la destruction thermique du composant, avec des conséquences catastrophiques au niveau circuit, système ou même mission.

A cause de la nature destructive et permanente du SEB, il doit être étudié pour concevoir des systèmes électroniques efficients et fiables. Les approches de fiabilité traditionnelles ne pouvant pas être appliquées au SEB, il devient nécessaire un outil de prédiction SEB.

A fin de construire un outil de prédiction, il faut partir d'une profonde connaissance physique du SEB, largement étudié dans les dernières 30 années. L'existence du SEB a été postulée pour la première fois déjà en 1985 ; ses conséquences au niveau composant étaient connues, et des études on été amenées pour connaître ses caractéristiques électriques au niveau semiconducteur.

Dans les années suivantes, il a été démontré que la sensibilité SEB augmente avec la tension de biais et l'énergie de la particule, et diminue avec la température et l'épaisseur de la zone épitaxiée. A partir de ces considérations, des solutions de durcissement ont été proposées au cours des années, même si le déclenchement du SEB ne paraît pas être empêché totalement.

Des protocoles de test on été aussi définis, spécialement les non destructifs, à fin d'économiser temps et coûts. Ils se basent sur la limitation de la charge injectée dans le composant, ou sur l'évacuation du courant.

C'est grâce aux tests non destructifs, ainsi qu'aux simulations numériques 2D et aux cartographies laser, que la caractérisation des composants à la sensibilité SEB apparaît un moyen relativement facile pour évaluer et essayer de prédire l'apparition du SEB dans certains composants. Cependant, il faut prendre en considération aussi d'autres facteurs, comme la variabilité parmi les différents lots de composants, et les coûts intrinsèques de toute démarche de caractérisation. Surtout, il faut considérer qu'aucune des méthodes citées assure une estimation complète et fiable de la sensibilité SEB d'un composant donné. Différentes configurations MOSFET ont aussi été caractérisées en termes de sensibilité SEB, comme par exemple le STRIPFET, Silicon Carbide (SiC) et Super-Junction (S-J).

En synthèse, la connaissance des mécanismes physiques du SEB a été améliorée, permettant la compréhension de sa dynamique. Toutefois, il manque toujours un outil de prédiction des taux SEB, ce qui permettrait d'évaluer le risque SEB pour une mission donnée, composant et conditions de travail.

La manque d'un outil de prédiction des taux SEB justifie l'étude ci-présentée. Elle porte sur le développement d'un modèle de prédiction opérationnelle des taux SEB dans les MOSFETs de puissance.

A fin de construire un modèle de prédiction des taux SEB, d'abord le SEB a été simulé dans un MOSFET de puissance, à fin d'étudier l'effet de différents paramètres sur le phénomène SEB. Pour cela, une structure 2D a été construite dans deux différentes configurations technologiques : HEXFET et STRIPFET. Une fois la structure validée par comparaison avec le datasheet, l'injection d'un ion lourd a été simulée pour déclencher un SEB dans le composant. Cette simulation basique a été répétée en changeant à chaque fois un seul parmi les paramètres : géométrie et dopage du composant, lieu et angle d'injection. Les effets de chacun de ces paramètres ont été modélisés en fonction du champ électrique moyen dans la région épitaxiée, et le critère de déclenchement considéré est la charge déposée dans la même région. Ainsi, tous les résultats des simulations ont été synthétisés à travers une loi empirique de déclenchement, qui présente la charge critique comme fonction du champ électrique moyen dans la zone épitaxiée à travers un coefficient qui décrit l'effet du lieu d'injection. (Voir § 3)

Cette loi empirique a été exploitée à travers un ajustement mathématique, et le critère de déclenchement a été déterminé comme comparaison entre la charge déposée et la charge critique, en établissant ainsi la base du modèle de prédiction DELPHY (Destructive effects prEdiction modeL based on PHysical analYsis). Cette partie du travail a été présentée pendant la conférence IEEE Conference on Radiation Effects on Components and Systems (RADECS) et a permis de développer une

estimation des taux SEB proton au cours d'une étude conjointe ONERA-CERN, à fin de caractériser les MOSFETs de puissance pour la génération future de convertisseurs de puissance dans le Large Hadron Collider.

Pour calculer les sections efficaces proton, une vaste base de données GEANT4 sur les réaction secondaires a été filtrée à l'ONERA, à fin d'extraire les réactions secondaires pertinentes à cette étude, et une probabilité différentielle de génération secondaire a été calculée. Elle a été donc convoluée avec les sections efficaces ion lourd pour déterminer la section efficace proton ; le calcul montre un bon accord dans l'ordre de grandeur avec la section efficace expérimentale. En effet, la technologie STRIPFET étant plus intégrée que celle HEXFET, les relatives sections efficaces calculées montrent un meilleur accord avec les données expérimentales. (Voir § 4)

La démarche utilisée pour la prédiction du SEB proton, a été exploitée davantage pour calculer la sensibilité SEB ion lourd à partir des données expérimentales proton, et vice-versa : dans les deux cas, l'ordre de grandeur de la section efficace estimée correspond à celle expérimentale, validant ainsi la procedure. (Voir § 5).

2 Single Event Burnout dans les MOSFETs de puissance

Le manuscrit en anglais contient une description détaillée des modèles SEB développés jusqu'à aujourd'hui et introduit les notions principales nécessaires pour l'étude du SEB.

3 Calcul des critères de déclenchement SEB à travers la simulation composant 2D TCAD

3.1 Construction d'une structure MOSFET 2D

La première étape a été faire le choix des composants à étudier. Ce choix se justifie par la disponibilité des données de reverse engineering sur la structure interne et les dimensions du composant ainsi que des données issues des tests sous irradiation. Pour ces raisons, deux composants différents ont été choisis, qui sont : une structure HEXFET, visible en fig. F.1a, et une structure STRIPFET, visible en fig. F.1b.

Un MOSFET est un dispositif multicellulaire où une structure de cellule simple est répétée plusieurs milliers de fois. Pour cette raison, il peut être efficace dans des simulations de le représenter par une seule cellule, la considérant comme totalement identique aux autres cellules et permettant ainsi d'appliquer les résultats dans chaque cellule.

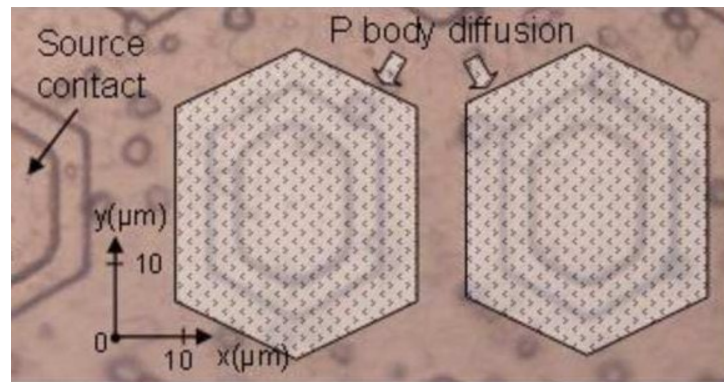

(a) *HEXFET [18]*

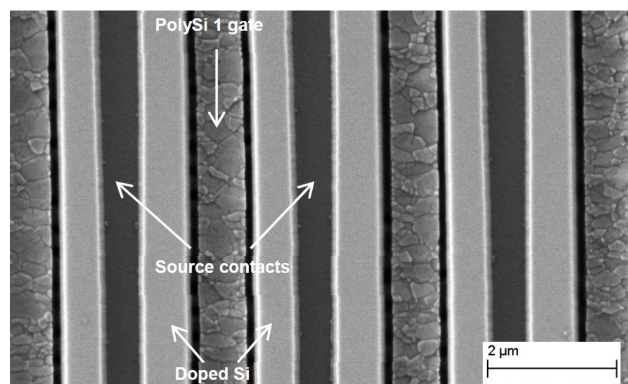

(b) *StripFET [88]*

Figure F.1 – Détails et dimensions de la surface des dispositifs étudiés

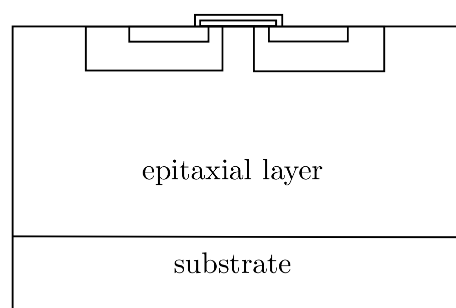

(a) *HEXFET*

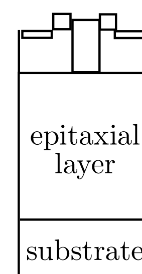

(b) *STRIPFET*

Figure F.2 – Cellule élémentaire étudiée dans les deux topologies MOSFET

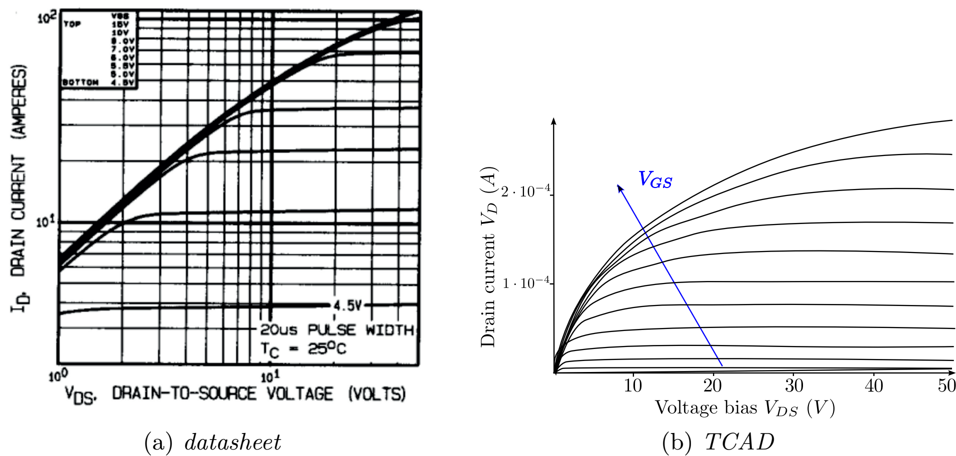

(a) *datasheet* (b) *TCAD*

Figure F.3 – Comparaison du courant de drain pour HEXFET

Introduction au modèles physiques simulés

Technology Computer-Aided Design (TCAD) résout les équations fondamentales de la physique des semi-conducteurs, tels que l'équation de Poisson et les équations de continuité. Le but est d'obtenir des valeurs électriques et physiques à l'intérieur du composant à travers la méthode Finite Elements Method (FEM). Dans ce travail, la version A-2007.12 a été utilisée, sous licence Synopsys, Inc.

A part les équations de Poisson et de continuité, les modèles physiques adoptés comprennent la dépendance du champ électrique et de la concentration de dopage pour la mobilité, le rétrécissement de bandgap, le modèle de recombination de Auger et Shockley-Red-Hall, et les effets du champ électrique sur la recombination d'avalanche. Ces modèles ont été utilisés dans les travaux précédents.

Comparaison avec le datasheet du composant

Une fois les structures construites, leurs caractéristiques électriques respectives ont été calculées et tracées, afin de déterminer le comportement électrique effectif des composants simulés, par rapport à ceux indiqués dans les fiches techniques respectives de International Rectifier.

La fig. F.3 montre les allures de courant de drain I_D : la différence quantitative s'explique par le fait que la simulation est une représentation 2D de la réalité, et le composant est constitué d'un grand nombre de cellules en parallèle.

Dans le manuscrit anglais une évaluation d'un facteur d'échelle entre les configurations 2D et 3D est présentée, ainsi qu'une comparaison du phénomène de diffusion dans les deux cas.

Table F.1 – Sélection des paramétrés simulés avec TCAD

Géométrie	Electrique	Particule
Lieu d'injection	Biais V_{DS}	LET
Angle d'injection	Dopage	Portée
Technologie composant		

3.2 Etude de la physique SEB par injection d'ions lourds

Le phénomène SEB est de nature complexe, où plusieurs effets physiques sont entrelacés: l'avantage de l'étudier avec des simulations TCAD est la possibilité de visualiser les effets d'un paramètre à la fois, en contrôlant ce qui est variable et permettant ainsi une meilleure compréhension des dépendances SEB à partir des dits paramètres, afin de les prendre en compte dans le modèle prédictif.

Dans le tableau F.1 il y a la liste des paramètres qu'ont une influence sur le SEB et qu'ont été simulés avec TCAD. Dans chaque configuration le but est d'évaluer la charge critique déposée dans la zone épitaxiée q_{th}, définie comme

$$q_{th} = LET_{th}\frac{h_{epi}}{cos\theta} \ . \tag{1}$$

Dans le manuscrit anglais il y a une description complète des résultats des simulations TCAD, pour les technologies HEXFET et STRIPFET. Pour chaque dépendance, l'effet du paramètre est mis en évidence, de façon à obtenir une vision générale sur les différentes allures de la charge critique en fonction de chaque paramètre.

3.3 Extraction d'une loi empirique de déclenchement basée sur le champ électrique et la charge critique

A partir de l'analyse TCAD, une loi empirique de déclenchement SEB a été extraite, visible en fig. F.4 pour le HEXFET et F.5 pour le STRIPFET.

A fin de synthétiser toutes les dépendances trouvées avec l'analyse TCAD, la fig. F.4 et la fig. F.5 représentent la charge seuil comme fonction du champ électrique respectivement dans les topologies HEXFET et STRIPFET. Les figures F.4 et F.5 étant à la base du modèle de prédiction développé, il a été nécessaire de les décrire à travers une loi d'ajustement mathématique

$$q_{th} = k \ EF^{-z} \tag{2}$$

où k and z sont coefficients d'ajustement qui dépendent du lieu d'impact.

On peut mettre en évidence que, indépendamment de la technologie et du lieu d'impact, les courbes ont une forme similaire, ce qui n'est pas surprenant, car elles représentent la même physique SEB.

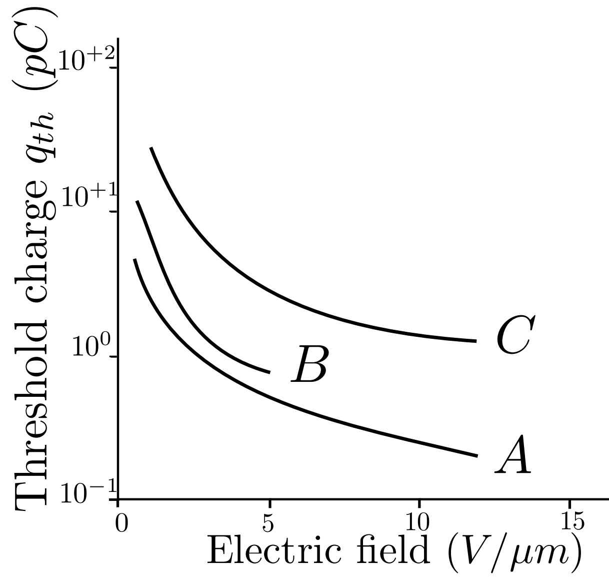

Figure F.4 – Charge seuil comme fonction du champ électrique moyen dans la topologie HEXFET. Les trois courbes représentent les trois lieux d'injection A, B, C

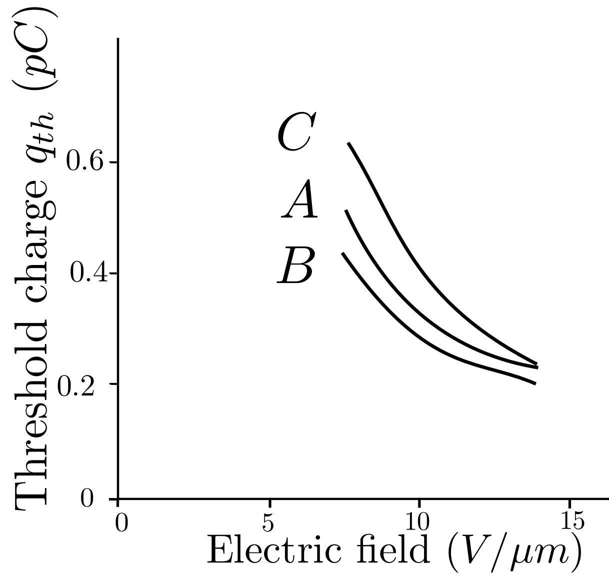

Figure F.5 – Charge seuil comme fonction du champ électrique moyen dans la topologie STRIPFET. Les trois courbes représentent les trois lieux d'injection A, B, C

4 Construction d'un modèle de prédiction SEB basé sur le champ électrique et la charge critique

DELPHY (Destructive effects prEdiction modeL based on PHysical analYsis) est développé comme modèle de prédiction de taux SEB, sur la base d'un critère de charge déposée en fonction du champ électrique à l'intérieur du MOSFET. Premièrement, les résultats de simulation TCAD sont discutés dans l'optique de la prédiction, afin de déterminer les entrées et sorties pour DELPHY. Ceci constitue une méthode générale utilisée pour une transition de l'analyse TCAD à un modèle de prédiction de SEB généré par ions lourds.

Une fois le domaine du modèle établi, le critère cité est appliqué pour construire DELPHY. La procédure de construction est détaillée et les sections efficaces ion lourd sont calculées. Ensuite, le même modèle est appliqué pour calculer les sections efficaces SEB proton, en prenant en compte la probabilité de génération des ions secondaires dans le composant.

4.1 Définition d'un critère de prédiction SEB

Le critère physique sur lequel DELPHY est basé est

$$q_{epi} \geqslant q_{th} \Longrightarrow SEB \tag{3}$$

qui devient

$$q_{epi} \geqslant k(x)EF^{-z} \Longrightarrow SEB\ . \tag{4}$$

Cela signifie que quand l'ion lourd impactant sur la surface du MOSFET à un endroit donné, dépose dans la zone épitaxiée une certaine charge qui est égale ou plus grande que la charge critique à cet endroit, alors le composant subira un SEB.

4.2 Développement de DELPHY pour SEB généré par ions lourds

Le modèle est construit sur la base du concept RPP (Rectangular Parallelepiped), qui se compose de la définition d'une structure sensible dans le composant et de l'évaluation du critère dans la même structure sensible.

Dans le cas d'un HEXFET la surface sensible est un hexagon (fig. F.7), et dans le cas d'un STRIPFET est un rectangle (fig. F.8).

Développer le modèle signifie imposer l'égalité

$$q_{epi} = q_{th}(x)\ |_{x=\xi} \tag{5}$$

qui devient

$$q_{epi} = k(\xi)EF^{-z}\ . \tag{6}$$

La solution donne la valeur de ξ et donc de $r = (R - \xi)$, qui est utilisé pour le calcul de la section efficace, comme montré par la fig. F.9.

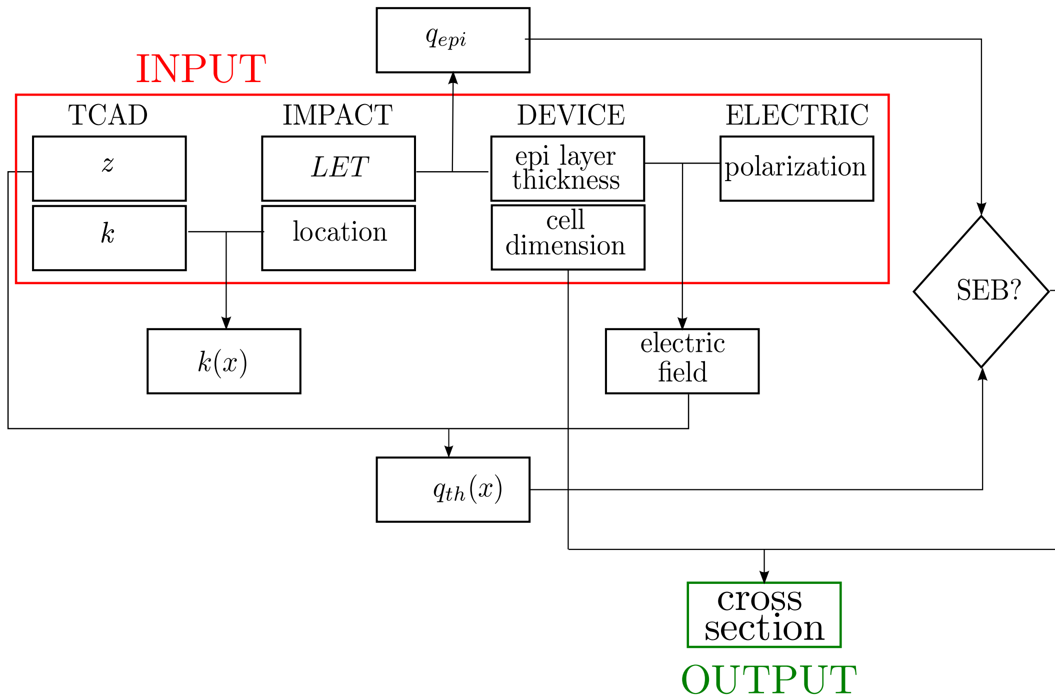

Figure F.6 – Entrées et sorties de DELPHY

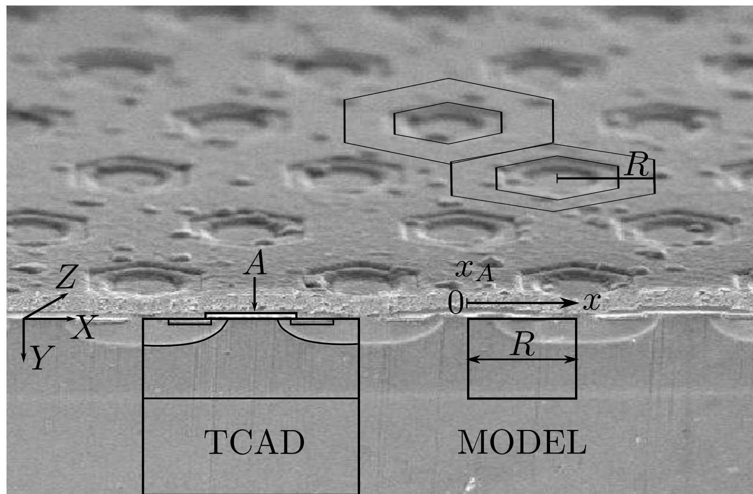

Figure F.7 – Transition de la géométrie TCAD à la géométrie du modèle pour une structure HEXFET

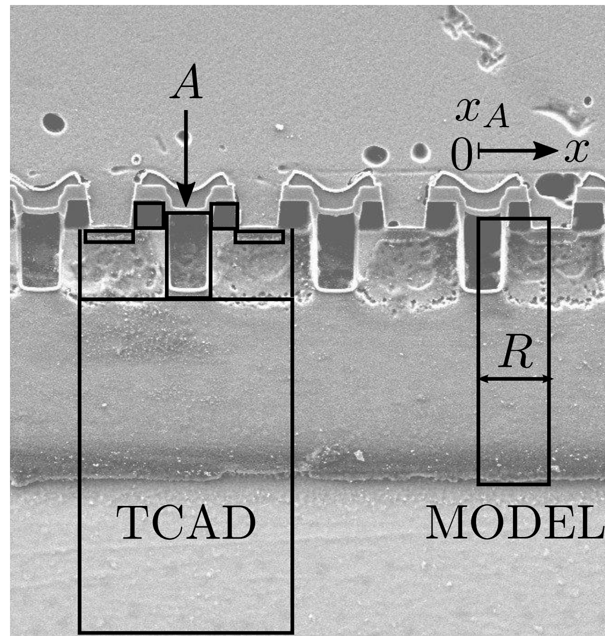

Figure F.8 – Transition de la géométrie TCAD à la géométrie du modèle pour une structure STRIPFET

La géométrie du calcul des sections efficaces est illustrée pour la topologie HEXFET dans les figures F.10 et F.11.

La géométrie du calcul des sections efficaces est illustrée pour la topologie STRIPFET dans les figures F.12 et F.13.

Dans chacune des configurations HEXFET ou STRIPFET, DELPHY calcule les courbes de section efficace (fig. F.14) et les cartographies de sensibilité SEB (fig. F.15).

4.3 Comparaison avec les données d'irradiation

La comparaison avec les données d'irradiation des IRF360 (données CNES, détaillées dans le manuscrit anglais), montrent que DELPHY surestime la sensibilité SEB. Les raisons de cette surestimation sont à chercher dans les approximations faites dans la construction du modèle.

4.4 Calcul des sections efficaces pour SEB proton

Pour calculer les section efficaces proton, il faut prendre en compte le fait que quand un proton impacte sur un composant, il génère des particules secondaires selon la nature du composant, de la particule et de leur interaction chimique.

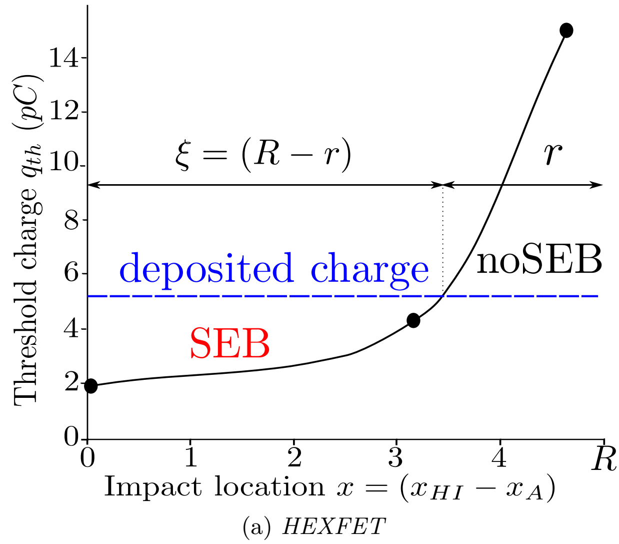

(a) *HEXFET*

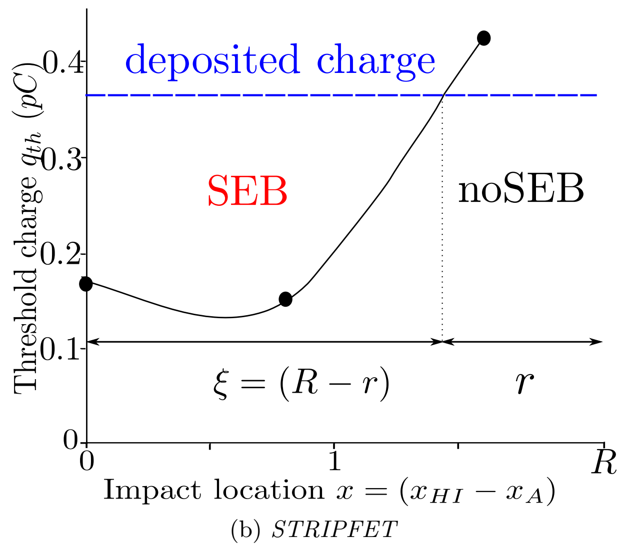

(b) *STRIPFET*

Figure F.9 – Illustration géométrique du critère SEB utilisé dans ces travaux pour les topologies HEXFET et STRIPFET

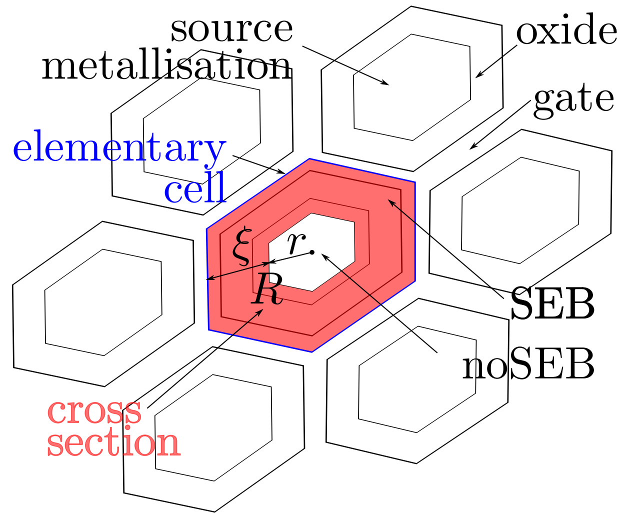

Figure F.10 – Cellule élémentaire et couronne hexagonale comme représentation visuelle de la section efficace σ_{HI} dans la technologie HEXFET

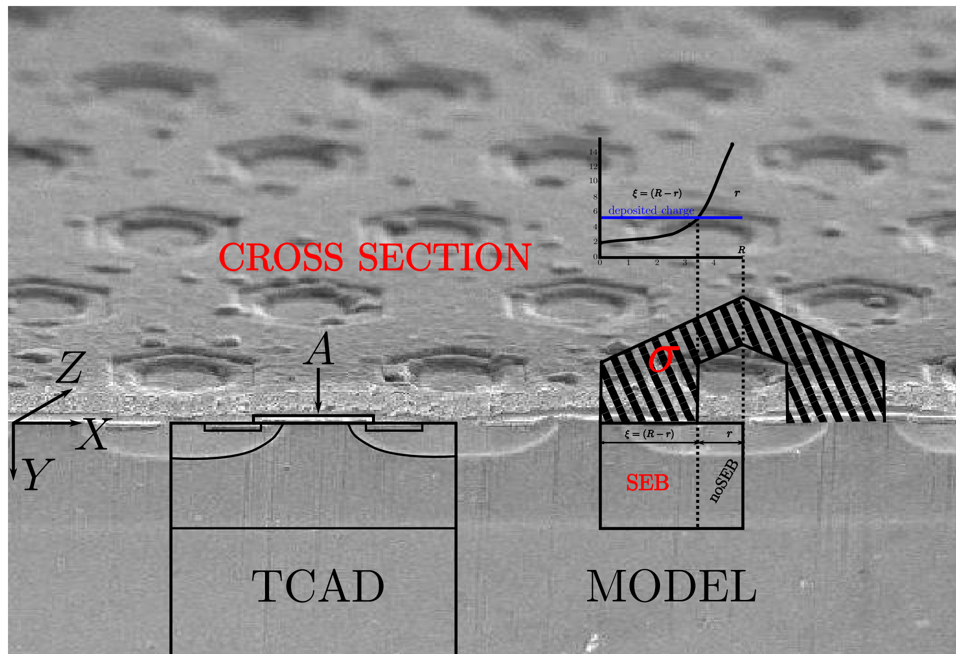

Figure F.11 – Transition des géométries TCAD et modèle au calcul de la section efficace σ_{HI} dans la technologie HEXFET

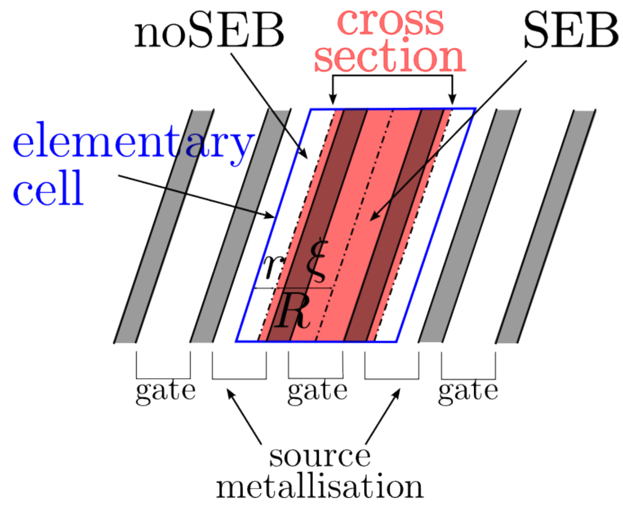

Figure F.12 – Cellule élémentaire et rectangle comme représentation visuelle de la section efficace σ_{HI} dans la technologie STRIPFET

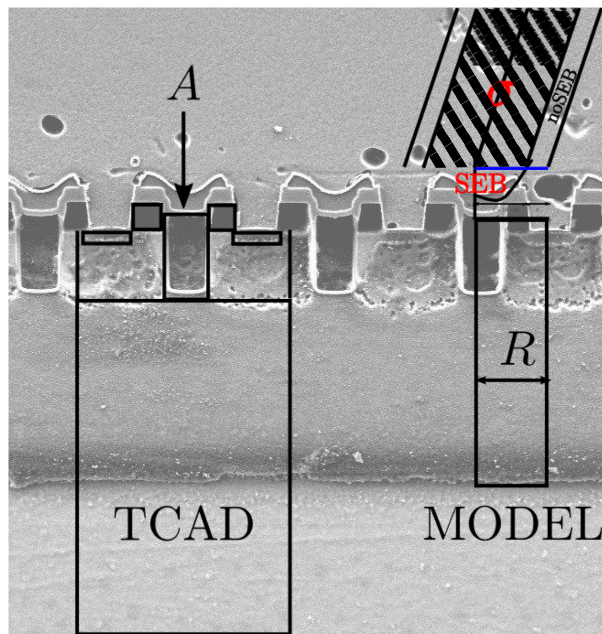

Figure F.13 – Transition des géométries TCAD et modèle au calcul de la section efficace σ_{HI} dans la technologie STRIPFET

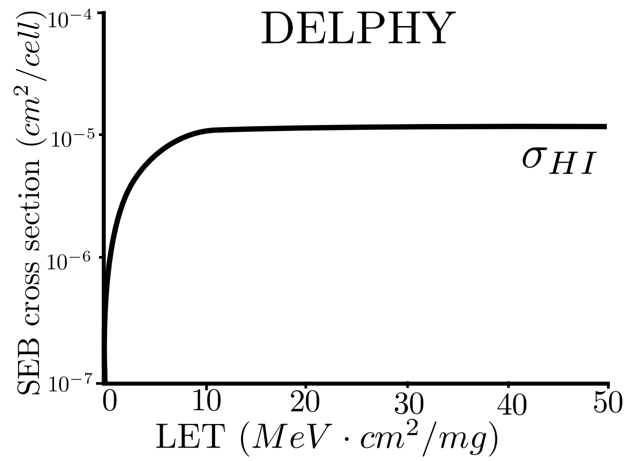

Figure F.14 – Section efficace σ_{HI} par cellule, en fonction du LET

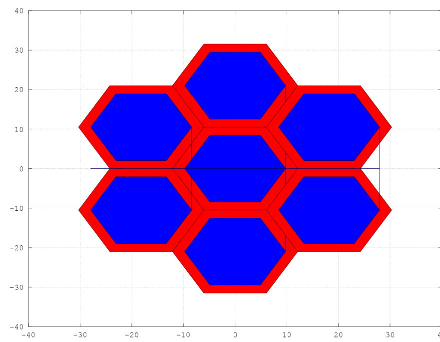

(a) $V_{DS} = 200\ V$

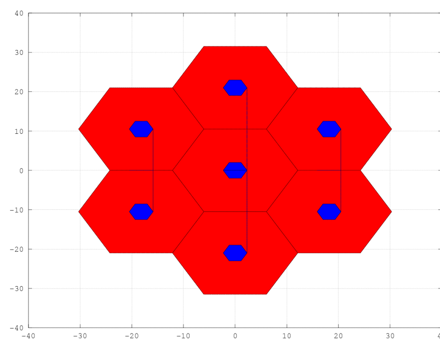

(b) $V_{DS} = 320\ V$

Figure F.15 – Cartographies SEB ion lourd pour le composant HEXFET, calculées par DELPHY. La partie rouge est sensible au SEB

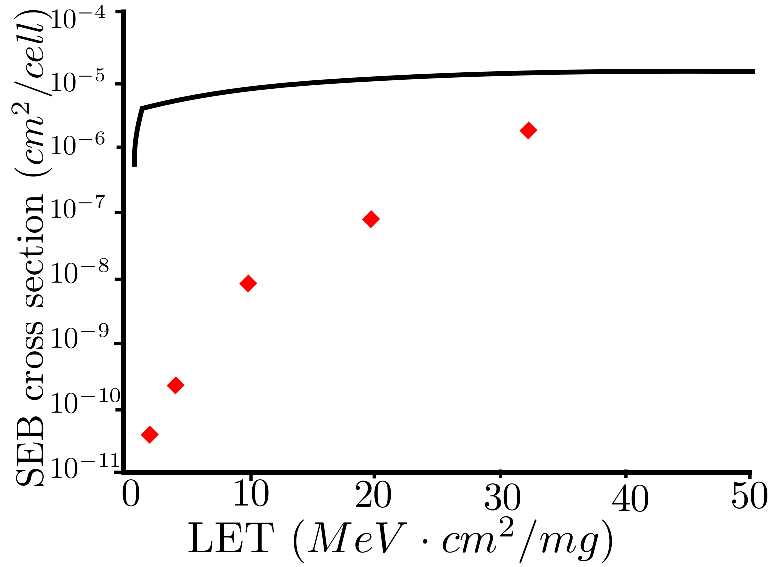

Figure F.16 – Section efficace σ_{HI} par cellule, en fonction du LET : la courbe continue noire est calculée avec le modèle de prédiction ; les points rouges viennent de [10]

La fig. F.17 montre que selon l'énergie du proton impactant, le spectre LET des probabilités de génération des ions secondaires générés est différent.

A partir de la matrice des probabilités de génération secondaire

$$C = \begin{bmatrix} c_{11} & c_{12} & \dots & c_{1n} \\ c_{21} & c_{22} & \dots & c_{2n} \\ \vdots & \vdots & \ddots & \vdots \\ c_{m1} & c_{m2} & \dots & c_{mn} \end{bmatrix} \tag{7}$$

DELPHY calcule les sections efficaces ion lourd H et proton P

$$H = \begin{bmatrix} h_1 \\ \vdots \\ h_n \end{bmatrix} \qquad P = \begin{bmatrix} p_1 \\ \vdots \\ p_m \end{bmatrix} , \tag{8}$$

avec la convolution

$$C \ \cdot H = P \ . \tag{9}$$

La fig. F.18 montre l'exemple du calcul de section efficace proton dans le cas d'un proton impactant avec une énergie de 200 MeV. En itérant le même calcul pour différentes énergies proton, DELPHY obtient la courbe de section efficace proton (fig. F.19).

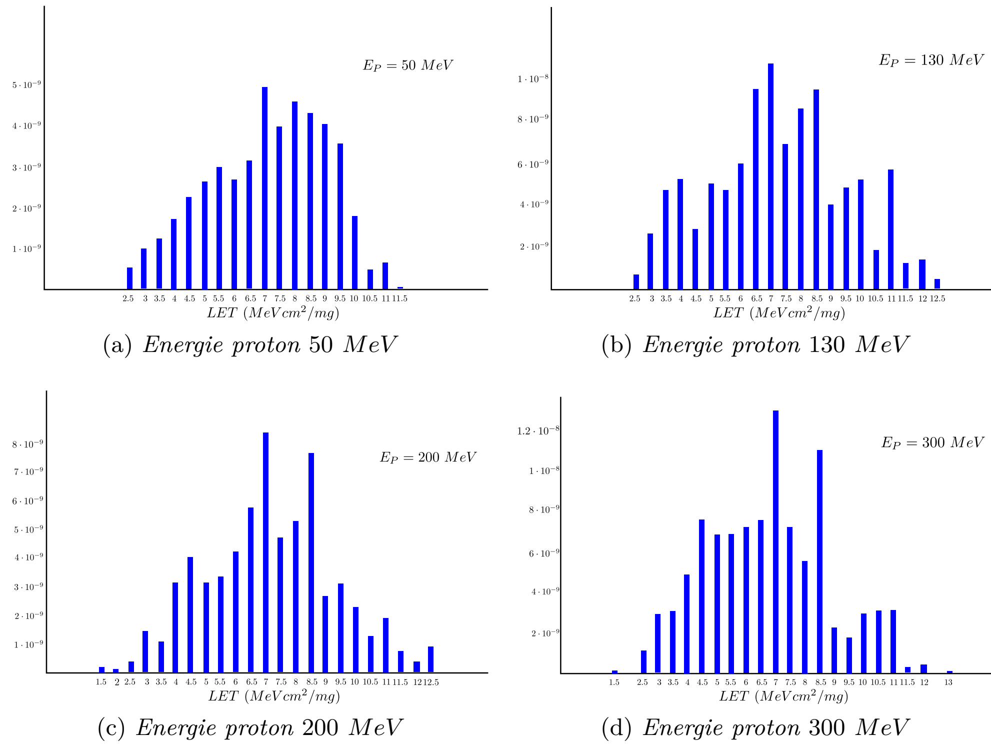

(a) *Energie proton* 50 MeV (b) *Energie proton* 130 MeV

(c) *Energie proton* 200 MeV (d) *Energie proton* 300 MeV

Figure F.17 – Spectre LET de la probabilité de génération des ions secondaires, en fonction de l'énergie du proton

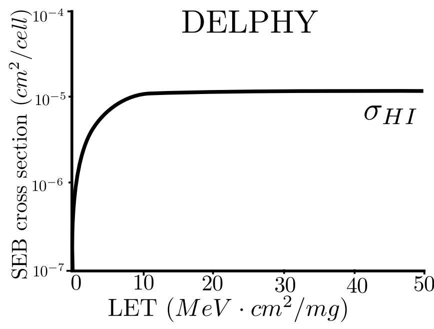

(a) *Section efficace SEB ions lourds secondaires*

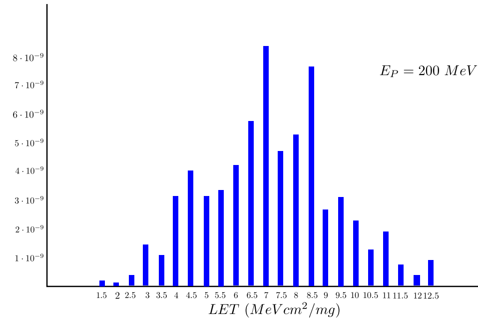

(b) *Probabilité différentielle de génération des ions lourds secondaires avec un proton d'énergie* 200 MeV

$$\sigma_P^{200} = 2 \cdot 10^{-9}\ cm^2$$

(c) *Protons SEB cross section*

Figure F.18 – Calcul des sections efficaces SEB proton, pour une énergie proton de 200 MeV

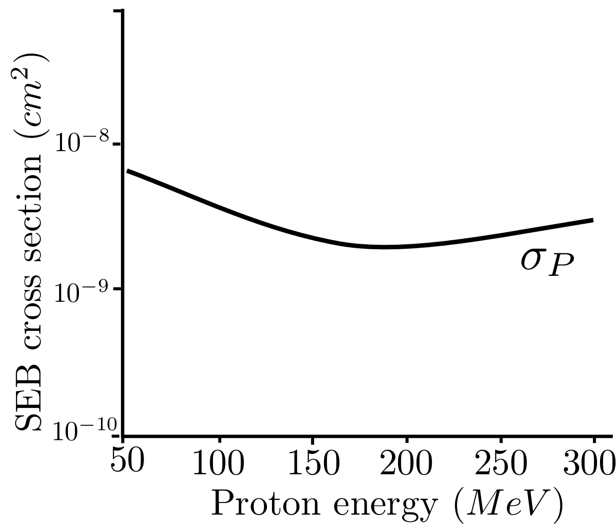

Figure F.19 – Section efficace SEB proton en fonction de l'énergie proton

Table F.2 – Sections efficaces SEB proton : données CERN et calcul DELPHY

	Cross section (cm^2)
CERN	$8.39E^{-10} < 9.46E^{-10} < 1.05E^{-9}$
DELPHY	$2.5E^{-9}$

4.5 Comparaison avec les données d'irradiation

La comparaison avec les données d'irradiation sur un composant STRIPFET (données CERN détaillées dans le manuscrit anglais), montre qu'il y a un bon accord dans l'ordre de grandeur, comme indiqué par le tableau F.2.

5 Extension du calcul des sections efficaces SEB à partir des données d'irradiation

5.1 Calcul des sections efficaces proton

Pour calculer la sensibilité SEB proton, il faut résoudre le système

$$C \cdot H = P \tag{10}$$

où la matrice des sections efficaces ion lourd H vient des données d'irradiation et non de la modélisation SEB. La solution donne une courbe qui a le même ordre de grandeur que les données expérimentales proton (fig. F.20).

5.2 Calcul des sections efficaces ion lourd

Pour calculer les sections efficaces ion lourd il faut résoudre le système

$$C \cdot H = P \ . \tag{11}$$

où la matrice des sections efficaces proton vient des données expérimentales. La comparaison avec les données d'irradiation ion lourd montre un bon accord dans l'ordre de grandeur (fig. F.21).

Une vision générale de méthodologie est données en fig. F.22.

6 Discussions

6.1 Choix des simulations 2D

Pour les technologies HEXFET et STRIPFET, une cellule élémentaire 2D a été identifiée et simulée, tout en vérifiant sa fonctionnalité électrique à travers la comparaison avec les datasheets des composants. Cela a permis d'estimer une troisième

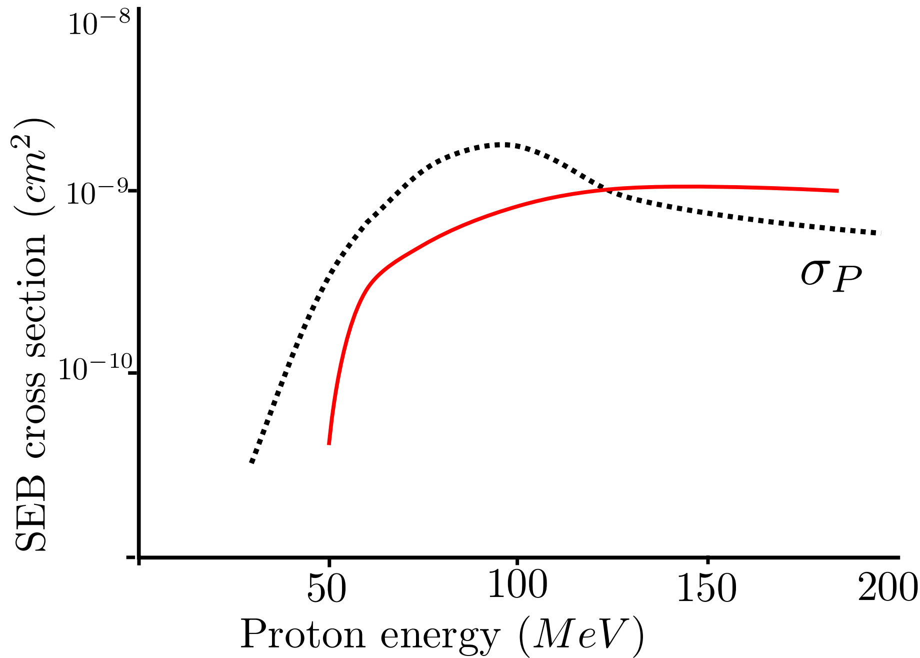

Figure F.20 – Section efficace proton calculée (en noir pointillé) comparée avec les données d'irradiation proton (en rouge continu) [10]

dimension équivalente, comme rapport entre le courant de drain du datasheet et celui des simulations.

Même si la littérature a démontré que la configuration 2D est suffisante à décrire la physique SEB, il y a un certain nombre de phénomènes physiques dont la représentation dynamique change dans les cas 2D et 3D.

Ces travaux donnent un petit exemple à travers l'étude de la diffusion. Un écart de 68% après $1 \cdot 10^{-9}$ s a été apprécié entre les configurations 2D et 3D. Cette valeur n'a pas une prétention d'exhaustivité dans l'évaluation de la différence 2D/3D, vu qu'il y a d'autres phénomènes physiques impliqués, et qui ne peuvent pas facilement être découplés.

Dans tous les cas, les coûts des simulations 3D ne conviennent pas au présent travail à cause du nombre élevé de simulations effectuées, et donc la configuration 2D a été choisie comme instrument de travail, en attendant de voir les conséquences de ce choix dans la sensibilité SEB prédite.

En effet, la surestimation de la sensibilité SEB calculée par DELPHY, pourrait être causée par la différence 2D/3D. Cette étude a démontré qu'il y a une concentration d'électrons plus élevée en 2D, et il est connu qu'un courant d'électrons plus élevé amène à une génération de trous plus élevée à la jonction $n_{epi} - n_{sub}$, qui donc augmente l'avalanche auto-alimentée et la mise en conduction du transistor BJT

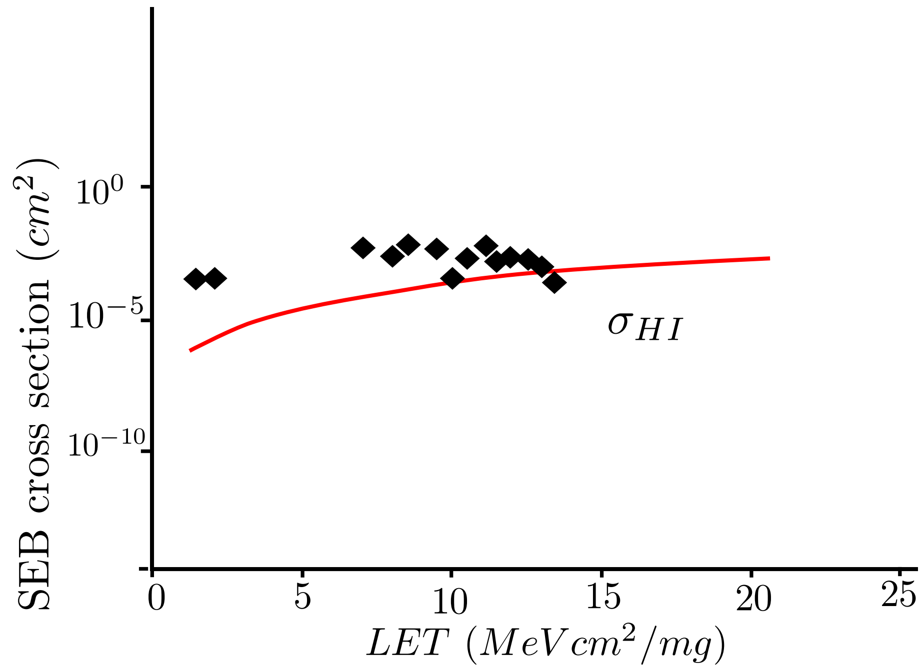

Figure F.21 – Section efficace ion lourd calcaluée (points) comparée avec les données d'irradiation ion lourd (en rouge continu) [10]

parasite.

Ça serait intéressant de vérifier ce concept avec des simulations jumelles en 2D et en 3D, à fin de prouver que la sensibilité au SEB est en effet mineure dans le cas 3D.

6.2 Choix du critère de déclenchement

Dans ces travaux le critère de déclenchement choisi est la charge critique dans la zone épitaxiée ; ce choix vient de la littérature. En effet, le rôle de la couche épitaxiée comme volume sensible a été démontré [82, 91, 55] et le même critère de déclenchement a été adopté par [75, 74].

Quelques travaux [48, 45, 44] avaient identifié la charge critique comme critère mais ils avaient relevé que sa valeur n'est pas dépendante du *LET* de la particule mais seulement de la technologie. La présente étude a démontré le contraire, avec la définition d'une charge critique qui dépend du *LET* et de la trace.

6.3 Choix des modèles physiques simulés

A part les équations de Poisson et de continuité, les modèles physiques adoptés comprennent la dépendance du champ électrique et de la concentration de dopage

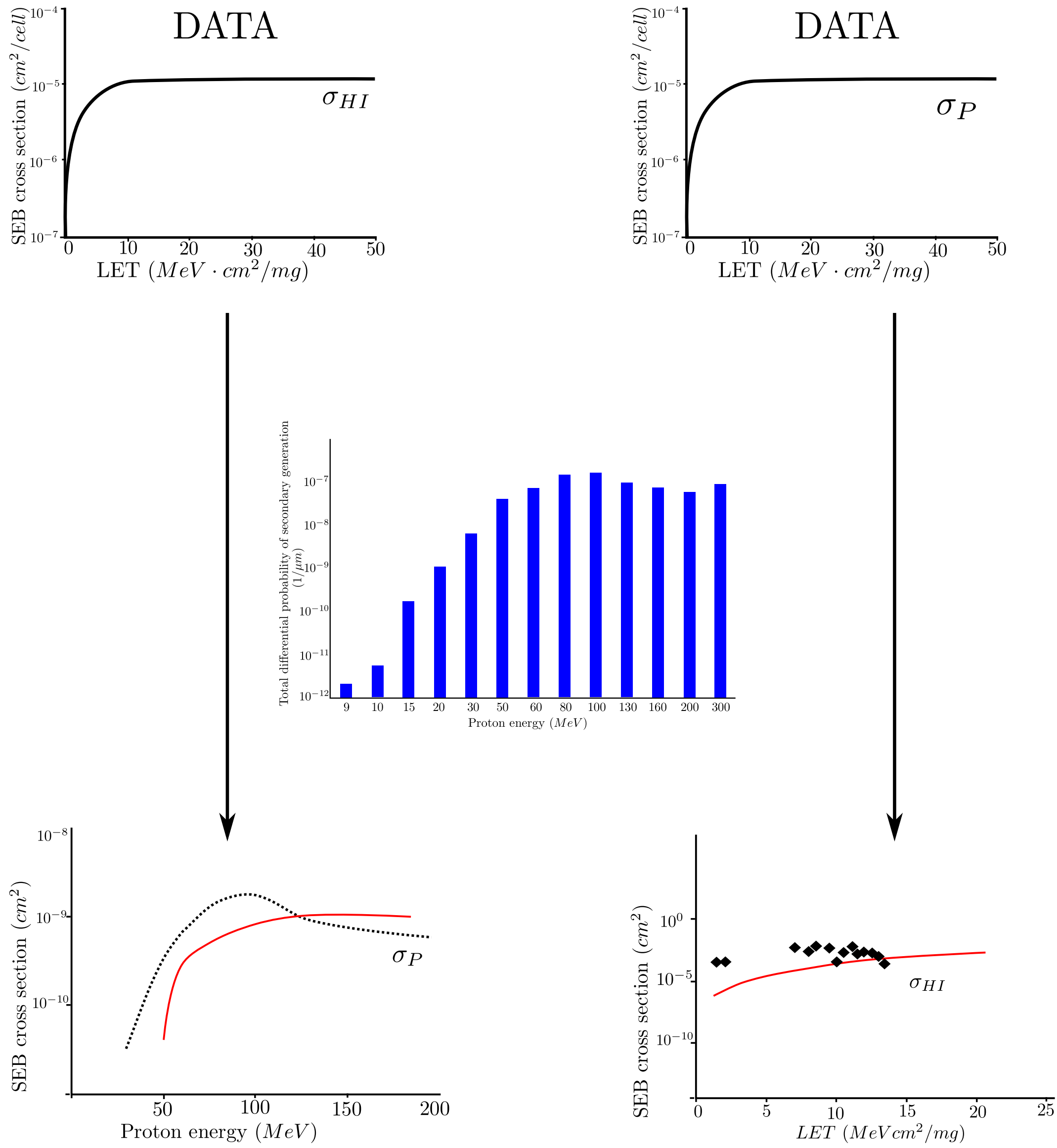

Figure F.22 – Vue générale de la méthodologie

pour la mobilité, le rétrécissement de bandgap, le modèle de recombination de Auger et Shockley-Red-Hall, et les effets du champ électrique sur la recombination d'avalanche. Ces modèles ont été utilisés dans les travaux précédents.

Toutefois, dans cette étude la dépendance du SEB de la température n'est pas prise en compte, donc le modèle dédié n'a pas été activé en TCAD. La surestimation des sections efficaces calculées peut être causée par ce choix, étant connu que la sensibilité SEB diminue avec une température croissante. Il serait intéressant de vérifier cette hypothèse avec deux simulations jumelles, dont la seule différence est dans l'activation du modèle thermique TCAD.

6.4 Confirmation des allures SEB

Dans les études précédentes, l'outil de simulation numérique (comme par exemple MEDICI [17] and SILVACO [55]) a été utilisé pour mettre en évidence l'effet de chaque paramètre sur le déclenchement du SEB.

Dans le présent travail, les paramètres étudiés à travers la simulation TCAD sont la position et l'angle d'injection, l'épaisseur et le dopage de la zone épitaxiée, tension de biais et longueur de trace. Ces simulations ont confirmé les allures disponibles dans la littérature, en validant les modèles physiques utilisés : la sensibilité SEB augmente avec la tension de biais te le *LET* de la particule, et diminue avec l'angle d'injection en fonction du lieu d'impact.

6.5 Identification de la loi de déclenchement

Des études antérieures ont démontré le rôle clé du champ électrique et de l'épaisseur de la couche épitaxiée comme volume sensible pour le SEB. Pour cette raison, tous les résultats de simulation ont été résumées avec une loi empirique de déclenchement, qui stipule que la charge de seuil dépend du champ électrique moyen dans la couche épitaxiée à travers un coefficient qui décrit l'effet du lieu d'injection.

Il serait intéressant d'exécuter des simulations 3D et d'évaluer la différence dans les coefficients de la loi. Ce serait coûteux mais pourrait offrir une appréciation de la différence 2D / 3D sur la loi de déclenchement. En outre, les deux topologies MOSFET étudiées étaient très différentes en termes de structure et dimensions caractéristiques, et pourtant elles ont montré le même comportement; l'enquête sur une troisième structure pourrait en effet donner une perspective plus large sur l'évaluation SEB et confirmer la validité de la loi de déclenchement tout en soulignant les effets de la topologie.

Une façon d'améliorer la prévision du modèle pour la section efficace, serait une meilleure description mathématique, avec donc un plus grand nombre de points dans la courbe, avec une conséquente calcul d'une nouvelle loi appropriée. D'un point de vue physique, cela signifierait l'évaluation de la charge seuil SEB dans plus de trois lieux d'impact.

6.6 Discussion de la méthodologie RPP

L'approche RPP représente une simplification extrême de SEB, en tenant compte que le phénomène dépend de nombreux paramètres entrelacées et se déroule relativement grandes structures comme les MOSFET de puissance.

En fait, les sections efficaces calculées par DELPHY sont mieux en accord avec les résultats expérimentaux dans le cas de la technologie STripFET, qui est bien plus intégrée que l'HEXFET, confirmant que le RPP rend une meilleure description de la réalité dans un petit dispositif. Cela confirme l'idée d'appliquer la même procédure sur d'autres topologies de composants et, par analyse comparative, essayer d'identifier les améliorations possibles pour DELPHY.

6.7 Calcul SEB à partir des données expérimentales

L'accord global entre les sections efficaces prédites et expérimentales, valide la méthodologie de DELPHY d'utiliser des données d'irradiation de prédire sensibilités de SEB complémentaires. La méthodologie est basée sur les effets secondaires protons à l'intérieur du dispositif, et implique donc une base de données de réactions nucléaires et un filtrage précis et cohérent des données brutes.

C'est dans le filtrage lui-même qui pourrait être la clé pour améliorer les sections efficaces prédites: des critères de filtrage sur le numéro atomique et la portée devraient être appliquées pour mieux décrire la physique SEB dans le composant étudié. Un matériau cible différente, ou une topologie différente, conduisent à des réactions nucléaires, et donc à différents produits secondaires en termes de nature des particules, de la portée et du *LET* [97].

Sur le même principe de filtrage nucléaire, on peut étendre la même méthodologie à d'autres composants, comme les IGBT, ou les mémoires CMOS ; et d'autres SEE, comme LATCH-UP ou SEU : avec une matrice adéquate de probabilité de génération différentielle, la physique de la génération secondaire est représentée de façon adéquate et utilisable.

7 Conclusions

Les MOSFETs de puissance sont des dispositifs électroniques très utilisés, capables de délivrer des niveaux importants de puissance. Ils sont sujets à des défaillances sévères causées par l'impact d'une particule radiative. Parmi les possibles effets de radiations, cette étude traite le Single Event Burnout (SEB), qui est déclenché par une particule déposant une charge dans le composant et ainsi mettant en conduction le structure BJT parasite. Cela conduit à un courant d'électrons qui active la jonction épitaxié/substrat et donc est à l'origine d'un courant de trous si un fort champ électrique est présent. Le phénomène est auto-alimenté et conduit à la destruction thermique du composant.

C'est dans ce cadre que la présente étude a ses raisons d'exister, son objectif étant la définition d'un modèle de prédiction SEB qui prend en compte la physique et la technologie. Le développement du modèle a été fait à partir de l'analyse TCAD, suivie par la synthèse des dépendances SEB et la définition d'un critère de déclenchement. Le modèle de prédiction DELPHY a été ainsi construit.

A travers l'outil de simulation TCAD, deux différentes technologies MOSFET ont été étudiées : un HEXFET et un STRIPFET, à fin de mettre en évidence l'effet de la technologie sur la dynamique SEB.

Les performances électriques des deux configurations ont été comparées avec les datasheets respectifs, confirmant le choix des modèles physiques simulés, et ensuite l'injection d'un ion lourd a été simulée. Les simulations de cette étude ont confirmé les allures SEB disponibles dans la littérature, mettant en évidence la dépendance de la sensibilité SEB des paramètres technologiques et d'injection.

Ces dépendances ont été synthétisées dans la définition d'une loi de déclenchement qui, à partir du champ électrique, calcule la charge minimale qu'il faut déposer dans la zone épitaxiée pour déclencher un SEB. Cette loi a été démontrée être valide dans les deux configurations étudiées à différents valeurs d'angle d'injection.

Cette loi a été exploitée à travers un ajustement mathématique, et le critère de déclenchement a été déterminé comme comparaison de la charge déposée avec la charge critique. Les deux charges font référence à la zone épitaxiée comme volume sensible.

A travers une approche RPP, l'application du critère dans le volume sensible est le cœur du modèle de prédiction DELPHY, qui a permis de calculer la section efficace des SEB ion lourd. Il fournit une surestimation de la sensibilité SEB mais trace la route comme un premier outil de prédiction SEB. Quelques suggestions pour l'améliorer ont aussi été données.

Au cours d'une étude conjointe ONERA-CERN, mise en place à fin de caractériser les MOSFETs de puissance pour la future génération de convertisseurs de puissance dans le Large Hadron Collider, les sections efficaces SEB proton ont été calculées dans la technologie STRIPFET ; la sensibilité calculée est en bon accord avec les données d'irradiation.

La démarche utilisée pour prédire la section efficace SEB proton, a été mise en place pour calculer la sensibilité SEB proton à partir des données de section efficace ion lourd, et vice-versa. Dans les deux cas, les ordres de grandeur des sections efficaces calculées sont en accord avec celles expérimentales, en validant ainsi la démarche.

En général, les résultats de prédiction DELPHY son encourageants pour continuer son développement dans le cas des topologies MOSFET différentes.

De plus, le fait que une physique complexe comme le SEB a été réduite à une déposition de charge dans un volume sensible, trace la route pour appliquer l'approche prédictive de DELPHY à des événements singuliers destructifs plus confinés dans

des autres composants.

Pour conclure, cette étude a répondu au manque de modèles de prédiction SEB, créant un modèle simple mais opérationnel. DELPHY étant le premier pas vers la prédiction SEB, il y a la marge pour plusieurs améliorations, en terme de meilleurs simulations TCAD, description mathématique plus précise, composants de puissance à étudier et plusieurs environnements radiatifs à prendre en compte.